ABSTRACT

A MICROSCOPIC STUDY OF NUCLEAR

MOLECULAR PHENOMENA

Ahmet Sait Umar

Yale University

1985

The concept of a "nuclear molecule" has been an intriguing topic in the low energy heavy-ion physics for the past quarter of a century. Despite the existence of a large body of experimental data, the theoretical understanding of the phenomena has been less than adequate. No theoretical calculation, which explains the details of the data in terms of the microscopic behavior of the nuclear system, has yet been presented. This dissertation gives a microscopic study of the phenomena. The fully microscopic nature of these calculations allows the consideration of the subject without making a priori assumptions as to the nature of a "nuclear molecule". The time-dependent Hartree-Fock formalism is used to study the nuclear dynamics leading to the formation of a molecule. The results establish a clear connection between the observed molecular resonances and the states built on the shape isomeric configurations of the composite nuclear system. These states are calculated by using the linear response theory and compared with experimental data.

A MICROSCOPIC STUDY OF NUCLEAR MOLECULAR PHENOMENA

A Dissertation

Presented to the Faculty of the Graduate School

of

Yale University

in Candidacy for the Degree of

Doctor of Philosophy

by

Ahmet Sait Umar

December 1985

ACKNOWLEDGEMENTS

My graduate school years have brought me into contact with many people whose contributions to the development of my perspective on physics I greatly value. First of all I would like to thank my thesis advisor, Michael R. Strayer, for excellent guidance throughout these years. His interest in diverse areas of physics has led me to develop a broad outlook to the field, but most of all, his treatment of me as a collaborator allowed me to build up confidence in my research.

A major factor in my decision for a dissertation topic was an enlightening course in nuclear theory offered by Prof. D. A. Bromley. In addition, I would like to thank him for his continuous support and constructive advice. I am also grateful to Prof. F. Iachello for his help and financial assistance.

Dr. J. B. McGrory and the members of the Physics Division at Oak Ridge National Laboratory deserve special thanks for their generous hospitality and financial support. Without the use of the computational facilities at ORNL, some of the work in this dissertation would not have been possible.

My acknowledgements would not be complete without thanking Althea Tate for her expert typing, not only of this dissertation but also of many other manuscripts. Also, for a critical reading of the manuscript, I want to thank Drs. A. Vazquez and A. B. Balantekin.

Finally, I would like to thank my wife, Verena, for her encouragement and patience during these difficult times, my friends Viktor Zekeriya and Atilla Öner for making my stay in New Haven more pleasant, and my parents for having fully supported my choice of physics as a carrier.

CONTENTS

LIST OF FIGURES

LIST OF TABLES

I. INTRODUCTION

The collisions of light heavy ions constitutes one of the most interesting areas of low-energy nuclear physics. The reactions of heavy systems are usually dominated by strong Coulomb repulsion at large impact parameters and strong attraction at small impact parameters, thus leading to a classical or semiclassical kind of phenomenon based on the gross features of the reaction partners. This could be understood from the fact that in these collisions the wavelength is short compared to the size of the nucleus which leads to the classical description of the relative motion of the ions.

However, among light systems, the scattering seems to display features reflecting details of the internal structure of the ions. The experimental observation of interesting structures in the scattering of light ions (in the Coulomb barrier region) dates as early as the heavy-ion reaction study by Bromley, Kuehner, and Almqvist, in 1960 (BK60). What characterized the scattering of light systems were unexpected structures in the excitation functions, with a very pronounced dependence on the scattering system. Since then, a tremendous amount of experimental and theoretical work has been done for the classification and understanding of these features (EB85). These structures also stimulated discussions about the possible existence of "nuclear molecules", a conjecture, which has been an outstanding problem in low-energy nuclear physics for the past quarter of a century. This chapter outlines some features of experimental observations together with some

of the theoretical calculations.

The experimental studies with light heavy ions reveal three separate kinds of structure in the excitation functions. These are classified according to their widths as gross- ($\Gamma \approx 3$-5 MeV), intermediate- ($\Gamma \approx 0.1$-0.5 MeV), and fine-structure ($\Gamma \approx 0.05$-0.1 MeV) resonances. The compound-nucleus states are still narrower and, in principle, could mix with all of the above structures. The gross structure is seen in all of the elastic scattering excitation functions, and they do not have explicit quantum numbers. The width and position of these structures vary systematically with mass number and scattering angle indicating a kind of diffraction phenomenon. These structures are explained as being due to the localization of the partial waves near the grazing angular momentum during the heavy-ion dynamics. More specifically, the gross structure is enhanced by the interference effects between waves reflected from the outer edge of the interaction potential and from the centrifugal barrier in its interior. The intermediate states show no correlation between different reaction channels. These structures arise from nearly random interferences between shape resonances in various asymptotic channels. A recent summary of the structures seen in the collisions of light heavy ions can be found in (EB85).

The more interesting structures are the fine-structure resonances. These resonances are most pronounced in the $^{12}C+^{12}C$ system although they are also seen in many other systems. Specific spin assignments have been made for most of these states and they are well correlated

between various asymptotic channels. The small resonance widths imply that we are dealing with a system having a relatively long lifetime. The occurrence of such fine structures in the reaction cross-section is generally viewed as an indication that the reaction proceeds through the formation of a composite system. This assertion also seems to be supported by the fact that the resonances are observed in reactions with different entrance and exit channels. For example, the structures seen through the reactions, $^{12}C(^{12}C,^{12}C)^{12}C$ (EN73,KE79), $^{12}C(^{12}C,^{4}He)^{20}Ne$ (AB63,EB76,BA76,VG77, GT77), $^{12}C(^{12}C,p)^{23}Na$ (CC75,BA76), $^{12}C(^{12}C,^{16}O)^{8}Be$ (EM75,WS77,JF78), $^{4}He(^{20}Ne,^{12}C)^{12}C$ (Da81), and $^{10}B(^{14}N,^{4}He)^{20}Ne$ (MV74,MH77) seem to fit onto a single classification scheme. Resonances were also observed in the electron-induced fission of ^{24}Mg into two ground state ^{12}C nuclei following monopole excitations (SK78). Similarly, the fusion cross-section of various systems ($^{12}C+^{12}C$, $^{12}C+^{16}O$) show characteristic oscillations (SB76). In Table 1 a compilation of the $^{12}C+^{12}C$ fine-structure resonances is given.

From the theoretical point of view the early calculations done for the understanding of these reactions were limited by the assumptions made concerning the nature of the "nuclear molecule". Subsequently, the two-center shell model calculations (PS74,PG77) have treated the shell structure of the $^{12}C+^{12}C$ fully microscopically. This was achieved by using a two-center shell model basis. The $^{12}C+^{12}C$ potential was calculated as a function of the relative distance between the two potential wells. This potential included an optical potential part

Table 1. A recent compilation of correlated resonances seen in $^{12}C+^{12}C$ system [(EB81) and references therein].

Table 1

Correlated resonances				
J = 0	J = 2	J = 4	J = 6	J = 8
(3.17)	(3.75)	(4.46)	(6.49)	9.65
(3.35)	4.62	5.96	7.55	9.84
4.25	4.88	6.85	8.86	10.30
5.80	5.00	(7.30)	9.05	10.63
	(5.37)	(7.45)	(9.33)	10.90
	5.64	7.71	9.98	11.38
	6.25	7.90	10.45	11.90
	6.63	8.26		12.36
	(7.05)	8.45		12.98

whose real part was determined by fitting the position and spacing of the observed sub-Coulomb resonances in the total cross-section. The calculations assumed adiabatic motion of the two ions which is appropriate in the weak-coupling limit. In addition, the potential included coupling potentials to the 4.43 MeV 2^+ state of ^{12}C. The coupling potentials depend strongly on the densities of the nuclei. This coupling was assumed to happen mainly in the touching region of the two nuclei. The solution of the coupled-channels equations with such a potential produced a qualitative description of the intermediate structure. This adiabatic picture would have worked well in the weak-coupling limit where the structure of the nuclear configuration is similar to that of the entrance channel. But it does not appear that this is the correct description of the potentials needed to reproduce the fine-structure resonances. Similar calculations of ion-ion potentials have been carried out using the constrained Hartree-Fock theory (CD79). These microscopic calculations computed the potential energy of the 24-particle system as a function of the relative separation coordinate, defined as the square root of the quadrupole moment. By also adding an imaginary part to simulate inelastic excitations of the intrinsic states, they computed the 90° excitation functions in the center-of-mass system. These calculations failed to reproduce in any quantitative way the intermediate and fine-structure resonances, although the gross-structure was reproduced. Other constrained Hartree-Fock calculations (CH76,BG80,FH80) have also produced similar potentials as a function of the ion-ion separation coordinate, R. These potentials have

no repulsive core due to the true adiabatic nature of the calculations. The strong attraction seen for short separation distances indicates that there is no mechanism to maintain a binary molecular shape. On the other hand, constrained Hartree-Fock calculations using the sudden approximation (ZM75,CS82) yield potentials that are similar to the ones obtained by making the adiabatic approximation except they become strongly repulsive at small separations. This strong repulsion is inconsistent with the long lifetime of the fine-structure resonances. An interesting outcome of one of these calculations (BG80) was the observation of a shape transition for small values of the separation coordinate. The α-^{16}O-α configuration was found to be energetically favorable in the large overlap region of the two carbons.

Figure 1 shows ion-ion potentials calculated for the $^{12}C+^{12}C$ system starting from different entrance channel configurations (St81). The $^{12}C(0_2^+)$ represents the 7.66 MeV 0_2^+ state in ^{12}C. This state is approximated by a shape isomeric configuration in Hartree-Fock calculations which is made up of three collinear alpha-like structures (see Fig. 8). These potentials were calculated using the adiabatic approximation for large ion-ion separations and the sudden approximation for small distances. They yield too large a radius as compared to the corresponding optical potentials, and they cannot reproduce the correct vibrational spacings of the fine-structure resonances.

The Nilsson-Strutinsky calculations (LL75) compute directly the collective potential energy surface of the composite system in terms of various shape parameters. Detailed calculations have revealed

Figure 1. $^{12}C+^{12}C$ potentials calculated from different entrance channel configurations. Here 0_1^+ denotes the 7.66 MeV 0^+ state of ^{12}C. Potentials were calculated using the adiabatic approximation for large ion-ion separations and sudden approximation for small distances (St81).

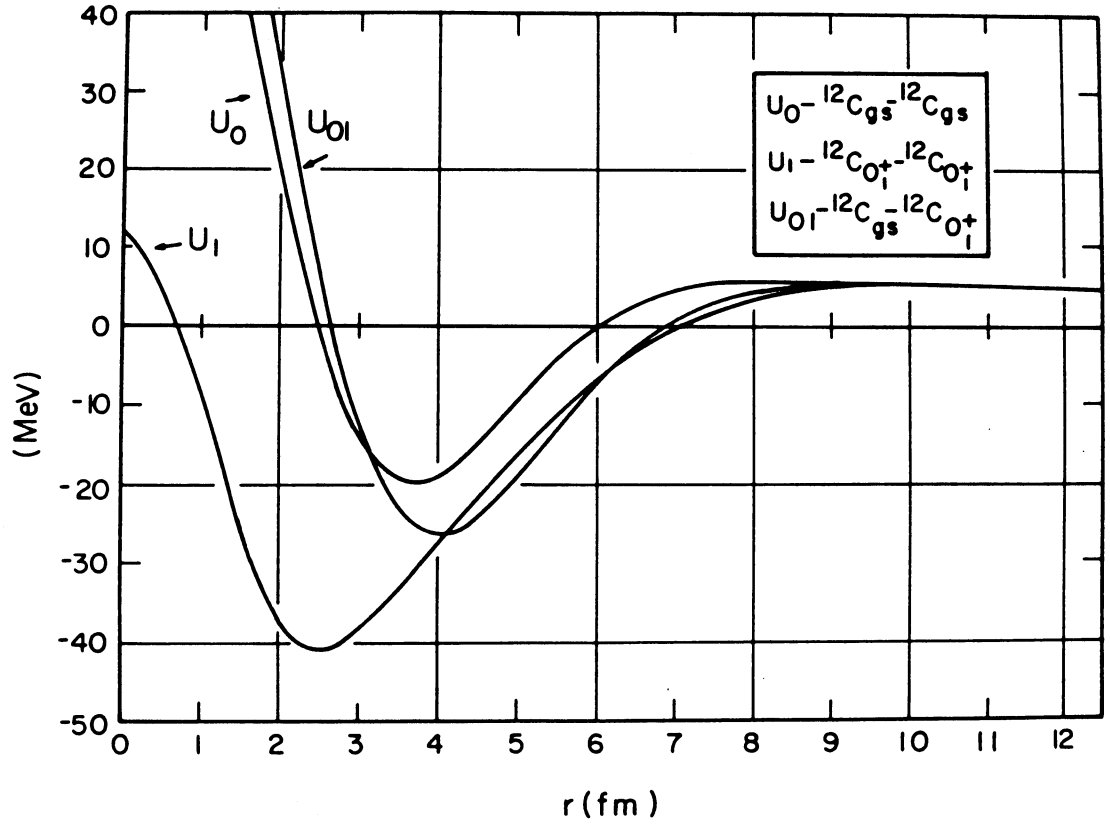
40
30
20
10
0
-10
-20
-30
-40
-50
(MeV)
0
1
2
3
4
5
6
7
8
9
10
11
12
r (fm)
U_0
U_{01}
U_1
$U_0 - {}^{12}C_{gs} - {}^{12}C_{gs}$
$U_1 - {}^{12}C_{0_1^+} - {}^{12}C_{0_1^+}$
$U_{01} - {}^{12}C_{gs} - {}^{12}C_{0_1^+}$

stationary shape isomers (minima) in the potential energy surface of the ^{24}Mg and other systems. These calculations could not address in any quantitative way the distinction between gross-, intermediate-, and fine-structure resonances. In later calculations (CM78) the Nilsson part was replaced by a two-center shell model basis, thus allowing the separation of the system into various asymptotic channels. As a consequence of difficulties in determining the correct potential parameters for light systems, there were no comparisons with experiments.

Recently a comprehensive description of the fine-structure data has been given in terms of the U(4) model (Ia81). This model considered a di-nuclear molecule with a prominent dipole degree of freedom. The approach was based on the use of a spectrum generating algebra, and it did not address the question of the interaction. On the other hand, it is possible to obtain a similar expression by studying the perturbative expansion of the Morse potential (or the anharmonic oscillator) about an equilibrium point r_o (EB81),

$$V(r) = V_o + A(r-r_o)^2 + B(r-r_o)^3 + C(r-r_o)^4. \qquad (1.1)$$

This results in an expression for the energies which is quadratic in oscillator quanta,

$$E(\nu,L) = -D + a\left(\nu + \tfrac{1}{2}\right) - b\left(\nu + \tfrac{1}{2}\right)^2 + CL(L+1), \qquad (1.2)$$

where ν denotes the vibrational quanta and L is the rotational quantum number. For D = -0.34 (MeV), a = 1.44 (MeV), b = 0.08 (MeV), and c = 0.076 (MeV), one obtains a relatively good fit of the 28 resonances of the ^{12}C+^{12}C system as shown in Fig. 2. The value 0.076 MeV for the rotational parameter corresponds to r_o = 6.75 fm as the equilibrium

Figure 2. A fit to the 28 resonances tabulated in Table 1. The energy expression is the one used by Erb and Bromley (EB81). The figure clearly demonstrates the vibrational-rotational nature of the resonances.

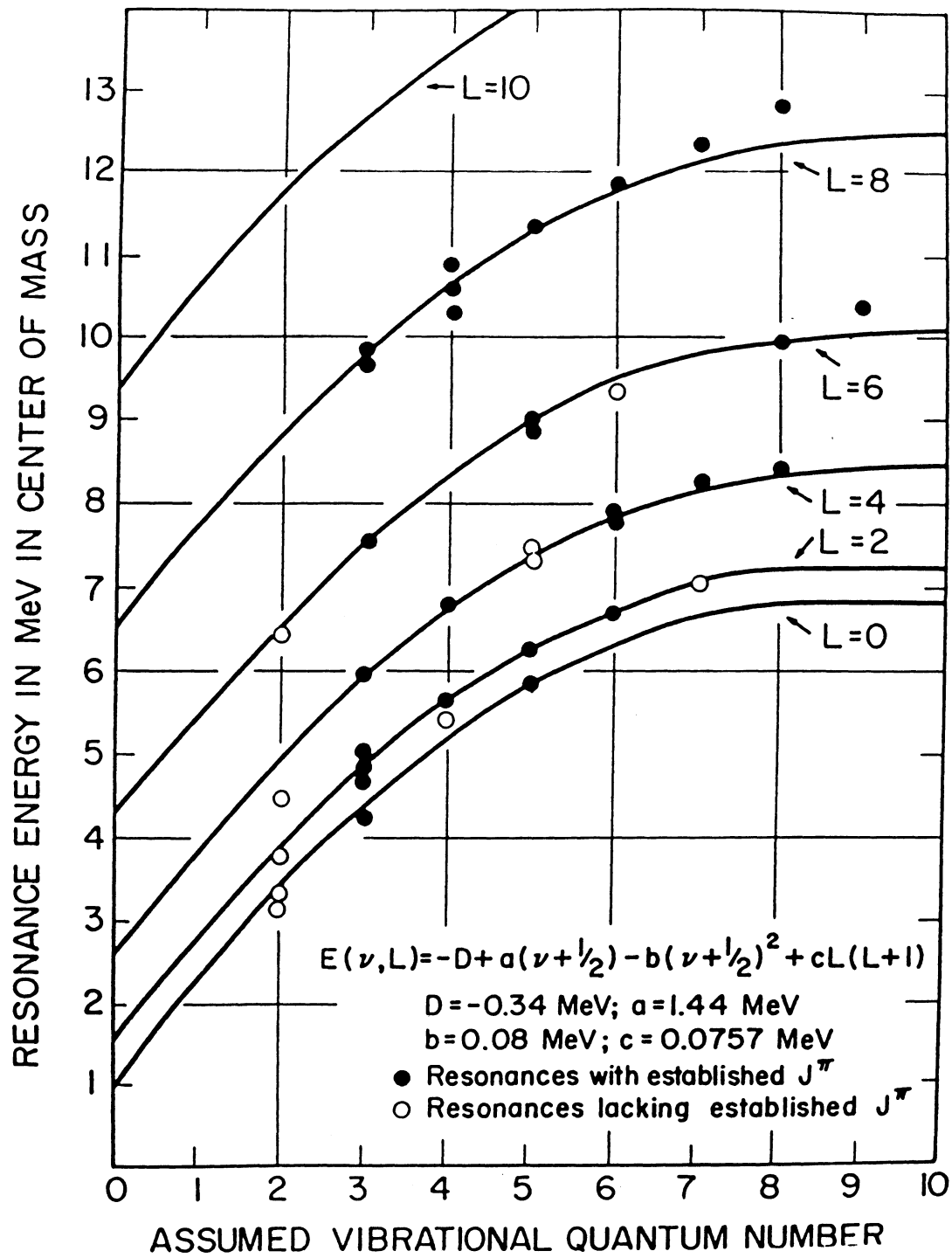
L=10
L=8
L=6
L=4
L=2
L=0
RESONANCE ENERGY IN MeV IN CENTER OF MASS
ASSUMED VIBRATIONAL QUANTUM NUMBER
E(ν,L)=-D+a(ν+½)-b(ν+½)²+cL(L+1)
D=-0.34 MeV; a=1.44 MeV
b=0.08 MeV; c=0.0757 MeV
Resonances with established J^π
Resonances lacking established J^π

separation of the two ^{12}C nuclei. This model was criticized because the potentials needed to fit the data had a considerable attraction at large distances where the two carbons could be considered asymptotic. This disagreement is probably due to the assumption of a di-nuclear system, and the true configuration of the composite system may be different.

A similar expression for the energies was also obtained by studying the axially symmetric quadrupole vibrations of the composite system with a large static quadrupole deformation (CG83). A collective Hamiltonian which depends only on the quadrupole degree of freedom was used. The addition of a quartic term yielded a vibrational-rotational energy expression identical to that of Eq. (1.2). The large static quadrupole deformation was interpreted as being due to the configuration of two touching carbon nuclei. Again, this model provided us with a parametrization of the data.

Although there are various theoretical models addressing the question of the gross and intermediate structures, the nature of the fine-structure states still remains undetermined. Most of the phenomenological models suffer from the so-called "intuitive approach" in which one makes plausible assumptions concerning the nature of these states. For example, the assumption of a di-nuclear complex is common to all of these models, but recent measurments (MK83) of γ-decay within the observed rotational band was found to be order of magnitude smaller than the expected collectively enhanced E2 radiation emitted from a rigidly rotating di-nuclear configuration. Similarly, the microscopic

models all rely on collective coordinates but it does not seem like the use of the quadrupole moment as the collective coordinate is the correct description of the potentials needed to reproduce fine-structure resonances. This makes it desirable to study these reactions in their full generality. The first part of this dissertation will look at various reactions using the time-dependent Hartree-Fock theory. Since these calculations are fully microscopic and no prior choice of collective degrees of freedom is made, they will help us to understand the reaction mechanisms leading to the formation of a "nuclear molecule". Equipped with this information, the question of fine-structure states will then be addressed.

II. STATIC AND TIME-DEPENDENT HARTREE-FOCK THEORIES

The early theoretical studies of heavy-ion dynamics have been done by using macroscopic models based on collective variables. One example is the Liquid-Drop Model (BM75), in which the nucleus is considered to be a drop of liquid. The characteristics of the nucleus are thus determined by properties like viscosity, compressibility, volume, pressure, etc. The vibrations of this liquid drop about an equilibrium shape have been used for the representation of collective states.

While these macroscopic models had some success in portraying certain aspects of heavy-ion phenomena, it has been beyond their range of applicability to describe heavy-ion dynamics including such phenomena as energy dissipation, transfer of relative energy into internal excitations, transfer of angular momentum, and mass and charge transfer. Although in a very limited number of cases (like the neck degree of freedom in fission), where use of collective variables may be justified, a general representation of the dynamics will require more than one, possibly infinite number of collective coordinates. In this sense, it is desirable to use a microscopic theory which avoids the arbitrary choice of collective and intrinsic variables and the need for parametrizing shapes.

One way of studying this many-body problem is through the Hartree-Fock approximation and its time-dependent generalization, the time-dependent Hartree-Fock (TDHF) theory (Di30,Ko75). The advantage of the TDHF theory is that it is built on the static Hartree-Fock (SHF) theory

which had some success in the description of low-lying states of nuclei (Ne70,VB72,BT75,BF75), properties of deformed nuclei, and fission barriers. The SHF and TDHF theories are based on the assumption that nucleons move in an average, one-body field generated self-consistently from an effective nucleon-nucleon interaction. The many-body wavefunctions are assumed to be of determinantal form which ensures the proper antisymmetrization. The mean-field approximation is easy to understand in the SHF case. Here, the collisions of nucleons are strongly inhibited due to the Pauli Exclusion Principle; thus, one can imagine the nucleons to be moving in an average field generated by themselves. The same argument also holds for the time-dependent case provided that the internal excitation energy of the ions is less than their respective Fermi energies. Another way of looking at the problem is through the fact that in heavy-ion collisions the wavelength is short compared to the size of the nucleus (at low energies) which leads to semiclassical or classical relative motion of the ions. In this case, the rate of change of the mean-field is slow enough to prevent large internal excitations in a short time interval.

In recent years the TDHF theory has been succesfully used in the description of large amplitude, collective, and dissipative phenomena such as fusion, fission, energy loss, and mass transfer in heavy-ion reactions. It has also been shown that in the small amplitude limit TDHF equations, when linearized, reduce to the Random Phase Approximation (RPA) equations (KK76). In this context, small amplitude TDHF calculations have been used in the study of giant resonance phenomena

(BF79). A recent summary of the applications of the TDHF theory can be found in (DD85).

This chapter will consider the various aspects of these theories including a detailed description of the numerical methods used. The introduction of new numerical methods is one of the major reasons enabling the calculations performed in this dissertation.

A. SKYRME INTERACTION

Before examining the derivation of SHF and TDHF equations, it is proper to mention the fact that the success of these theories largely depends on the development of the density-dependent effective interactions. For this reason, a brief description of the effective interactions, and in particular the Skyrme interaction, will be presented.

Since the nucleon-nucleon force in free-space only contains the momentum-conserving part of this interaction, it cannot be directly used for calculations in the nuclear medium. The G-matrix formalism (Be71) outlines a derivation of this interaction for nuclear matter. Here, the Lippmann-Schwinger equation for the scattering matrix of two particles is replaced by the one in the nuclear medium,

$$G_{ij,k\ell}(E) = V_{ij,k\ell} + \frac{1}{2} \sum_{\substack{m,n \\ >\varepsilon_F}} V_{ij,mn} \frac{1}{E-\varepsilon_m-\varepsilon_i+i\eta} G_{mn,k\ell}(E)$$

where i,j,... denote the shell model indices replacing the two-particle momenta, ε_F is the Fermi energy, ε_m and ε_i are the single-particle energies, and V is the nucleon-nucleon potential. In this sense, the effective interaction (G-matrix) is an infinite sum of scattering

processes in the nuclear medium.

An extension of these ideas to finite size nuclei has been achieved through the Local Density Approximation (Ne70). In this formalism the G-matrix for a finite nucleus has been taken to be the same as that for nuclear matter at the same density. However, for a quantitative description of the experimental data, one still needs phenomenological renormalization parameters. In this respect, one is led to investigate phenomenological effective interactions that would simulate the general features of the G-matrix.

One of the most important properties of the effective nucleon-nucleon force is its short range. In fact, zero-range forces of the form $\delta(\vec{r}_1-\vec{r}_2)$ (where $\vec{r}_1$ and $\vec{r}_2$ denote the space coordinates of the nucleon 1 and nucleon 2, respectively) have been used extensively in the description of nuclear properties (SF74). We also note that this force satisfies the Galilean invariance, since it only depends on the relative two-nucleon distance $\vec{r} = (\vec{r}_1-\vec{r}_2)$. It is easy to see from the Fourier transform,

$$v_{12}(\vec{p},\vec{p}') = \int d^3r\ e^{-i(\vec{p}-\vec{p}')\cdot\vec{r}}\ v_{12}(\vec{r}), \tag{2.1}$$

that a finite range in coordinate space would necessarily imply a momentum dependence for $v_{12}(\vec{p},\vec{p}')$. For a delta function force $v_{12}(\vec{p},\vec{p}')$ is a constant. As a simplest generalization, one can consider the quadratic expansion in momentum space (Sk59,Ko69,Mo70),

$$v_{12}(\vec{p},\vec{p}') = v_0 + v_1\ \vec{p}'^2 + v_1\ \vec{p}^2 + v_2\ \vec{p}\cdot\vec{p}'. \tag{2.2}$$

This form is Galilean invariant since it depends only on the relative two-nucleon momentum. Furthermore, it is also invariant under space

reflection, time-reversal ($\vec{p}$--> - $\vec{p}$), and space exchange ($v_{12} = v_{21}$). In coordinate space v_{12} can be written as

$$v_{12}(\vec{r}) = v_o\delta(\vec{r}) + v_1(\vec{p}^2\delta(\vec{r}) + \delta(\vec{r})\vec{p}'^2) + v_2\vec{p}\delta(\vec{r})\cdot\vec{p}'. \tag{2.3}$$

Various forms of this momentum expansion have been used as an effective interaction for nuclear many-body calculations. One particular interaction, the Skyrme potential (Sk56,Sk59), is given by

$$V \equiv V^{(2)} + V^{(3)} = \sum_{i<j} v_{ij} + \sum_{i<j<k} v_{ijk}, \tag{2.4}$$

where v_{ij} and v_{ijk} denote two- and three-body interactions,

$$\begin{aligned} v_{12} = {} & t_0(1 + x_o P_\sigma)\delta(\vec{r}) + \frac{1}{2} t_1[\delta(\vec{r})\vec{k}^2 + \vec{k}'^2 \delta(\vec{r})] \\ & + t_2\vec{k}'\cdot\delta(\vec{r})\vec{k} + i W_o(\vec{\sigma}_1 + \vec{\sigma}_2)\cdot\vec{k}' \times \delta(\vec{r})\vec{k} \end{aligned} \tag{2.5a}$$

$$v_{123} = t_3\delta(\vec{r}_1-\vec{r}_2)\delta(\vec{r}_2-\vec{r}_3). \tag{2.5b}$$

In this expression P_σ is the spin exchange operator,

$$P_\sigma = \frac{1 + \sigma_1\cdot\sigma_2}{2}, \tag{2.6}$$

$\vec{k}$ denotes the operator $(\vec{\nabla}_1-\vec{\nabla}_2)/2i$ acting on right, and $\vec{k}'$ is the operator $-(\vec{\nabla}_1-\vec{\nabla}_2)/2i$ acting on left. The W_o term depends explicitly on spin and denotes a spin-orbit contribution. The three-body term was introduced as an explicit density dependence (Sk59), and as we will see later, this term can also be written in an equivalent two-body form (VB72),

$$\frac{1}{6} t_3(1 + P_\sigma)\delta(r)\rho^\alpha\left(\frac{\vec{r}_1+\vec{r}_2}{2}\right). \tag{2.7}$$

In the original definition $\alpha = 1$. The power α can be adjusted to yield

better fits to nuclear properties in the Hartree-Fock approximation (see section D). The parameters t_0, t_1, t_2, t_3, W_o, and x_o are to be determined from experimental fits, and they will be constants throughout the periodic table.

The Skyrme interaction can be considered as a parametrization of a G-matrix, which includes the effects of the short-range correlations through its dependence on the density. In this sense, it is an approximate description of the effective potential which is only valid for small relative momenta. The problem of relating the empirical parameters of the Skyrme interaction to the nucleon-nucleon potential has also been studied by expanding the nuclear density matrix in powers of k^2 (NV72,NV75). This leads to an effective Hamiltonian density which relates the nucleon-nucleon potential to the effective interaction.

B. THE HARTREE-FOCK ENERGY DENSITY

In the Hartree-Fock approximation the many-body wavefunction, X, is usually assumed to be of determinantal (Slater) form,

$$X \equiv \frac{1}{\sqrt{A!}} \det \left| \chi_\alpha(\vec{r}_1,\sigma,q) \right| , \tag{2.8}$$

where $\vec{r}$, σ, and q denote spatial, spin, and isospin coordinates of the single-particle states χ_α respectively (q = +1/2 for protons, -1/2 for neutrons). The subscript α denotes all other quantum labels, (i.e. n, l, j, m, etc.), and A is the nuclear mass number. In the second quantized representation (SF74), to each single-particle state χ_α we can associate a creation operator $a_\alpha^\dagger$, and an annihilation operator a_α.

Since we are dealing with fermions, these operators obey the anticommutation relations,

$$\{a_\alpha^\dagger, a_\beta\} = \delta_{\alpha\beta} \quad ; \quad \{a_\alpha^\dagger, a_\beta^\dagger\} = 0$$
$$\{a_\alpha, a_\beta\} = 0. \tag{2.9}$$

We can define the vacuum $|\, 0\rangle$ in the usual sense as

$$a_\alpha \,|\, 0\rangle = 0 \quad ; \quad \langle 0 \,|\, a_\alpha^\dagger = 0. \tag{2.10}$$

In what follows we will use Latin letters i, j, k, .. to denote the states in X (occupied states), and Greek letters α, β, γ, ... to denote states in general (occupied and unoccupied). In this representation the wavefunction X is written as

$$|\, X\rangle = a_1^\dagger a_2^\dagger \ldots a_n^\dagger \,|\, 0\rangle, \tag{2.11}$$

and Eq.(2.9) guarantees X to be antisymmetric in the quantum labels. These identities will be useful in the following calculations,

$$a_i^\dagger \,|\, X\rangle = 0 \quad ; \quad \langle X \,|\, a_i = 0$$
$$a_\alpha \,|\, X\rangle = 0 \quad ; \quad \langle X \,|\, a_\alpha^\dagger = 0 \text{ for } \alpha > A. \tag{2.12}$$

The total energy E of the nucleus is given by

$$E = \langle X \,|\, H \,|\, X\rangle = \langle X \,|\, T + V^{(2)} + V^{(3)} \,|\, X\rangle, \tag{2.13}$$

where H is the many-body Hamiltonian,

$$H = \sum_{\alpha,\beta} \langle \alpha \,|\, t \,|\, \beta\rangle \, a_\alpha^\dagger a_\beta + \frac{1}{2} \sum_{\alpha\beta\gamma\delta} \langle \alpha\beta \,|\, v_{12} \,|\, \gamma\delta\rangle \, a_\alpha^\dagger a_\beta^\dagger a_\delta a_\gamma + \ldots, \tag{2.14}$$

and T is the one-body kinetic energy operator. The calculation of the expectation value is straightforward (VB70,VB72,EB75,Pa76) and is given in Appendix A. Here we just quote the result for a spin-saturated system (EB75),

$$E = \int d\vec{r}\, H(\vec{r})$$

$$H(\vec{r}) = \frac{\hbar^2}{2m}\tau + \frac{1}{2}t_o\left[\left(1+\frac{x_o}{2}\right)\rho^2 - \left(\frac{1}{2}+x_o\right)\sum_q \rho_q^2\right]$$
$$+ \frac{t_3}{8}\rho^\alpha\left(\rho^2 - \sum_q \rho_q^2\right) + \frac{(t_1+t_2)}{4}(\rho\tau - \vec{j}^2) + \frac{(t_2-t_1)}{8}\sum_q(\rho_q\tau_q - \vec{j}_q^2)$$
$$+ \frac{1}{16}(t_2-3t_1)\rho\nabla^2\rho + \frac{(t_2+3t_1)}{32}\sum_q \rho_q \nabla^2 \rho_q, \qquad (2.15)$$

where we have neglected the spin-orbit part. The quantity $H(\vec{r})$ is the energy density. The nuclear density ρ, kinetic energy density τ, and current density $\vec{j}$ are

$$\rho_q(\vec{r}) = \sum_{i\varepsilon q} |\chi_i(\vec{r})|^2$$
$$\tau_q(\vec{r}) = \sum_{i\varepsilon q} |\nabla\chi_i(\vec{r})|^2 \qquad (2.16)$$
$$j_q(\vec{r}) = \sum_{i\varepsilon q} \mathrm{Im}\left|\chi_i^*(\vec{r})\vec{\nabla}\chi_i(\vec{r})\right|$$

with $\rho = \rho_p + \rho_n$, $\tau = \tau_p + \tau_n$, and $\vec{j} = \vec{j}_p + \vec{j}_n$. Frequently, to account for the finite-range effects in the energy density, the terms proportional to $\rho\,\nabla^2\,\rho$ are replaced by a sum of Yukawa interactions of the form (HN77),

$$E_y = \int d\vec{r}\, d\vec{r}' \frac{e^{-|\vec{r}-\vec{r}'|/a}}{|\vec{r}-\vec{r}'|/a}\left[\frac{v_u}{2}\rho(\vec{r})\rho(\vec{r}') + \frac{(v_\ell - v_u)}{2}\sum_q \rho_q(\vec{r})\rho_q(\vec{r}')\right], \qquad (2.17)$$

where v_ℓ and v_u denote the interaction strengths between "like" and "unlike" nucleons, respectively. As shown in Appendix B, the first-order expansion of this expression reproduces the $\rho\,\nabla^2\,\rho$ terms of Eq.

(2.15) provided the parameters v_ℓ and v_u are chosen to be

$$2\pi a^5 \, v_u = \frac{(t_2 - 3t_1)}{16}$$

$$2\pi (v_\ell - v_u) a^5 = \frac{1}{32} (t_2 + 3t_1). \tag{2.18}$$

As a consequence of this expansion, we also get terms proportional to ρ^2; this leads to the modification of the parameters t_o and x_o. The new parameters $\tilde{t}_o$ and $\tilde{x}_o$ are (Appendix B) given by

$$\tilde{t}_o = t_o - \frac{8\pi}{3} a^3 (v_\ell + v_u)$$

$$\tilde{x}_o = \frac{2}{\tilde{t}_o} (t_o - \tilde{t}_o) + \frac{t_o}{\tilde{t}_o} x_o - 8\pi \, a^3 \frac{v_u}{\tilde{t}_o}. \tag{2.19}$$

In addition, the distinction between neutrons and protons arises from a contribution to the Hamiltonian due to the Coulomb interaction (HN77). The direct part of this interaction has the familiar form

$$E_C^D = \frac{e^2}{2} \int d\vec{r} \, d\vec{r}' \, \frac{\rho_p(\vec{r}) \rho_p(\vec{r}')}{|\vec{r} - \vec{r}'|}, \tag{2.20}$$

and the exchange part is chosen to be the Slater's approximation,

$$E_C^E = -\frac{3}{4} \left(\frac{3}{\pi}\right)^{1/3} e^2 \int d^3r \, [\rho_p(\vec{r})]^{4/3}. \tag{2.21}$$

C. VARIATION OF THE ENERGY

The final form for the nuclear energy used in this dissertation can be written as

$$E_N = \int d\vec{r} \left\{ \frac{\hbar^2}{2m} \tau + \frac{1}{2} \tilde{t}_o \left[\left(1 + \frac{\tilde{x}_o}{2} \right) \rho^2 - \left(1/2 + \tilde{x}_o \right) \sum_q \rho_q^2 \right] \right.$$

$$\left. + \frac{t_3}{8} \rho^\alpha \left(\rho^2 - \sum_q \rho_q^2 \right) + \frac{(t_1+t_2)}{4} \left(\rho\tau - \vec{j}^2 \right) + \frac{(t_2-t_1)}{8} \sum_q \left(\rho_q \tau_q - \vec{j}_q^{\,2} \right) \right\}$$

$$+ \int d\vec{r}\, d\vec{r}' \, \frac{e^{-|\vec{r}-\vec{r}'|/a}}{|\vec{r}-\vec{r}'|/a} \left[\frac{v_u}{2} \rho(\vec{r})\rho(\vec{r}') + \frac{(v_\ell - v_u)}{2} \sum_q \rho_q(\vec{r})\rho_q(\vec{r}') \right]$$

$$+ \frac{1}{2} e^2 \int d\vec{r}\, d\vec{r}' \, \frac{\rho_p(\vec{r})\rho_p(\vec{r}')}{|r-r'|} - \frac{3}{4} \left(\frac{3}{\pi} \right)^{1/3} e^2 \int d\vec{r} \left[\rho_p(\vec{r}) \right]^{4/3} . \quad (2.22)$$

The SHF equations are obtained through the variational principle (VB72),

$$\delta_{n,p} \left(E_N - \sum_i \varepsilon_i \int d\vec{r} \, |\, \chi_i(\vec{r}) \,|^2 \right) = 0, \quad (2.23)$$

where the variation is with respect to the single-particle states χ_α, and the normalization condition is imposed by the Lagrange multipliers ε_i. The subscripts n and p indicate variations with respect to neutrons and protons, respectively. The variation of E_N can be written as,

$$\delta_{n,p} E_N = \int d\vec{r} \left[\frac{\hbar^2}{2m^*_{n,p}(\vec{r})} \delta\tau_{n,p}(\vec{r}) + U_{n,p}(\vec{r}) \delta\rho_{n,p} + T_{n,p}(\vec{r}) \delta j_{n,p} \right], \quad (2.24)$$

where we have defined the effective mass m^* through

$$\frac{\hbar^2}{2m^*_{n,p}(\vec{r})} = \frac{\hbar^2}{2m} + \frac{(t_1+t_2)}{4} \rho(\vec{r}) + \frac{(t_2-t_1)}{8} \rho_{n,p}(\vec{r}) \quad (2.25)$$

and

$$U_{n,p}(\vec{r}) = \tilde{t}_o \left[\left(1 + \frac{\tilde{x}_o}{2}\right)\rho(\vec{r}) - \left(\frac{1}{2} + \tilde{x}_o\right)\rho_{n,p}\right] + \frac{t_3}{8}\left[(\alpha+2)\rho^{\alpha+1} - \alpha\rho^{\alpha-1}\sum_q \rho_q{}^2 - 2\rho^\alpha \rho_{n,p}\right] + \left[\frac{(t_1+t_2)}{4}\tau + \frac{(t_2-t_1)}{8}\tau_{n,p}\right]$$
$$+ v_u \int d\vec{r}' \frac{e^{-|\vec{r}-\vec{r}'|/a}}{|\vec{r}-\vec{r}'|/a}\rho(\vec{r}') + (v_\ell - v_u)\int d\vec{r}' \frac{e^{-|r-r'|/a}}{|\vec{r}-\vec{r}'|/a}\rho_{n,p}$$
$$+ \left[e^2 \int d\vec{r}' \frac{\rho_p(\vec{r}')}{|\vec{r}-\vec{r}'|} - \left(\frac{3}{\pi}\right)^{1/3} e^2 \left[\rho_p\right]^{1/3}\right]\delta_{qp} \qquad (2.26)$$

$$T_{n,p}(\vec{r}) = -\left[\frac{t_1+t_2}{2}\vec{j} + \frac{t_2-t_1}{4}\vec{j}_{n,p}\right].$$

For the SHF equations, because of the time-reversal invariance ($\vec{j} = -\vec{j}$), the current terms vanish. Then,

$$\delta_{n,p}E_N = \sum_{i\varepsilon n,p} \int d\vec{r}\,(\delta_{n,p}\chi_i{}^*)\left\{-\vec{\nabla}\frac{\hbar^2}{2m^*_{n,p}(\vec{r})}\vec{\nabla} + U_{n,p}(\vec{r})\right\}\chi_i(\vec{r}), \qquad (2.27)$$

where we have performed an integration by parts in the calculation of the $\delta\tau$ variation. Using this expression in Eq.(2.23), we obtain the SHF equations in the absence of the spin-orbit interaction,

$$\left\{-\vec{\nabla}\frac{\hbar^2}{2m^*_{n,p}(\vec{r})}\vec{\nabla} + U_{n,p}(\vec{r})\right\}\chi_i(\vec{r}) \equiv h_{n,p}(\vec{r})\chi_i(\vec{r}) = \varepsilon_i\chi_i(\vec{r}). \qquad (2.28)$$

As we can see in the single-particle Hamiltonian h, the one-body potential U is local and the only non-locality appears through the effective mass. In determining $U(\vec{r})$ we have replaced the original $\rho\nabla^2\rho$ terms with the finite-range Yukawa interaction. The numerical solution of Eq. (2.28) will be discussed later in this chapter.

One of the problems of the SHF theory is the spurious center-of-mass motion. All of our equations have implicitly assumed the

existence of an origin of the body-fixed coordinate system. However, in this case the A vectors $r_1,\ldots,r_A$ are not independent since they have to satisfy the condition,

$$\sum_i \vec{r}_i = 0.$$

Unfortunately, the handling of the Schroedinger equation with nonindependent variables is very complicated, and the problem of the spurious center-of-mass motion remains unresolved. The consequences of this problem will be discussed later.

D. PARAMETERS OF THE SKYRME INTERACTION - NUCLEAR MATTER

The early SHF calculations (VB70,VB72) used the radii and binding energies of the doubly-magic closed-shell nuclei to determine the parameters t_0, t_1, t_2, t_3, x_0, and W_0 (α =1) of the Skyrme interaction, (Sk I and Sk II). The strength W_0 of the spin-orbit interaction, was determined (after fitting t_0, t_1, t_2, t_3 and x_0) to adjust the 6.15-MeV splitting of the 1p states of ^{16}O. Although the spin-orbit interaction constitutes an important contribution to the nuclear force, its strength has not been determined for a wide range of nuclei. These forces have a large t_3 value indicating a strong dependence on the density (BF75).

Later, calculations were extended to many other spherical nuclei (BF75,BG76,B180) determining new sets of parameters for the Skyrme forces Sk III-VI. One consequence of these calculations was to discover a very strong dependence of the single-particle energies ε_i on the parameter t_3. Sk III force yields reasonable results for all of

these quantities (BF75). For most of these forces calculations of angular distributions for electron scattering also gave good agreement with experiment.

Systematic studies with the Skyrme interaction have generalized this force to powers $\alpha \neq 1$ (KT80). Apart from the spherical nuclei, this new force (Sk M^*) fits the quadrupole and hexadecapole moments of ^{166}Er and ^{240}Pu together with the liquid-drop fission barrier of ^{240}Pu (BQ82). The calculation of monopole resonances with a fluid dynamical Lagrangian yielded reasonable results for a large number of nuclei (KT80). On the other hand, the RPA (SZ73,KK77) and linear response calculations (Be73,BT75,LB76,B180) of isoscalar and isovector giant resonances for closed shell nuclei failed to show any systematic agreement with these forces.

It is fair to conclude from the above discussion that while all of these parametrizations yield good results for ground state properties, the situation for other observables is considerably different. For completeness, Table 2 contains the various parametrizations of the Skyrme force to date. The last line of the table gives the parameters for the BKN force (BK76). This force replaces the t_1 and t_2 terms of the Skyrme interaction by a finite-range Yukawa potential.

In nuclear matter, with no Coulomb force, the wavefunctions are translationally invariant plane waves,

$$\chi_{\vec{k}}(\vec{r},\sigma,q) = e^{i\vec{k}\cdot\vec{r}} \mid \sigma q\rangle. \tag{2.29}$$

The nuclear density becomes

Table 2. Various Parametrizations of the Skyrme Interaction

Table 2

Skryme parameters

Yukawa radius parameter a_o = 0.45979 fm

Force	t_o (fm^3 MeV)	$\tilde{t}_o$ (fm^3 MeV)	x_o (fm^3 MeV)	$\tilde{x}_o$	t_1 (fm^5 MeV)	t_2 (fm^5 MeV)	t_3 (fm^6 MeV)	alpha	v_u (MeV)	v_l (MeV)
I	-1057.3	- 540.31	0.56	1.2417	235.9	-100.0	14463.5	1.0	- 390.98	-243.9
II	-1169.9	- 104.44	0.34	4.0132	585.6	-27.10	9331.10	1.0	- 863.52	-444.88
III	-1128.75	- 334.47	0.45	1.7436	395.0	- 95.0	14000.0	1.0	- 619.60	-355.79
IV	-1205.6	116.89	0.05	-0.27964	765.0	35.0	5000.0	1.0	-1094.0	-530.05
V	-1248.29	367.66	-0.17	0.8071	970.56	107.22	0.0	1.0	-1357.5	-626.87
VI	-1101.81	- 483.59	0.583	1.5538	271.67	-138.33	17000.0	1.0	- 461.48	-297.7
SKM	-2645.0	-1843.8	0.09	0.18042	385.0	-120.0	15595.0	1.6	- 617.18	-366.68
SKM*	-2645.0	-1784.7	0.09	0.19302	410.0	-135.0	15595.0	1.6	- 660.75	-395.72
BKN	- 497.73				0.0	0.0	12952.5	1.0	- 363.04	-363.04

$$\rho = \sum_{\vec{k}\sigma q} \left| \chi_{\vec{k}}(\vec{r},\sigma,q) \right|^2 = \int_{|\vec{k}| < k_F} \frac{d\vec{k}}{(2\pi)^3} \sum_{\sigma q} \left| \chi_k(\vec{r},\sigma,q) \right|^2 = \frac{2}{3\pi^2} k_f^3, \tag{2.30}$$

where k_f denotes the Fermi momentum. Similarly,

$$\tau = \frac{3}{5} \rho k_f^2. \tag{2.31}$$

Also, since χ is translationally invariant $\vec{\nabla}\rho = \vec{\nabla}j = 0$. Putting $\rho_p = \rho_n = 1/2\rho$, $\tau_n = \tau_p = 1/2\tau$, the Hamiltonian density of Eq. (2.15) becomes

$$H_\infty = \frac{\hbar^2}{2m} \tau + \frac{3}{8} t_0 \rho^2 + \frac{1}{16} t_3 \rho^{\alpha+2} + \frac{1}{16} (3t_1 + 5t_2)\rho\tau. \tag{2.32}$$

The total energy is simply

$$E_\infty = \int d\vec{r}\, H_\infty = H_\infty \Omega \quad (\Omega = \text{volume}). \tag{2.33}$$

After defining the density as $\rho = A/\Omega$, the binding energy of nuclear matter is given by

$$\frac{E_\infty}{A} = \frac{H_\infty}{\rho} = \frac{\hbar^2}{2m} \frac{3}{5} k_f^2 + \frac{3}{8} t_0 \rho + \frac{1}{16} t_3 \rho^{\alpha+1} + \frac{1}{16} (3t_1 + 5t_2)\tau. \tag{2.34}$$

The incompressibility coefficient K_∞ of nuclear matter is defined to be

$$K_\infty = k_f^2 \frac{\partial^2 (E_\infty/A)}{\partial k_f^2} = \frac{\hbar^2}{2m} \frac{6}{5} k_f^2 + \frac{9}{4} t_1 \rho + \frac{9}{11} t_3 (\alpha+1) \left(\alpha + \frac{2}{3}\right) \rho^{\alpha+1} + \frac{5}{4} (3t_1 + 5t_2)\tau. \tag{2.35}$$

These two equations, together with the condition for the saturation of the binding energy $\partial(E_\infty/A)/\partial k_f = 0$, determine the parameters t_0, t_3, and $(3t_1 + 5t_2)$ with

$$\frac{m^*}{m} = \left[1 + \frac{1}{16}\ \frac{2m}{\hbar^2}\ (3t_1 + 5t_2)\rho\right]^{-1}. \qquad (2.36)$$

From this equation we conclude that the combination $(3t_1 + 5t_2)$ is important for the density dependence of the effective mass. For a fixed value of k_f the density is fixed, but the power α of the t_3 term can be used to change the incompressibility coefficient K_∞. All of the parametrizations given in Table 2 give $E_\infty/A \approx -16$ MeV for $k_f = 1.30$ fm^{-1}. This value of k_f corresponds to a nuclear matter density $\rho = 0.145$ nucleons/fm^3. The only parameters which cannot be pinned down simultaneously are the effective mass ratio m^*/m and the incompressibility coefficient K_∞.

To some extent the same arguments also hold for finite nuclei. In addition, the coefficient of $(\vec{\nabla}\rho)^2$ terms, $(9t_1 - 5t_2)$, will be a measure of the surface effects. In fact, in the Thomas-Fermi approximation this quantity completely determines the surface thickness (VB72). In Table 3 we tabulate some of these quantities for various parametrizations of the Skyrme potential.

E. TDHF EQUATIONS

The TDHF equations can be obtained from the variation of the many-body action S (KK76),

$$S = \int_{t_1}^{t_2} dt\ \langle\Phi(t)\ \Big|\ i\hbar\frac{\partial}{\partial t} - H\ \Big|\ \Phi(t)\rangle. \qquad (2.37)$$

In this expression the many-body Hamiltonian H is the one defined previously for the static case, and the A-nucleon wavefunction $\Phi(t)$ is chosen to be of determinantal form, constructed from time-dependent

Table 3. Properties of Nuclear Matter Using the Skyrme Interaction

Table 3

Nuclear matter properties

Fermi momentum k_f = 1.30 (fm^{-1})

Nuclear matter density $\rho = 2/(3\pi^2)\, k_f^3 = 0.145$ n/fm^3

Force	$(9t_1 - 5t_2)$ (fm^5 MeV)	$(3t_1 + 5t_2)$ (fm^5 MeV)	m^*/m	K (MeV)	E/A (MeV)
I	2623.1	207.7	0.915	325.3	-15.95
II	5405.9	1621.3	0.580	341.7	-15.94
III	4030.0	710.0	0.760	376.8	-15.84
IV	6710.0	2470.0	0.475	310.6	-15.96
V	8189.9	3447.8	0.401	273.8	-16.02
VI	3136.7	123.36	0.950	399.3	-15.73
SKM	4065.0	555.0	0.800	184.2	-15.71
SKM*	4365.0	555.0	0.800	184.2	-15.71
BKN	0.0	0.0	1.000	410.7	-11.15

single-particle states $\phi_\alpha(t)$,

$$\Phi(t) = \frac{1}{\sqrt{A!}} \det \left|\phi_\alpha(\vec{r},t)\right| \ . \tag{2.38}$$

For notational simplicity, we have dropped the spin and isospin indices. As in the case of SHF theory, the variation of Eq. (2.37) is an independent variation with respect to single particle states ϕ_α and ϕ_α^* and yields the equations of motion,

$$i\hbar \frac{\partial \phi_\alpha(r,t)}{\partial t} = \frac{\delta \langle H \rangle}{\delta \phi_\alpha^*(\vec{r},t)}, \tag{2.39}$$

and a similar expression for ϕ_α^*. The classical nature of these equations can be put into a better perspective via the definition of classical field coordinates $\psi_\alpha(\vec{r},t)$ and conjugate momenta $\Pi_\alpha(\vec{r},t)$,

$$\phi_\alpha(\vec{r},t) = \left(\psi_\alpha(\vec{r},t) + i\Pi_\alpha(\vec{r},t)\right)/\sqrt{2}. \tag{2.40}$$

In terms of these fields, the equations of motion become

$$\begin{aligned} i\hbar \frac{\partial}{\partial t}\left[\frac{\psi_\alpha(\vec{r},t) + i\Pi_\alpha(\vec{r},t)}{\sqrt{2}}\right] &= \frac{\partial \langle H \rangle}{\partial \phi_\alpha^*} \\ &= \frac{\partial \langle H \rangle}{\delta \psi_\alpha} \frac{\delta \psi_\alpha}{\delta \phi_\alpha^*} + \frac{\delta \langle H \rangle}{\delta \Pi_\alpha} \frac{\delta \Pi_\alpha}{\delta \phi_\alpha^*} \end{aligned} \tag{2.41}$$

leading to Hamilton's equations of motion,

$$\begin{aligned} \hbar \frac{\partial \psi_\alpha}{\partial t} &= \frac{\delta \langle H \rangle}{\delta \pi_\alpha} \\ \hbar \frac{\partial \pi_\alpha}{\partial t} &= -\frac{\delta \langle H \rangle}{\delta \psi_\alpha}. \end{aligned} \tag{2.42}$$

As it will be explained in the next section, the TDHF Eqs. (2.39) are

solved on a three-dimensional space and time lattice with initial wavefunctions of the form

$$\lim_{t\to-\infty} \psi_\alpha(\vec{r},t) = \sqrt{2}\cos\left(\vec{k}_\alpha\cdot\vec{r} - \varepsilon_\alpha t\right)\chi_\alpha\left(\vec{r}-\vec{k}_\alpha/m\ t-\vec{\beta}_\alpha\right)$$
$$\lim_{t\to-\infty} \Pi_\alpha(\vec{r},t) = \sqrt{2}\sin\left(\vec{k}_\alpha\cdot\vec{r} - \varepsilon_\alpha t\right)\chi_\alpha\left(\vec{r}-\vec{k}_\alpha/m\ t-\vec{\beta}_\alpha\right), \tag{2.43}$$

where χ_α is the solution to the SHF Eqs. (2.28) and $\vec{k}_\alpha$ and $\vec{\beta}_\alpha$ are parameters of the initial boost (BK76,Ko80). To study a heavy-ion collision, the initial wavefunction is taken to be two non-overlapping SHF solutions which are given boosts appropriate for the initial conditions of the collision.

F. LINEAR RESPONSE

Linear response theory, in its various forms, has been widely used in nuclear physics to approximate the excited states of the nucleus (Be73,BT75,LB76,SB75,Bl80). This is achieved by studying the response of a many-body system to a weak external field. To provide a general background, we shall first look at the linear response theory for a many-body quantum system (FW71).

Consider an interacting system which has a time-independent Hamiltonian H, to which belongs a complete set of eigenstates $|\ X_N\rangle$,

$$H\,|\ X_N\rangle = E_N\,|\ X_N\rangle, \tag{2.44}$$

and assume that at time t=0 the system is in one of its eigenstates, say N=0. The system is then perturbed by an external, time-dependent Hamiltonian $H'(t)$. The new state $|\ \Phi(t)\rangle$ satisfies the time-dependent Schroedinger's equation,

$$i\hbar \frac{\partial}{\partial t}|\Phi(t)\rangle = [H + H'(t)]|\Phi(t)\rangle, \qquad t > 0. \tag{2.45}$$

All of the physical information is contained in the matrix elements of the operator $\hat{O}(t)$, which may depend explicitly on time. The linear response of the expectation value of this operator is given by

$$\delta \langle\hat{O}(t)\rangle \equiv \langle\Phi(t) \mid \hat{O}(t) \mid \Phi(t)\rangle - \langle X_o \mid \hat{O}(t) \mid X_o\rangle. \tag{2.46}$$

This expectation is calculated to first order in H', which equals

$$\delta \langle\hat{O}(t)\rangle = i/\hbar \int_o^t dt' \, \langle X_o|[H'_H(t'), \hat{O}_H(t')]|X_o\rangle, \tag{2.47}$$

where the subscript H denotes operators in Heisenberg representation. Upon turning on a weak external field $K(\vec{r},t) = f(\vec{r})g(t)$, the corresponding external perturbation is the coupling of this field to the density of the system,

$$H'(t) = \int d^3r \, \hat{\rho}(\vec{r},t)K(\vec{r},t), \tag{2.48}$$

where $\hat{\rho}$ is the exact density operator for the unperturbed system. The response of the density is related to the density-density correlation function and is defined as

$$\begin{aligned} R[f]_t &\equiv \delta \langle\hat{\rho}(\vec{r},t)\rangle \\ &= i/\hbar \int_o^t dt' \int d^3r' \, K(\vec{r}',t') \, \langle X_o|[\hat{\rho}_H(\vec{r}',t'), \hat{\rho}_H(\vec{r},t)]|X_o\rangle. \end{aligned} \tag{2.49}$$

As shall be seen below, the information about the excited states of the system is contained in the overlap of the linear response with the probe,

$$R[f,f] \equiv \int d^3r \, f(\vec{r})R[f]_\omega = \int_{-\infty}^{+\infty} dt \, e^{i\omega t} \int d^3r \, f(\vec{r})R[f]_t. \tag{2.50}$$

When computed explicitly, R[f,f] becomes

$$R[f,f] = \sum_N \frac{\langle X_o \mid F \mid X_N\rangle\langle X_N \mid F \mid X_o\rangle}{\hbar\omega - (E_N - E_o) + i\eta} - \frac{\langle X_o \mid F \mid X_N\rangle\langle X_N \mid F \mid X_o\rangle}{\hbar\omega + (E_N - E_o) + i\eta}, \quad (2.51)$$

where F stands for

$$F = \int d^3r\, f(\vec{r})\hat{\rho}(\vec{r}). \quad (2.52)$$

Consequently, one can also show that the strength function $S(\omega)$, which measures the transition strength of the operator F, is given by (LB76),

$$S(\omega) = \frac{1}{\pi}\,\mathrm{Im}R[f,f] = \sum_N |\langle X_N \mid F \mid X_o\rangle|^2\, \delta(\hbar\omega - (E_N - E_o)). \quad (2.53)$$

This expression shows that when exact eigenstates are used, the S-function has discrete peaks at the excited energies of the system.

In practice, one usually approximates the true nuclear many-body wavefunction with the corresponding Hartree-Fock state (BT75). The time-dependent states $\Phi(t)$ are then given by the solution of the TDHF equations (Eq. 2.39) with a weak, one-body, time-dependent external field. If one assumes a perfectly harmonic evolution of the nuclear density, it is possible to show that small-amplitude TDHF equations lead to RPA equations (Ro66,KK76). In the Hartree-Fock theory the response function can be written in terms of the nuclear density $\hat{\rho}$, which is obtained from the one-body density matrix ρ with the assumption that the many-body wavefunction is a Slater determinant $(\hat{\rho}^2 = \hat{\rho})$ as

$$R[f]_t = \rho(\vec{r},t) - \rho_o(\vec{r}). \quad (2.54)$$

Here $\rho(\vec{r},t)$ is constructed from the time-dependent single-particle states obtained by solving the TDHF equations, and ρ_o is the SHF density of [Eq. (2.16)] the unperturbed system. Consequently, the functions R[f,f] and $S(\omega)$ can be obtained from Eqs. (2.50, 2.53). In this

case, the exact solution of the time-dependent Schroedinger equation will be replaced by the associated TDHF wavefunction. This leads to a continuous S-function with peaks centered about the excited states of the system. Previous to this work, small amplitude TDHF equations have been used in the study of giant resonances (BF79) under a different theoretical framework.

This direct calculation of the S-function has the natural extension for treating deformed nuclei, and, as will be seen in Chapter IV, it succesfully reproduces the RPA eigenfrequencies for various transition operators F.

G. NUMERICAL METHODS

The SHF and TDHF calculations contained in this dissertation involve extensive amounts of computation time. As a consequence, the optimization of the numerical techniques becomes neccesary for the realistic application of these theories to the study of the nuclear molecular phenomenon, which neccesarily involves the long-time evolution of the TDHF equations.

The discrete approximations to the SHF and TDHF equations which enable a numerically stable algorithm are obtained in cylindrical polar coordinates appropriate for axially deformed nuclei. The methods discussed in this section closely follow those of (DK81,HN77) with the exception of the new numerical methods.

1. Cylindrical Polar Coordinates.

In cylindrical polar coordinates (r,z,ϕ) the single-particle wave

functions can be written as (Va73,HN77)

$$\phi_\alpha(r,z,\phi) = \psi_\alpha(r,z)e^{i\mu_\alpha\phi}, \tag{2.55}$$

where $\psi_\alpha(r,z)$ depends only on the magnitude but not the sign of μ_α (the z-component of angular momentum $j_z \pm 1/2$), and for notational simplicity we have dropped the implicit time index. The quantities ρ_q, τ_q, and $\vec{j}_q$ in these coordinates take the forms

$$\begin{aligned}
\rho_q(\vec{r}) &= \sum_{\ell\varepsilon q} \left| \psi_\ell(r,z) \right|^2 \\
\tau_q(\vec{r}) &= \sum_{\ell\varepsilon q} \left(\frac{\partial \phi_\alpha^*}{\partial r}\hat{r} + \frac{i\mu_\ell}{r}\phi_\ell^*\hat{\phi} + \frac{\partial \phi_\ell^*}{\partial z}\hat{z} \right)\cdot(\text{c.c.}) \\
&= \sum_{\ell\varepsilon q} \left(\left|\frac{\partial \psi_\ell}{\partial z}\right|^2 + \left|\frac{\partial \psi_\ell}{\partial r}\right|^2 + \frac{\mu_\ell^2}{r^2}\left|\psi_\ell\right|^2 \right) \\
\vec{j}_q(\vec{r}) &= \sum_{\ell\varepsilon q}\left[\text{Im}\ \phi_\ell^*(\vec{r}) \left(\frac{\partial \phi_\ell}{\partial r}\hat{r} + \frac{\partial \phi_\ell}{\partial z}\hat{z} + \frac{i\mu_\ell}{r}\phi_\ell\hat{\phi} \right) \right] \\
&= \sum_{\ell\varepsilon q} \text{Im}\left[\psi_\ell^* \frac{\partial \psi_\ell}{\partial r}\hat{r} + \psi_\ell^* \frac{\partial \psi_\ell}{\partial z}\hat{z} + \frac{i\mu_\ell}{r}\psi_\ell{}^2\hat{\phi} \right].
\end{aligned} \tag{2.56}$$

The term proportional to μ_ℓ vanishes upon the summation over ℓ, since the $\pm\mu_\ell$ states are occupied equally. The following definitions are for notational convenience,

$$\tau_{zq} = \sum_{\ell\varepsilon q} \left|\frac{\partial\psi_\ell}{\partial z}\right|^2$$

$$\tau_{rq} = \sum_{\ell\varepsilon q} \left|\frac{\partial\psi_\ell}{\partial r}\right|^2$$

$$s_q = \sum_{\ell\varepsilon q} \frac{\mu_\ell^2}{r^2}\left|\psi_\ell\right|^2 \tag{2.57}$$

$$j_{zq} = \sum_{\ell\varepsilon q} \mathrm{Im}\left[\psi_\ell^* \frac{\partial\psi_\ell}{\partial z}\right]$$

$$j_{rq} = \sum_{\ell\varepsilon q} \mathrm{Im}\left[\psi_\ell^* \frac{\partial\psi_\ell}{\partial r}\right].$$

In this representation the nuclear energy E_N of Eq. (2.22) can be written as

$$E_N = E_o + E_V + E_H, \tag{2.58}$$

where E_o contains the derivative-independent parts, and, E_V and E_H contain those terms in E_N which include r- and z-derivatives respectively,

$$E_o = \int d^3r \left\{\frac{1}{2}\tilde{t}_o\left[\left(1+\frac{\tilde{x}_o}{2}\right)\rho^2 - \left(\frac{1}{2}+\tilde{x}_o\right)\sum_q \rho_q^2\right] + \frac{t^3}{8}\rho^\alpha\left(\rho^2 - \sum_q \rho_q^2\right)\right\} + E_Y + E_C^D + E_C^E$$

$$E_V = \int d^3r \left\{\frac{\hbar^2}{2m}(\tau_r+s) + \frac{t_1+t_2}{4}\left[(\tau_r+s)\rho - j_r^2\right] + \frac{t_2-t_1}{8}\sum_q\left[\rho_q(\tau_{rq}+s_q) - j_{rq}^2\right]\right\} \tag{2.59}$$

$$E_H = \int d^3r \left\{\frac{\hbar^2}{2m}\tau_z + \frac{t_1+t_2}{4}(\rho\tau_z - j_z^2) + \frac{t_2-t_1}{8}\sum_q(\rho_q\tau_{zq} - j_{zq}^2)\right.$$

2. Spatial Discretization of TDHF Equations.

For the numerical solution of SHF and TDHF equations it is more advantageous to define a discrete approximation to the energy density prior to the application of variational principle to the resulting wavefunctions defined on the mesh points (HN77). As a consequence, one obtains a numerical procedure where all of the constants of motion of the continuous equations also remain constant in the discrete solution.

On the uniform cylindrical mesh the r and z points are defined as

$$\begin{aligned} r_i &= (i-1/2)\Delta r \qquad i = 1,\ldots,N_R \\ z_j &= (j-1)\Delta z \qquad -N_z < j < N_z. \end{aligned} \tag{2.60}$$

The choice of half-integer values in the r-direction arises from the boundary conditions defined on the z-axis. This point will become clear in the course of this section. With the above definition, the volume element d^3r becomes

$$\Delta V_i = 2\pi\, r_i\, \Delta r \Delta z, \tag{2.61}$$

and the normalization of the single-particle states can be written as

$$\sum_{ij} \Delta V_i \left| \psi_\ell(i,j) \right|^2 = 1. \tag{2.62}$$

In this expression i,j is a shorthand for r_i, z_j. It is conventional to take out a factor $\sqrt{r}$ from the wavefunction by defining

$$g_\ell(i,j) = (i-1/2)^{1/2}\, \psi_\ell(i,j). \tag{2.63}$$

Before we proceed, it is proper to mention a few details. In cylindrical polar coordinates the single-particle states g_ℓ have a definite z-parity (even or odd), which implies that at the point z=0 either g_ℓ or $\partial g_\ell / \partial z$ must vanish. For the SHF calculations of reflection symmetric nuclei, it is more convenient to deal only with positive z. Here a

weight factor of 2 is needed for the integration. As a consequence, the integrand at z = 0 will be double counted and should be multiplied by 1/2. This can be achieved by defining

$$\Delta V_{ij} = \Delta V_i\left(1 - \frac{1}{2}\,\delta_{j1}\right). \tag{2.64}$$

Finally, the wavefunctions have to vanish on the boundaries of the box,

$$\psi_\ell\left(N_R, j\right) = \psi_\ell\left(i, \pm N_z\right) = 0. \tag{2.65}$$

The integrals in the expression for the energy, E_N, contain terms which are functions of τ and $\vec{j}$. These densities contain derivatives in r- and z-directions which are calculated using the first-order finite-difference form for the derivatives,

$$\frac{\partial f(r)}{\partial r} = \frac{f(i+1)-f(i)}{\Delta r} \tag{2.66}$$

The discrete forms for the various quantities are defined as follows

$$\begin{aligned}
\rho_q(i,j) &= \frac{1}{(i-1/2)} \sum_{\ell \varepsilon q} \left| g_\ell(i,j) \right|^2 \\
\rho_q(i,j+1/2) &\equiv \frac{1}{2}\left[\rho_q(i,j) + \rho_q(i,j+1)\right] \\
\rho_q(i+1/2,j) &\equiv \frac{1}{2}\left[\rho_q(i,j) + \rho_q(i+1,j)\right] \\
\tau_{zq}(i,j+1/2) &\equiv \frac{1}{(i-1/2)(\Delta z)^2} \sum_{\ell \varepsilon q} \left| g_\ell(i,j) - g_\ell(i,j+1) \right|^2 \\
\tau_{rq}(i+1/2,j) &\equiv \frac{r_{i+1/2}}{r_i} \frac{1}{\Delta r} \sum_{\ell \varepsilon q} \left| \frac{g_\ell(i,j)}{\sqrt{r_i}} - \frac{g_\ell(i+1,j)}{\sqrt{r_{i+1}}} \right|^2 \\
s_q(i,j) &= \frac{1}{(i-1/2)} \frac{1}{r_i^{\,2}} \sum_{\ell \varepsilon q} \mu_\ell^{\,2} \left| g_\ell(i,j) \right|^2
\end{aligned} \tag{2.67}$$

$$j_{zq}(i,j+1/2) \equiv \frac{1}{(i-1/2)\Delta z} \sum_{\ell \varepsilon q} \mathrm{Im}\left[g_\ell^*(i,j) g_\ell(i,j+1)\right]$$

$$= \frac{1}{(i-1/2)\Delta z} \sum_{\ell \varepsilon q} \left[\frac{g_\ell^*(i,j) g_\ell(i,j+1) - g_\ell(i,j) g_\ell^*(i,j+1)}{2\sqrt{-1}}\right]$$

$$j_{rq}(i+1/2,j) \equiv \frac{1}{\sqrt{(i^2-1/4)}} \sqrt{\frac{r_{i+1/2}}{r_i}} \frac{1}{\Delta r} \sum_{\ell \varepsilon q} \mathrm{Im}\left[g_\ell^*(i,j) g_\ell(i+1,j)\right]$$

$$= \frac{1}{\sqrt{(i^2-1/4}} \sqrt{\frac{r_{i+1/2}}{r_i}} \frac{1}{\Delta r} \sum_{\ell \varepsilon q} \left[\frac{g_\ell^*(i,j) g_\ell(i+1,j) - g_\ell(i,j) g_\ell^*(i+1,j)}{2\sqrt{-1}}\right],$$

where imaginary i is explicitly denoted by $\sqrt{-1}$. In the calculation of current densities the fact that $\mathrm{Im}[\,|\,g(i,j)\,|^2] = 0$ was used. All of these expressions are straightforward discretizations of their defined forms with the exception of τ_{rq} and j_{rq}. Since these terms are evaluated by using the wavefunction at ith and (i+1)th points, the factor r_i in the volume element ΔV_i should be replaced by $r_{i+1/2}$. This is achieved by multiplying τ_{rq} and j_{rq} by $r_{i+1/2}/r_i$ and using the same definition of ΔV_i for all of the integrals. For j_{rq} this factor comes with a square root since j is only used in squared form.

With these conventions the discrete forms for E_o, E_V, and E_H become

$$E_o = \sum_{i,j} \Delta V_i \left\{\frac{1}{2}\tilde{t}_o\left[\left(1+\frac{\tilde{x}_o}{2}\right)\rho^2(i,j) - \left(\frac{1}{2}+\tilde{x}_o\right)\sum_q \rho_q(i,j)\right]\right.$$

$$\left. + \frac{t_3}{8}\rho^\alpha(i,j)\left[\rho^2(i,j) - \sum_q \rho_q{}^2(i,j)\right] - \frac{3}{4}\left(\frac{3}{\pi}\right)^{1/3} e^2\, \rho_p{}^{4/3}(i,j)\right\} + E_Y + E_C{}^D$$

$$E_V = \sum_{i,j} \Delta V_i \left\{ \frac{\hbar^2}{2m} \left[\tau_r(i+1/2,j) + s(i,j) \right] \right.$$

$$+ \frac{t_1+t_2}{4} \left[\tau_r(i+1/2,j)\rho(i+1/2,j) + s(i,j)\rho(i,j) - j_r{}^2 (i+1/2,j) \right] \tag{2.68}$$

$$\left. + \frac{t_2-t_1}{8} \sum_q \left[\rho_q(i+1/2,j)\tau_{rq}(i+1/2,j) + \rho_q(i,j)s_q(i,j) - j_{rq}(i+1/2,j) \right] \right\}$$

$$E_H = \sum_{i,j} \Delta V_i \left\{ \frac{\hbar^2}{2m} \tau_z(i,j+1/2) + \frac{t_1+t_2}{4} \left[\rho(i,j+1/2)\tau_z(i,j+1/2) \right. \right.$$

$$\left. \left. - j_z{}^2(i,j+1/2) \right] + \frac{t_2-t_1}{8} \sum_q \left[\rho_q(i,j+1/2)\tau_{zq}(i,j+1/2) - j_{zq}{}^2(i,j+1/2) \right] \right\}.$$

The Yukawa and direct Coulomb contributions to E_o can be calculated by solving the discrete Helmholtz and Poisson equations (KD77) respectively.

Similarly, the action S of Eq. (2.37) can be written in the discretized form as

$$S = \int dt \left\{ \sum_{i,j} \frac{\Delta V_i}{(i-1/2)} \left[\sum_\ell g_\ell{}^*(i,j) i\hbar \frac{\partial g_\ell(i,j)}{\partial t} \right] - E_o - E_V - E_H \right\}, \tag{2.69}$$

where now the variational principle becomes

$$\frac{\delta}{\delta g_\ell^*(i',j')} S = 0. \tag{2.70}$$

The result of the variation are the TDHF equations of the form

$$i\hbar \frac{\partial g_\ell(i,j)}{\partial t} = (Hg_\ell)(i,j) + (Vg_\ell)(i,j). \tag{2.71}$$

The action of the "horizontal" Hamiltonian H is defined to be

$$(Hg_\ell)(i,j) = B_q^{(+)}(i,j)g_\ell(i,j+1) + B_q^{(+)*}(i,j-1)g_\ell(i,j-1)$$

$$+ \left[B_q^{(o)}(i,j) + \frac{1}{2} h_{oq}(i,j) \right] g_\ell(i,j), \tag{2.72}$$

where the B_q terms arise from the variation of E_H. For completeness, the details of the variation need to be shown. Firstly, the variation is explicitly defined as follows,

$$\frac{\delta}{\delta g_{\ell'}^{*}(i',j')} g_{\ell}^{*}(i,j) = \delta_{ii'}\delta_{jj'}\delta_{\ell\ell'} \cdot \tag{2.73}$$

With this convention the variation of E_H becomes

$$\begin{aligned}
(i-1/2)\delta E_H = &- \frac{\hbar^2}{2m(\Delta z)^2}\left[g_\ell(i,j+1) - 2g_\ell(i,j) + g_\ell(i,j-1)\right] \\
&+ \frac{t_1+t_2}{4}\frac{1}{(\Delta z)^2}\left[\rho(i,,j+1/2)g_\ell(i,j) - \rho(i,j+1/2)g_\ell(i,j+1)\right. \\
&\left. - \rho(i,j-1/2)g_\ell(i,j-1) + \rho(i,j-1/2)g_\ell(i,j)\right] \\
&+ \frac{t_1+t_2}{4}\frac{1}{2}\left[\tau_z(i,j+1/2)g_\ell(i,j) + \tau_z(i,j-1/2)g_\ell(i,j)\right] \\
&- \frac{t_1+t_2}{4}\frac{1}{\Delta z\sqrt{-1}}\left[j_z(i,j+1/2)g_\ell(i,j+1) - j_z(i,j-1/2)g_\ell(i,j-1)\right] \\
&+ \frac{t_2-t_1}{8}\frac{1}{(\Delta z)^2}\left[\rho_q(i,j+1/2)g_\ell(i,j) - \rho_q(i,j+1/2)g_\ell(i,j+1)\right. \\
&\left. - \rho_q(i,j-1/2)g_\ell(i,j-1) + \rho_q(i,j-1/2)g_\ell(i,j)\right] \\
&+ \frac{t_2-t_1}{8}\frac{1}{2}\left[\tau_{zq}(i,j+1/2)g_\ell(i,j) + \tau_{zq}(i,j-1/2)g_\ell(i,j)\right] \\
&- \frac{t_2-t_1}{8}\frac{1}{\Delta z\sqrt{-1}}\left[j_{zq}(i,j+1/2)g_\ell(i,j+1) - j_{zq}(i,j-1/2)g_\ell(i,j-1)\right].
\end{aligned} \tag{2.74}$$

Collecting terms and comparing with Eq. (2.72), we can write

$$B_q^{(o)}(i,j) = \frac{\hbar^2}{m(\Delta z)^2} + \frac{t_1+t_2}{4}\left\{\frac{\rho(i,j+1/2)+\rho(i,j-1/2)}{(\Delta z)^2} + \frac{1}{2}\left[\tau_z(i,j+1/2)\right.\right.$$

$$\left.\left. + \tau_z(i,j-1/2)\right]\right\} + \frac{t_2-t_1}{8}\left\{\frac{\rho_q(i,j+1/2)+\rho_q(i,j-1/2)}{(\Delta z)^2}\right.$$

$$\left. + \frac{1}{2}\left[\tau_{zq}(i,j+1/2) + \tau_{zq}(i,j-1/2)\right]\right\} \qquad (2.75)$$

$$B_q^{(+)}(i,j) = -\frac{\hbar^2}{2m(\Delta z)^2} - \frac{t_1+t_2}{4(\Delta z)^2}\left[\rho(i,j+1/2) + \frac{\Delta z}{\sqrt{-1}}\, j_z(i,j+1/2)\right]$$

$$- \frac{t_2-t_1}{8(\Delta z)^2}\left[\rho_q(i,j+1/2) + \frac{\Delta z}{\sqrt{-1}}\, j_{zq}(i,j+1/2)\right].$$

Note the error in the Eq. (4.9a) of (DK81). The contribution $1/2h_{oq}(i,j)$ to the diagonal part is half of the variation of E_o and is given by

$$h_{oq}(i,j) = \tilde{t}_o\left[\left(1 + \frac{\tilde{x}_o}{2}\right)\rho(i,j) - \left(\frac{1}{2} + \tilde{x}_o\right)\rho_q(i,j)\right]$$

$$+ \frac{t_3}{8}\left[(\alpha+2)\rho^{\alpha+1}(i,j) - \alpha\rho^{\alpha-1}(i,j)\sum_{q'}\rho_{q'}^2(i,j) - 2\rho^{\alpha}(i,j)\rho_q(i,j)\right] \qquad (2.76)$$

$$+ V_u U_y(i,j) + (V_\ell - V_u)U_{yq}(i,j)$$

$$+ \delta_{qp}\left[U_C(i,j) - \left(\frac{3}{\pi}\right)^{1/3} e^2\, \rho_p^{1/3}(i,j)\right].$$

In this expression U_y and U_c denote the discrete approximations to the Yukawa and direct Coulomb parts,

$$U_{yq}(\vec{r}) = \int d\vec{r}' \frac{e^{-|\vec{r}-\vec{r}'|/a}}{|\vec{r}-\vec{r}'|/a}\rho_q(\vec{r}')$$

$$U_C(\vec{r}) = e^2 \int d\vec{r} \frac{\rho_p(\vec{r}')}{|\vec{r}-\vec{r}'|}. \qquad (2.77)$$

The action of the "vertical" Hamiltonian V is similarly defined as

$$(Vg_\ell)(i,j) = A_q^{(+)}(i,j)g_\ell(i+1,j) + A_q^{(+)*}(i-1,j)g_\ell(i-1,j) + \left[A_{\mu q}^{(o)}(i,j) + \frac{1}{2}\, h_{oq}(i,j)\right]g_\ell(i,j), \tag{2.78}$$

where the terms $A_q^{(+)}$, $A_{\mu q}^{(o)}$ arise from the variation of E_V and are given by

$$A_q^{(+)}(i,j) = \frac{1}{\sqrt{(i^2-1/4)}}\left[-\frac{\hbar^2}{2m(\Delta r)^2} - \frac{(t_1+t_2)}{4(\Delta r)^2}\,\rho(i+1/2,j) - \frac{(t_2-t_1)}{8(\Delta r)^2}\,\rho_q(i+1/2,j)\right]$$
$$- \frac{\Delta r}{\sqrt{-1}}\left(\frac{i}{i-1/2}\right)^{1/2}\left[\frac{(t_1+t_2)}{4(\Delta r)^2}\, j_r(i+1/2,j) + \frac{(t_2-t_1)}{8(\Delta r)^2}\, j_{rq}(i+1/2,j)\right]$$

$$A_{\mu q}^{(o)}(i,j) = C_{\mu q}(i,j) + D_q(i,j)$$

$$C_{\mu q}(i,j) = \frac{\mu_\ell^2}{r_i^2}\left[\frac{\hbar^2}{2m} + \frac{(t_1+t_2)}{4}\,\rho(i,j) + \frac{(t_2-t_1)}{8}\,\rho_q(i,j)\right] \tag{2.79}$$

$$D_q(i,j) = \frac{\hbar^2}{m(\Delta r)^2} + \frac{t_1+t_2}{4}\, s(i,j) + \frac{(t_2-t_1)}{8}\, s_q(i,j)$$
$$+ \frac{(t_1+t_2)}{4}\left[\left(\frac{i}{i-1/2}\,\rho(i+1/2,j) + \frac{i-1}{i-1/2}\,\rho(i-1/2,j)\right)/(\Delta r)^2\right.$$
$$\left. + \frac{1}{2}\left(\tau_r(i+1/2,j) + \frac{i-3/2}{i-1/2}\,\tau_r(i-1/2,j)\right)\right]$$
$$+ \frac{(t_2-t_1)}{8}\left[\left(\frac{i}{i-1/2}\,\rho_q(i+1/2,j) + \frac{i-1}{i-1/2}\,\rho_q(i-1/2,j)\right)/(\Delta r)^2\right.$$
$$\left. + \frac{1}{2}\left(\tau_{rq}(i+1/2,j) + \frac{i-3/2}{i-1/2}\,\tau_{rq}(i-1/2,j)\right)\right].$$

3. Time Evolution.

The TDHF Eqs.(2.71) formally have the solution

$$g_\ell(t) = G(t,t_o)g_\ell(t_o), \tag{2.80}$$

where $g_\ell(t_o)$ represents the solution at time t_o and $G(t,t_o)$ is the propagator,

$$G(t,t_o) = T \exp\left[- i/\hbar \int_{t_o}^{t} d\tau\ (H+V)(\tau)\right]. \tag{2.81}$$

In this expression we have dropped the spatial indices, and T denotes the time-ordering. For short time intervals, the propagator can be approximated by

$$G_\Delta(t_{n+1},t_n) = \exp[- i/\hbar\ \Delta t\ \hat{h}(t_{n+1/2})], \tag{2.82}$$

where we have defined the single-particle Hamiltonian $\hat{h}$ as

$$\hat{h}(t_n) = (H+V)(t_n), \tag{2.83}$$

and in terms of the discretized time,

$$t_k = k\Delta t. \tag{2.84}$$

The half-step Hamiltonian is obtained by taking a step with Δt replaced by $\Delta t/2$. Among many available prescriptions for approximating G_Δ, we have used the method of Peaceman and Rachford (DK81), in which

$$G_\Delta \approx G_{PR} = \left[1 + \frac{i\Delta t}{2\hbar} V\right]^{-1} \left[1 - \frac{i\Delta t}{2\hbar} H\right]\left[1 + \frac{i\Delta t}{2\hbar} H\right]^{-1} \left[1 - \frac{i\Delta t}{2\hbar} V\right]. \tag{2.85}$$

One of the advantages of G_{PR} is that it involves inversions of small, tridiagonal matrices. The details of this inversion are given in Appendix C. Although this operator is not unconditionally unitary, its successive application results in unitary propagation, and it is an approximation to G up to order $(\Delta t)^2$.

4. Static Hartree-Fock Solutions.

In this subsection we will discuss the gradient iteration method (RC82) for the solution of SHF equations. The basis for the method is the use of the imaginary-time propagator (DF80). The TDHF equations for the single-particle states g_ℓ are

$$i\hbar\dot{g}_\ell(t) = \hat{h}(t)g_\ell(t). \tag{2.86}$$

The imaginary-time step method consists of the transformation $\Delta t \rightarrow -i\Delta t$ for the propagator G_Δ,

$$g_\ell(t_{k+1}) = \exp[-\varepsilon\left(\hat{h}(t_k) - \varepsilon_\ell(t_k)\right)]\, g_\ell(t_k), \tag{2.87}$$

where $\varepsilon = \Delta t/\hbar$, and a phase from $g_\ell(t_k)$ has been removed. For all practical purposes, the gradient iteration step corresponds to the first-order expansion of the exponential operator,

$$g_\ell(t_{k+1}) = \mathcal{O}\left\{g_\ell(t_k) - \varepsilon[\hat{h}(t_k) - \varepsilon_\ell(t_k)]g_\ell(t_k)\right\}. \tag{2.88}$$

The operation $\mathcal{O}$ denotes the necessary orthonormalization of the single-particle states. As is clearly seen from Eq. (2.87), the exponential operator acts as a filter in selecting the lowest eigenvalues of $\hat{h}$ and leads to the minimization of the SHF energy. Furthermore, the dampening parameter ε can be replaced by an operator $\hat{D}(k_o)$ to yield

$$g_\ell(t_{k+1}) = \mathcal{O}\left\{g_\ell(t_k) - \hat{D}(k_o)[\hat{h}(t_k) - \varepsilon_\ell(t_k)]g_\ell(t_k)\right\}. \tag{2.89}$$

For $\hat{D}(k_o)$ we choose

$$\hat{D}(k_o) = \varepsilon(1 + \hat{T}/k_o)^{-1}. \tag{2.90}$$

Here $\hat{T}$ is the kinetic energy operator defined on the spatial mesh points. This choice for $\hat{D}$ is motivated by the fact that the high-energy components of $\hat{h}$ will be dominated by the eigenvalues of the kinetic energy operator. These parameters were chosen to be

$\varepsilon = 0.015$ and $k_o = 40$ MeV.

The convergence of the method is shown in Fig. 3 for three different nuclear configurations, ground state ^{20}Ne, ground state ^{12}C, and the shape isomeric SHF solution of $^{12}C(0^+)$. The ordinate of Fig. 3 shows the fractional change in the SHF energy,

$$\Delta E^k = \frac{E_N(t_{k+1}) - E_N(t_k)}{E_N(t_k)}, \tag{2.91}$$

as a function of the iteration number k. The Hartree-Fock iteration sequence is fully self-consistent, and the structure in the ^{20}Ne curve results from a reordering of the single-particle states due to three separate shell-crossings. The extension of the gradient iteration method to the constrained Hartree-Fock calculations and particularly to the density constrained Hartree-Fock (DCHF) method (CR85) is dicussed in Appendix D. In recent years other types of numerical methods have also been proposed for the solution of SHF and constrained Hartree-Fock equations (BT77,DR80).

The gradient iteration and DCHF methods will be the essential ingredients in the numerical calculations carried out in the next chapter.

Figure 3. Convergence of the gradient iteration method for the nuclei ^{12}C, $^{12}C(0^+)$, and ^{20}Ne. The structure in the ^{20}Ne curve arises from the reordering of the single-particle states due to three separate shell crossings.

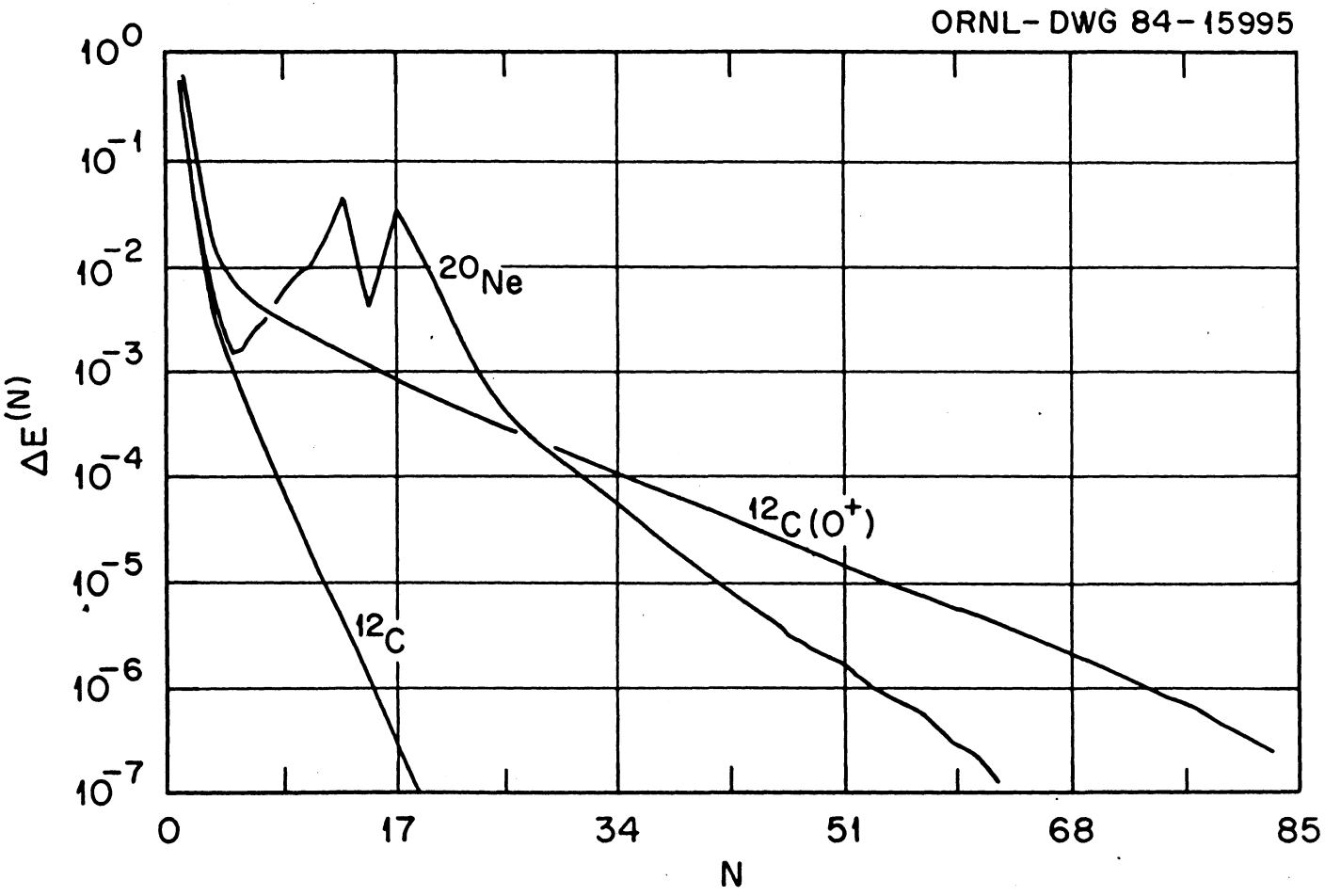
ORNL-DWG 84-15995
10^{0}
10^{-1}
10^{-2}
10^{-3}
10^{-4}
10^{-5}
10^{-6}
10^{-7}
$\Delta E^{(N)}$
^{20}Ne
$^{12}C(0^{+})$
^{12}C
0
17
34
51
68
85
N

III. TDHF STUDIES OF NUCLEAR MOLECULES

In what follows we will examine the long-time behavior of the TDHF equations (Eq. 2.71) by initiating head-on (zero impact parameter) collisions with bombarding energies near the Coulomb barrier.

The TDHF evolution of nuclear dynamics is different from the stationary-state scattering theory in the sense that in TDHF theory we actually follow the motion of the wavepackets (KK76). Initially, both nuclei are approximated by their Hartree-Fock wavefunctions. These wavefunctions are then given a boost appropriate for the initial conditions of the collision (Eq. 2.43). By solving the TDHF equations, we follow these wavepackets during and after the collision. One problem with this scenario arises from the fact that the TDHF wavefunction stays as a single Slater determinant for all times, evolving in a non-linear, self-consistent fashion. This evolution differs from that of the exact Schroedinger equation. In the TDHF case the wavefunction does not decompose into a linear combination of channel eigenstates. Also, the initial TDHF determinant is a wavepacket in the space of channel eigenstates which makes it difficult to isolate a given incident channel. As a consequence, the calculation of specific quantum-mechanical information is complicated, and one usually deals with inclusive quantities (as opposed to exclusive). A more detailed discussion of the applications of the TDHF theory can be found in (DD85).

On the other hand the long-time collective motion arising from the solution of the TDHF equations can be interpreted through the language

of chaos (He81). The theory of chaos concerns the long-time behavior of non-integrable mechanical systems and addresses questions as to the nature of energy dissipation and equilibration of energy. Within the context of nuclear physics, these ideas were first used by Fermi, Pasta, and Ulam (FP57). Similarly, the hydrodynamic models of heavy-ion reactions (Be75) exhibit dissipative fluid flow behavior, where the details of momentum transfer and particle multiplicities may be considered as evidence for the formation of attractor regions in the reaction phase space. Various limits of the TDHF motion depend on the initial conditions (i.e. initial energy, initial separation, etc.). In the small amplitude limit, TDHF solutions yield unquantized vibrational frequencies with the classical interpretation of being the most probable RPA frequencies (Ro66,KK76). In this context, TDHF calculations of isoscalar and isovector giant resonances have been found to be in good agreement with the corresponding RPA calculations (BF79). The functional integral theories formulate the bound-states of the many-body system in terms of the periodic TDHF solutions (LN80,Bl81), but the numerical solution of the resulting equations are presently not possible.

Below we will study the collisions of $^{4}He+^{14}C$, $^{12}C+^{12}C(0^{+})$, and $^{4}He+^{20}Ne$ systems (SC84,US85). The important collective degrees of freedom of the composite system will be identified in terms of the moments of the density defined by

$$M_{LI}(t) = \int d^3x \; R^L \; Y_{LO}(\hat{R})\rho_I(\vec{x},t), \tag{3.1}$$

where $\vec{R}$ denotes a vector in spherical coordinates. The isoscalar

density ρ_o and the isovector density ρ_1 are given by the expectation of the operator

$$\rho_I(\vec{x}) = \sum_{i=1}^{A} \delta(\vec{x}-\vec{x}_i)\hat{a}_I(i) \tag{3.2}$$

with

$$\langle q \mid a_I \mid q' \rangle = \begin{cases} \delta_{qq'} & , \ q = \text{proton} \\ (-1)^I \delta_{qq'} & , \ q = \text{neutron.} \end{cases} \tag{3.3}$$

In terms of these quantities, isoscalar and isovector densities can be written as

$$\rho_I(\vec{x},t) = \begin{cases} \rho_p(\vec{x},t) + \rho_n(\vec{x},t) & , \ I = 0 \\ \rho_p(\vec{x},t) - \rho_n(\vec{x},t) & , \ I = 1. \end{cases} \tag{3.4}$$

Using the newly developed DCHF method, we also calculate the position of the TDHF trajectory with respect to the multi-dimensional energy surface of the composite system. The BKN force was used in all of the calculations presented below.

A. ^{4}He+^{14}C SYSTEM

In these calculations THDF equations were evolved for times greater than about 3×10^3 fm/c with a time-step of $\Delta t = 0.75$ fm/c. The spatial discretization used a NR×NZ=10×45 point grid with a uniform mesh spacing of 0.5 fm. The total energy was conserved to better than 10^{-3} over the entire time interval. The initial ^{14}C nucleus was obtained as a spherical approximation to the ground state using the filling approximation. In this approximation the levels of the open shell are occupied with fractional occupation numbers leading to the closure of the shell. The initial separation and the c.m. kinetic

energy were 15 fm and 7.5 MeV respectively.

After the initial contact at about 40 fm/c, the system relaxes into a configuration and undergoes quasiperiodic motion. The density contours in Fig. 4 are shown in the (y,z) plane (x=0), where the separation of the centers of the ^{4}He and ^{14}C nuclei is initially aligned along the z-axis. Density contours are shown at six different times beginning at about 500 fm/c and extending roughly for half a period of the oscillations. In a schematic interpretation the density shows an alpha-particle-like structure and a ^{14}C-like structure which are exchanging about the center of mass of the ^{18}O system. Figures 5-6 show the time and frequency dependence of the isoscalar quadrupole and octupole moments and the isovector dipole moment. From Fig. 5, we observe oscillations for times longer than the typical nuclear reaction times (10^{-21} sec). Figure 6 shows a relatively pure 4-MeV frequency in the isoscalar octupole mode and 8- and 15-MeV frequencies in the isoscalar quadrupole mode. The isovector dipole has 4- and 9-MeV frequencies. The 4-MeV frequency could be a result of the coupling of isoscalar octupole and isovector dipole channels. The 4-MeV dipole frequency may correspond to the 4.4-MeV 1^{-} state observed in the ^{4}He+^{14}C molecular band (GR83).

The position of the TDHF path with respect to the multi-dimensional static energy surface of the composite system, ^{18}O, is computed using the DCHF method. At certain time intervals along the collective path, one obtains the SHF energy subject to the constraint that the isoscalar density remains fixed. The energy surface shown in Fig.

Figure 4. Density contours (I = 0) in the collision plane for ^{18}O system, starting from the initial $^{4}He+^{14}C$ configuration. The times are considerably after the initial contact and exhibit the quasiperiodicity of the system. The density contours 1, 3, 5, and 6 are respectively 0.028, 0.084, 0.14, and 0.168 nucleons/fm^3.

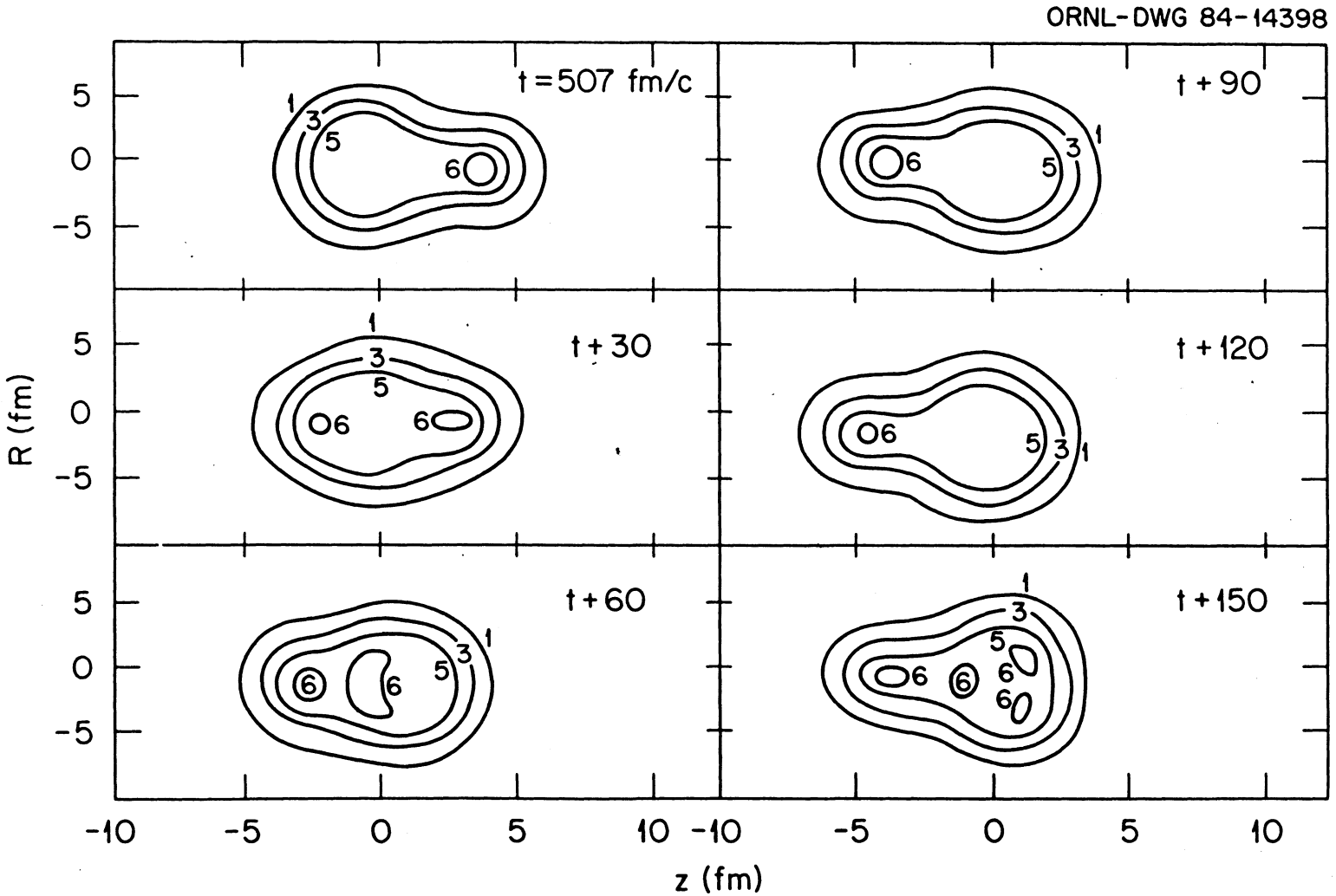
ORNL-DWG 84-14398
t = 507 fm/c
t + 90
t + 30
t + 120
t + 60
t + 150
R (fm)
z (fm)
5
0
-5
-10
10

Figure 5. The time dependence of the isoscalar octupole, isoscalar quadrupole, and the isovector dipole moments for the ^{18}O system.

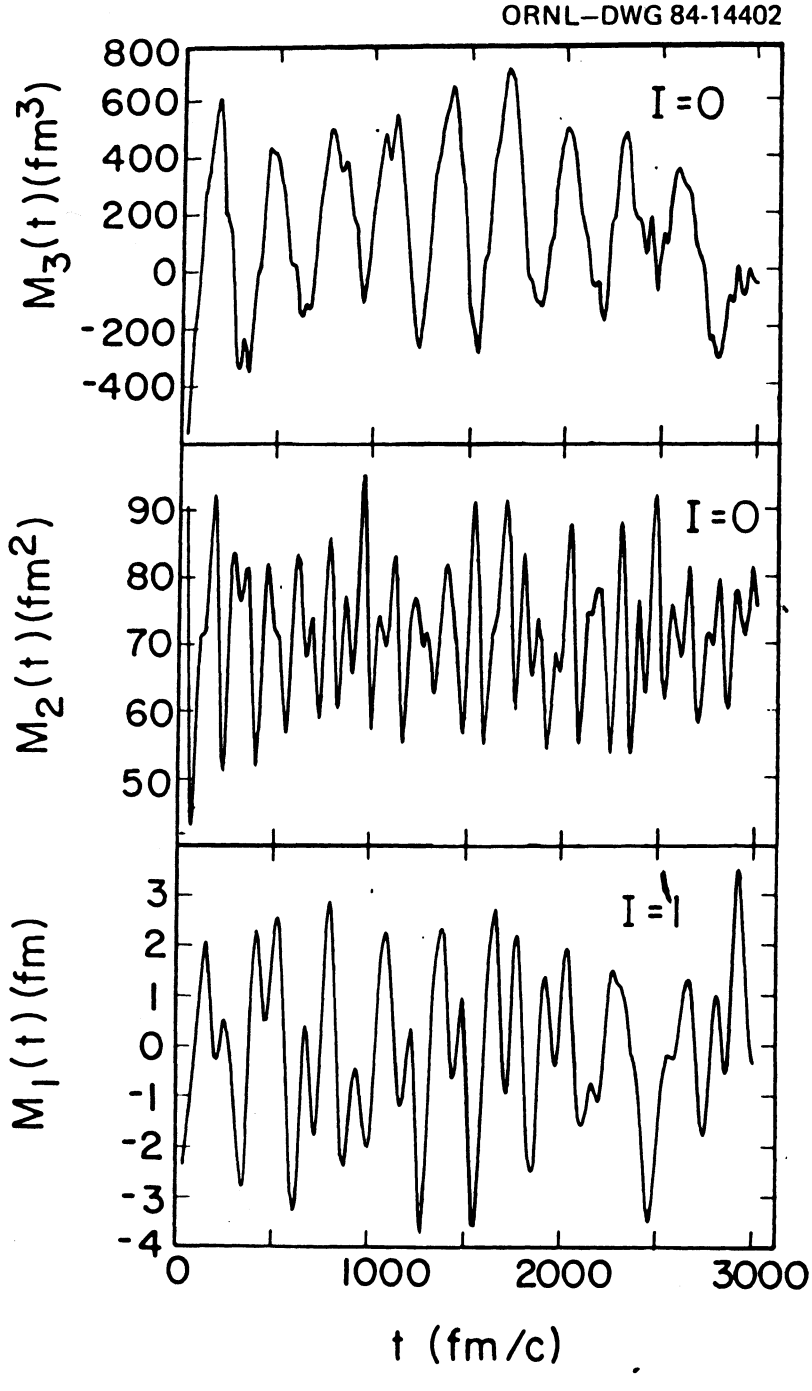
ORNL–DWG 84-14402
800
600
400
200
0
-200
-400
$M_3(t)(fm^3)$
I=0
90
80
70
60
50
$M_2(t)(fm^2)$
I=0
3
2
1
0
-1
-2
-3
-4
$M_1(t)(fm)$
I=1
0
1000
2000
3000
t (fm/c)

Figure 6. The frequency dependence of the isoscalar octupole, isoscalar quadrupole, and the isovector dipole moments for the ^{18}O system.

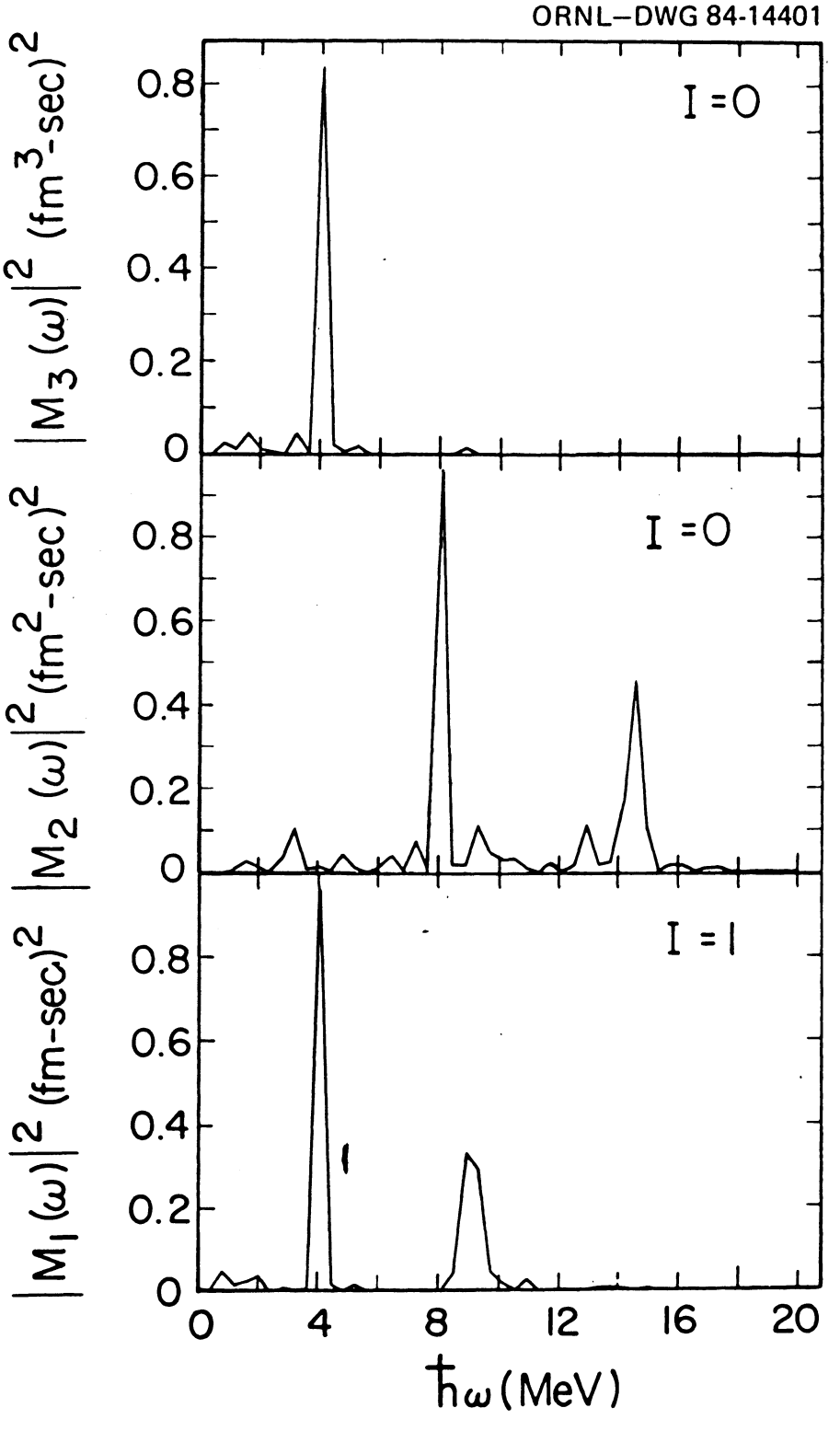
ORNL–DWG 84-14401
$|M_3(\omega)|^2$ (fm^3-sec)^2
$|M_2(\omega)|^2$ (fm^2-sec)^2
$|M_1(\omega)|^2$ (fm-sec)^2
I = 0
I = 0
I = 1
1
0
0.2
0.4
0.6
0.8
0
4
8
12
16
20
$\hbar\omega$ (MeV)

7 is obtained by plotting the DCHF energy as a function of the octupole (q_3) and quadrupole (q_2) degrees of freedom. The DCHF equations were solved at approximately 450 different time points along the trajectory. The plot is obtained using a least-squares fit to the DCHF energies. The initial configuration corresponds to the coordinates $q_2/q_{20} = 1.7$, and $q_3/q_{30} = -2.5$. The system quickly evolves into the region shown in Fig. 7. The minimum energy in Fig. 7 corresponds to an axially symmetric shape isomer of the ^{18}O system and is a stable solution of the unconstrained SHF equations.

The focusing of the TDHF trajectory to the vicinity of the shape isomeric minimum of the composite nuclear system is evidence for the formation of an attractor region in the reaction phase space. We should also note that this long-lived configuration is different from the one arising from the formation of a compound nucleus where the energy is equilibrated among all of the nucleons in the system.

B. $^{12}C+^{12}C(0^+)$ SYSTEM

The same analysis is also performed for the reaction $^{12}C+^{12}C(0^+)$. Here 0^+ denotes the 7.66-MeV excited state of ^{12}C. Choice of this state follows from the suggestion that this state may represent one of the building blocks of the $^{12}C+^{12}C$ molecule (EB81). Experimentally, this level lies at 7.66 MeV (just above the α-threshold energy at 7.3 MeV) and has a very large α-decay width (TA71). In the α-particle model of the ^{12}C nucleus this state has a collinear three-alpha configuration (TA71). The ground and low-lying states (for example, the

Figure 7. Density constrained static Hartree-Fock energies. $E = E(\text{constrained}) - E_o$, $E_o = -122.3$ MeV, as a function of the isoscalar quadrupole and octupole degrees of freedom. Contours are labeled in MeV. The constants q_{20}, q_{30} are $q_{20} = 56.6$ fm^2, and $q_{30} = -412.6$ fm^3. The point having the energy E_o is a shape isomer of the ^{18}O system.

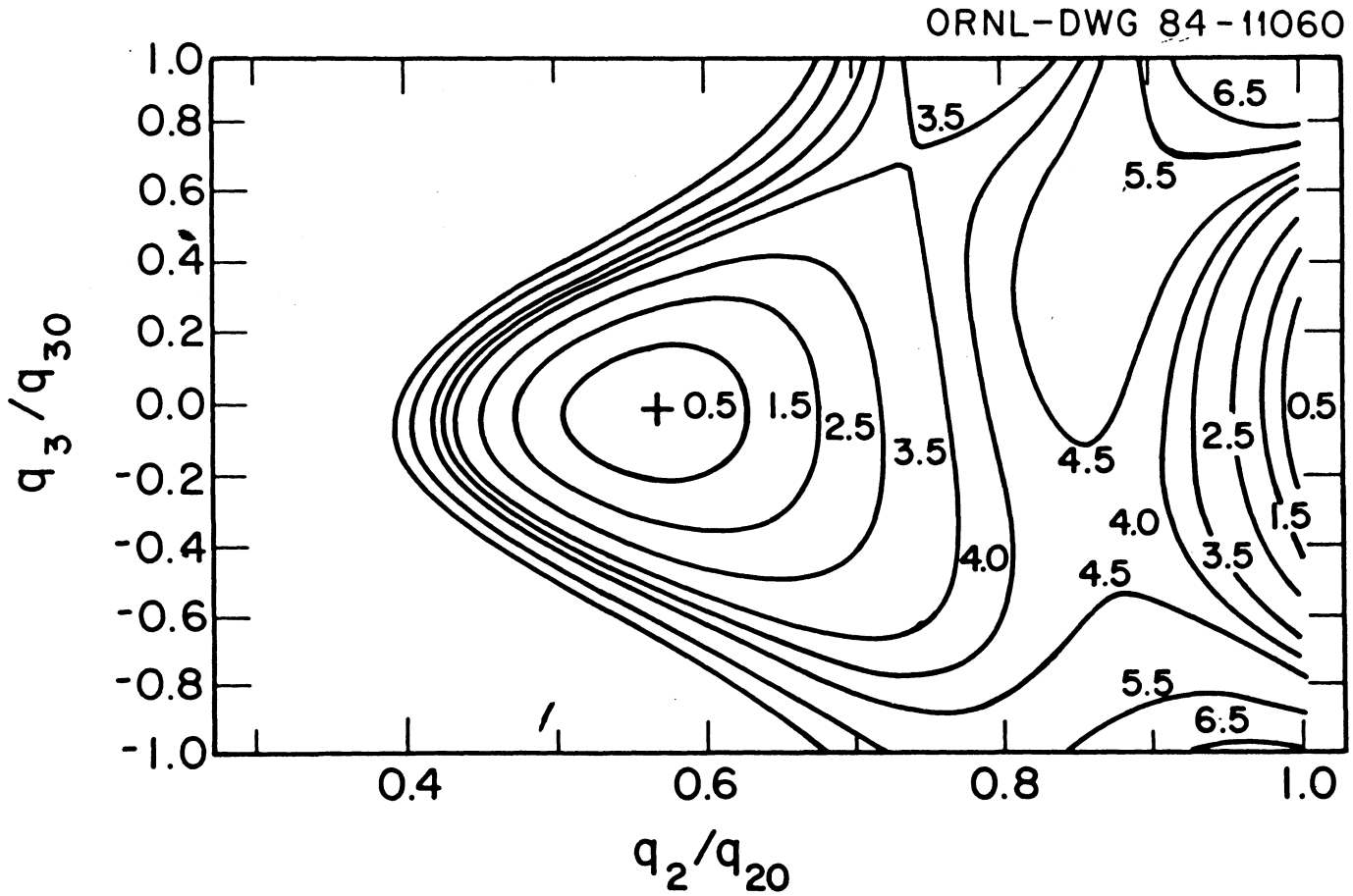
ORNL-DWG 84-11060
1.0
0.8
0.6
0.4
0.2
0.0
-0.2
-0.4
-0.6
-0.8
-1.0
0.4
0.6
0.8
1.0
q_3/q_{30}
q_2/q_{20}
+0.5
1.5
2.5
3.5
4.0
4.5
5.5
6.5
0.5
1.5
2.5
3.5
4.0
4.5
5.5
6.5

4.43-MeV 2^+ state) are below this threshold. In Fig. 8 we show the density contours corresponding to the ground state Hartree-Fock wavefunction (configuration A) and to the Hartree-Fock shape isomeric wavefunction (configuration B) of ^{12}C. On the same figure the change in the SHF energy as a function of the deformation parameter β and the precise locations of configurations A and B are also shown (CH76). As seen in the figure, the unaccounted center-of-mass motion (see section II.C) in SHF theory introduces an error on the excitation energy of the isomer with respect to the ground state. Detailed studies (TA71) have shown that in order to be able to obtain the experimental electromagnetic transition probabilities, the true ground state and the 0^+ state should be formed as a linear combination of configurations A and B. Specifically, these states are given by

$$\begin{aligned} |0_1^+\rangle &= 0.9777\,|A\rangle + 0.21\,|B\rangle \\ |0^+\rangle &= 0.21\,|A\rangle - 0.9777\,|B\rangle \end{aligned} \tag{3.5}$$

with

$$\langle 0_1^+ | 0^+\rangle = 0.$$

In principle, this admixture will explain the excitation of the configuration B during the collision. Unfortunately, in Hartree-Fock theory the construction of such correlated wavefunctions is not possible, and here the collision between two Hartree-Fock wavefunctions corresponding to configurations A and B will be studied.

Initially, the ions are 12 fm apart with c.m. kinetic energy of 7.5 MeV. The time-evolution was performed with a time-step of $\Delta t = 0.5$ fm/c and the reaction was followed up to 1.2×10^4 fm/c. The spatial

Figure 8. The structure of the $^{12}C(0^+)$ configuration obtained by constrained Hartree-Fock calculations.

CALCULATIONS ON CARBON
CONSTRAINED HARTREE FOCK

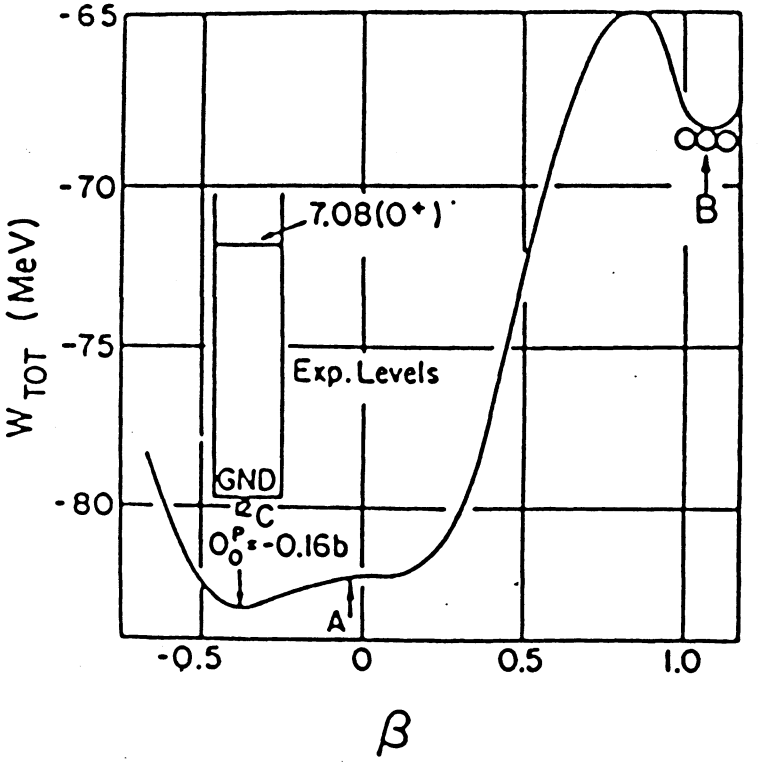

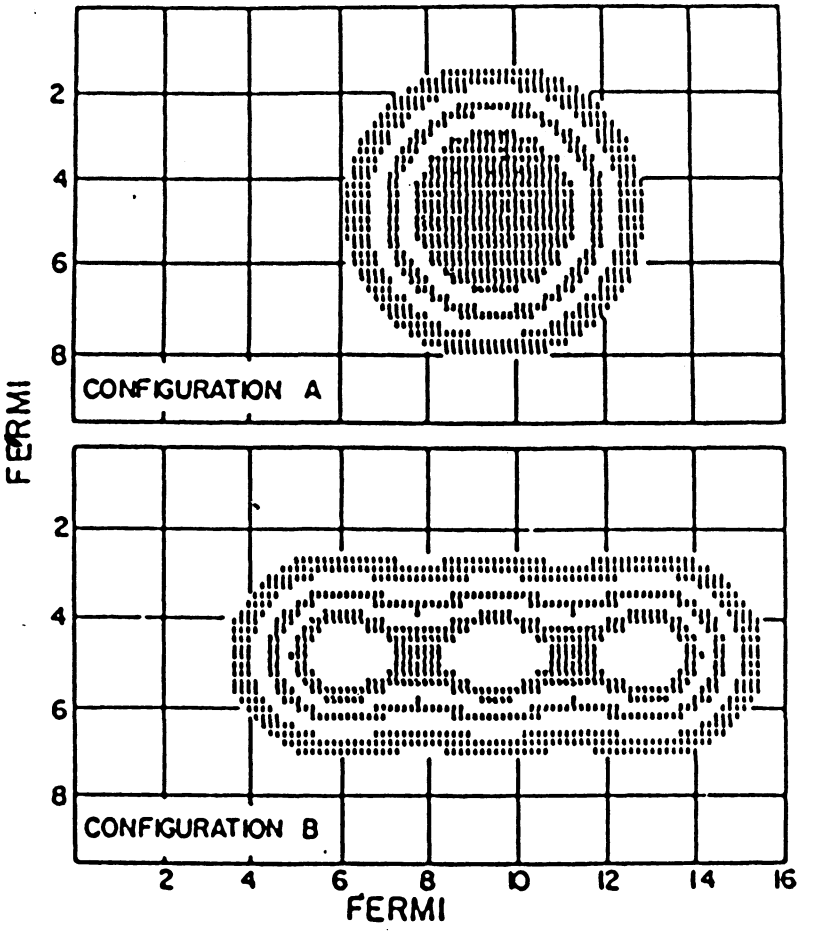

discretization used a NR×NZ=15×80 grid with a uniform mesh spacing of 0.5 fm. Figure 9 shows the evolution of the isoscalar density in the (y,z) plane at various times. Again, we see a quasiperiodic motion arising from a complicated matter flow. Similarly, Fig. 10 shows the rapid oscillations in the isovector density at various times. The oscillations are induced by the Coulomb force, and they correspond to high multipole structures. The associated time-dependence of the isovector dipole, isoscalar quadrupole, and the isoscalar octupole are shown in Fig. 11. The corresponding frequency spectra of Fig. 12 show a 1.5-MeV isoscalar octupole peak, 2.5- and 8-MeV isoscalar quadrupole peaks, and 6- and 8.5-MeV isovector dipole peaks.

The position of the TDHF trajectory with respect to the multidimensional energy surface of the ^{24}Mg system is shown in Fig. 13. As before, the contours are shown in the quadrupole (q_2) and octupole (q_3) subset of the full collective Hilbert space. The path for ^{24}Mg starts from the initial point at $q_2/q_{20} = 1.5$ and $q_3/q_{30} = 2.9$ and traverses a complex route about the shape isomer which has an energy of -143.8 MeV. The axially symmetric ground state of ^{24}Mg occurs at $q_2 = 42.3$ fm^2 with an energy of -179.9 MeV.

C. ^{4}He+^{20}Ne SYSTEM

A similar collision study was also performed for the ^{4}He+^{20}Ne system with a c.m. kinetic energy of 6.5 MeV. The frequency spectrum for isovector dipole, isoscalar quadrupole, and isoscalar octupole motions is shown in Fig. 14. The similarities between the ^{12}C+^{12}C(0^+) spectra

Figure 9. Density contours (I = 0) in the collision plane for the ^{24}Mg system, starting from an initial $^{12}C+^{12}C(0^+)$ configuration. Different times exhibit the quasi-periodicity of the system. The outer dark contour corresponds to 9×10^{-4}, the adjacent grey contour to 3×10^{-3}, the adjacent white contour to 8×10^{-3}, the adjacent grey contour to 3×10^{-2}, the adjacent white area to 7.2×10^{-2}, and the central dark region to 1.5×10^{-1} nucleons/fm^3.

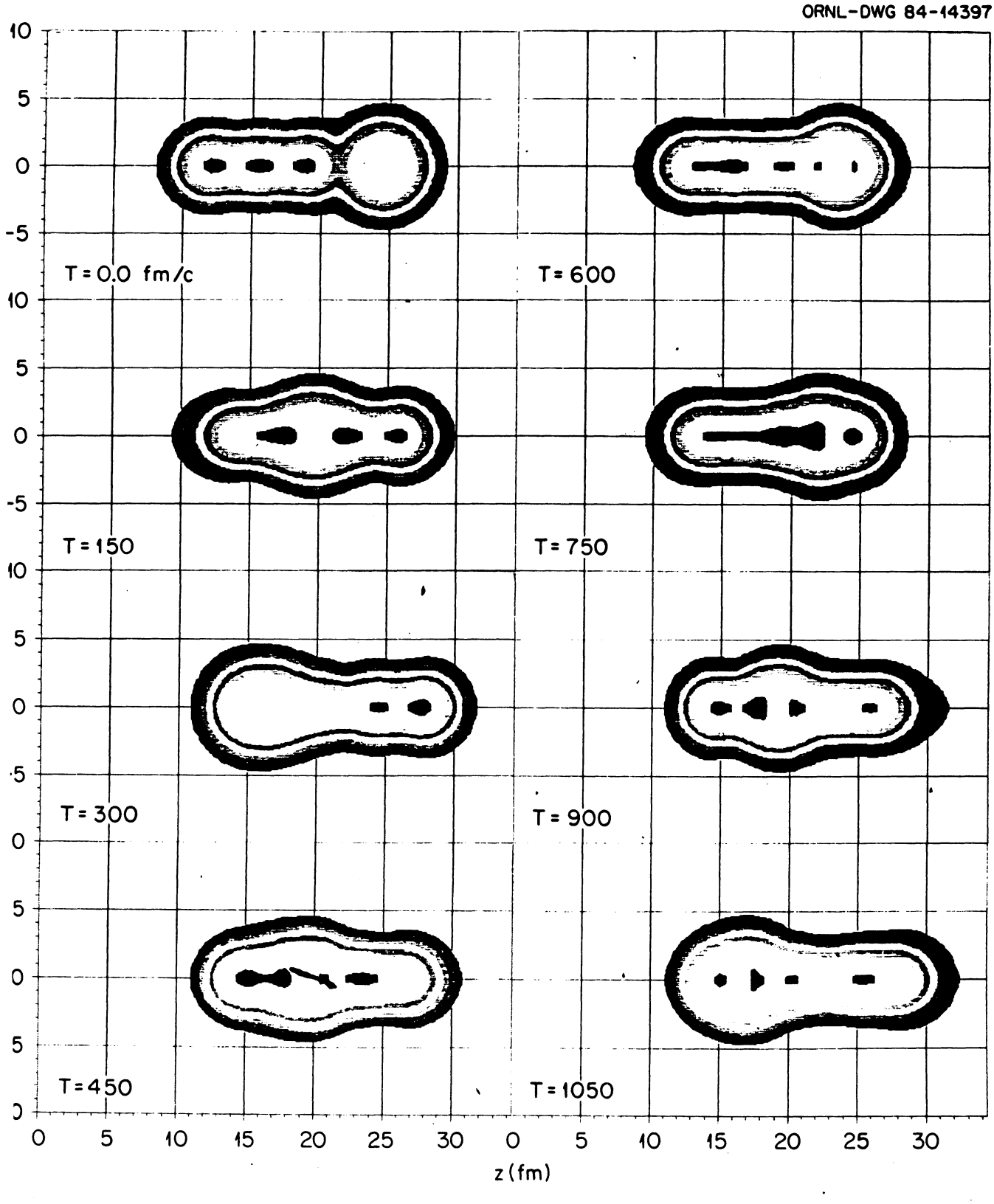
ORNL-DWG 84-14397
T = 0.0 fm/c
T = 600
T = 150
T = 750
T = 300
T = 900
T = 450
T = 1050
z (fm)

Figure 10. Density contours (I = 1) in the collision plane for the ^{24}Mg system, starting from an initial $^{12}C+^{12}C(0^+)$ configuration. The isovector densities change more rapidly in time, and they correspond to high multipole structures. The darkest contour corresponds to 8.8×10^{-4}, the grey contour always circled by the darkest contour to 3×10^{-3}, the isolated grey contours to -6×10^{-3}, the white regions to -4.4×10^{-3}, and the grey contours encircled by the white region to -1.0×10^{-2} e^2/fm^3.

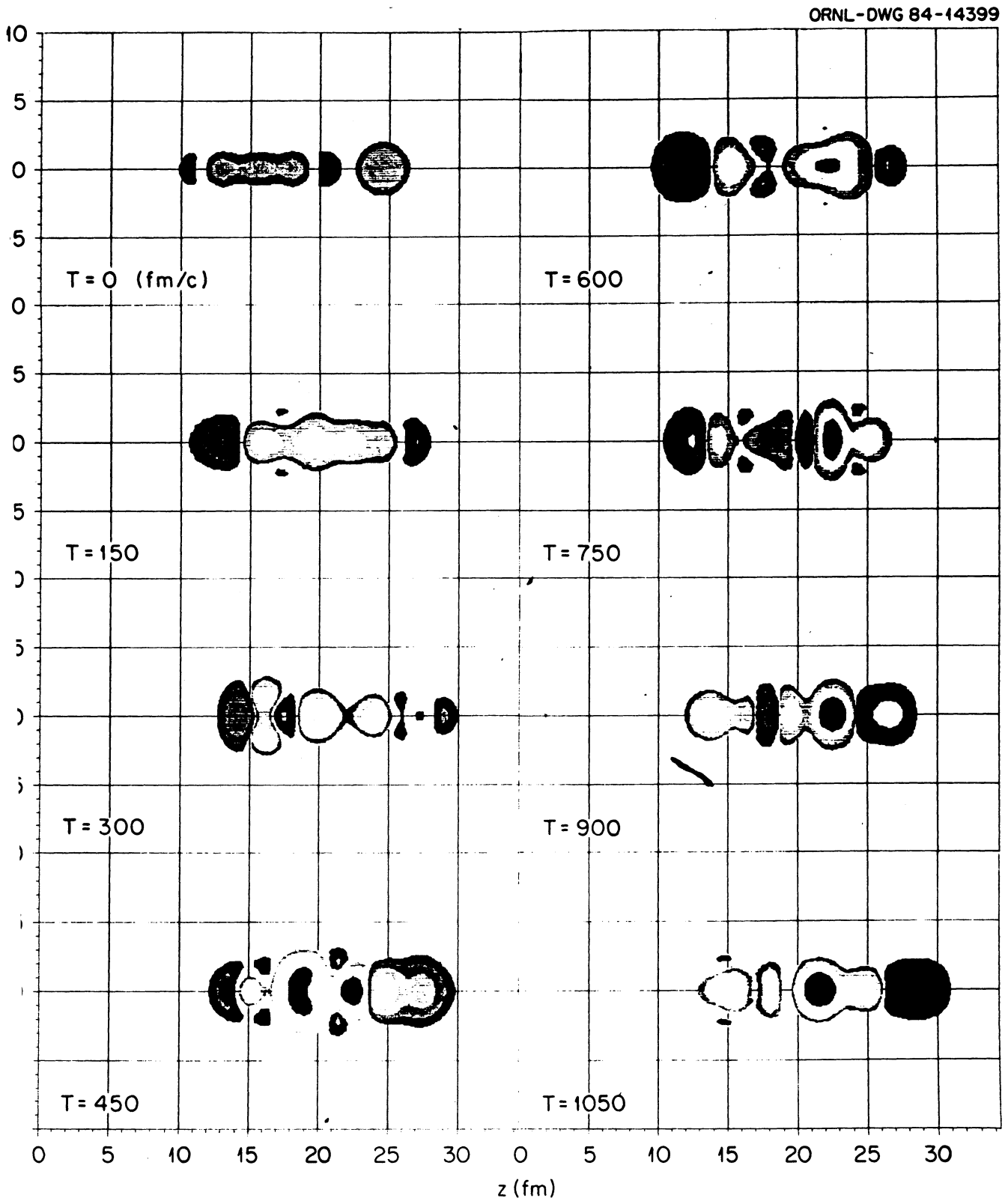
ORNL-DWG 84-14399
T = 0 (fm/c)
T = 150
T = 300
T = 450
T = 600
T = 750
T = 900
T = 1050
10
5
0
5
0
5
0
5
0
5
0 5 10 15 20 25 30
0 5 10 15 20 25 30
z (fm)

Figure 11. The time dependence of the isovector dipole, isoscalar quadrupole, and the isoscalar octupole moments for the ^{24}Mg system.

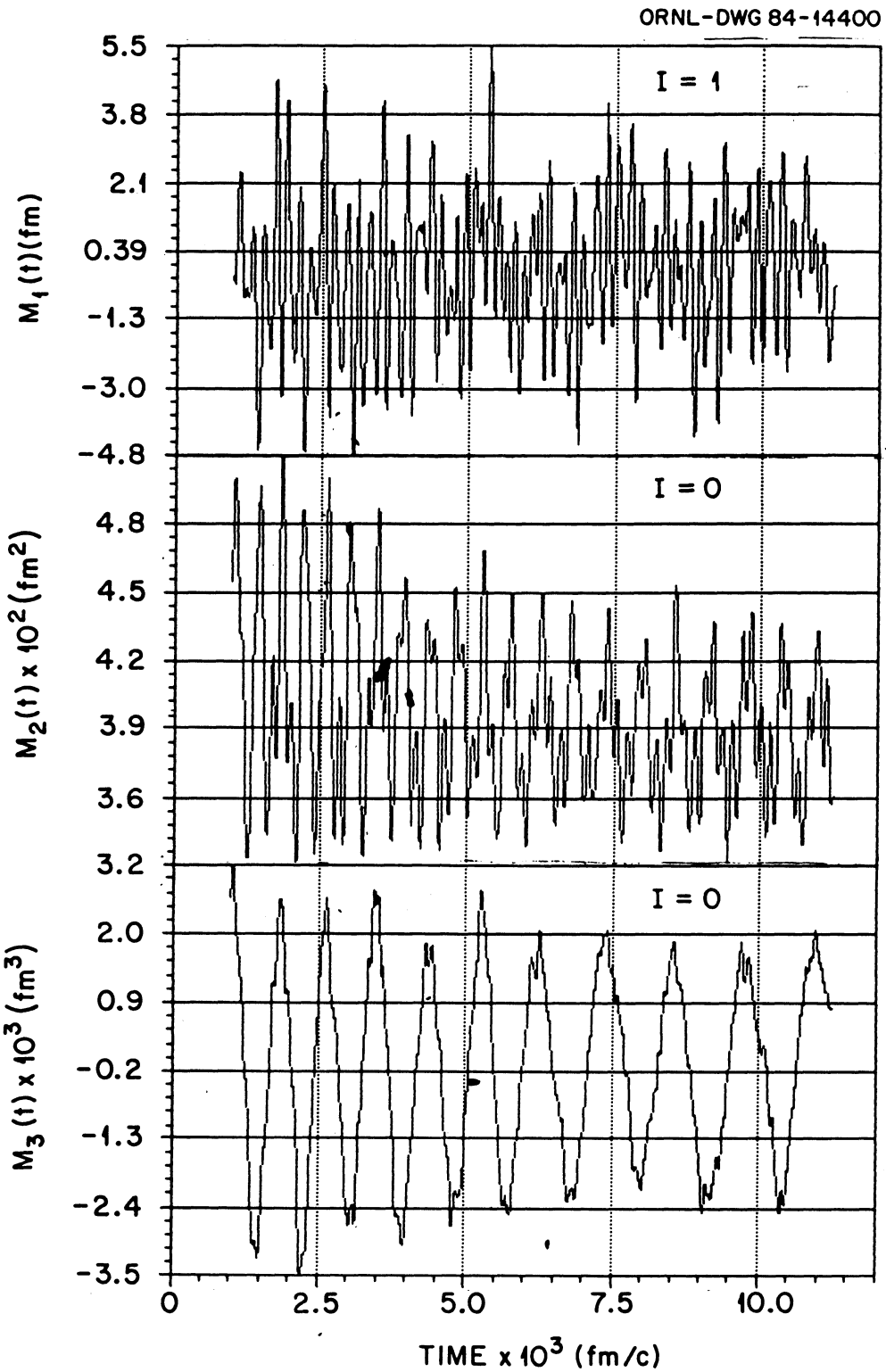
ORNL-DWG 84-14400
I = 1
I = 0
I = 0
$M_1(t)$(fm)
$M_2(t) \times 10^2$(fm^2)
$M_3(t) \times 10^3$(fm^3)
5.5
3.8
2.1
0.39
-1.3
-3.0
-4.8
4.8
4.5
4.2
3.9
3.6
3.2
2.0
0.9
-0.2
-1.3
-2.4
-3.5
0
2.5
5.0
7.5
10.0
TIME x 10^3 (fm/c)

Figure 12. The frequency dependence of the isovector dipole, isoscalar quadrupole, and the isoscalar octupole moments for the ^{24}Mg system.

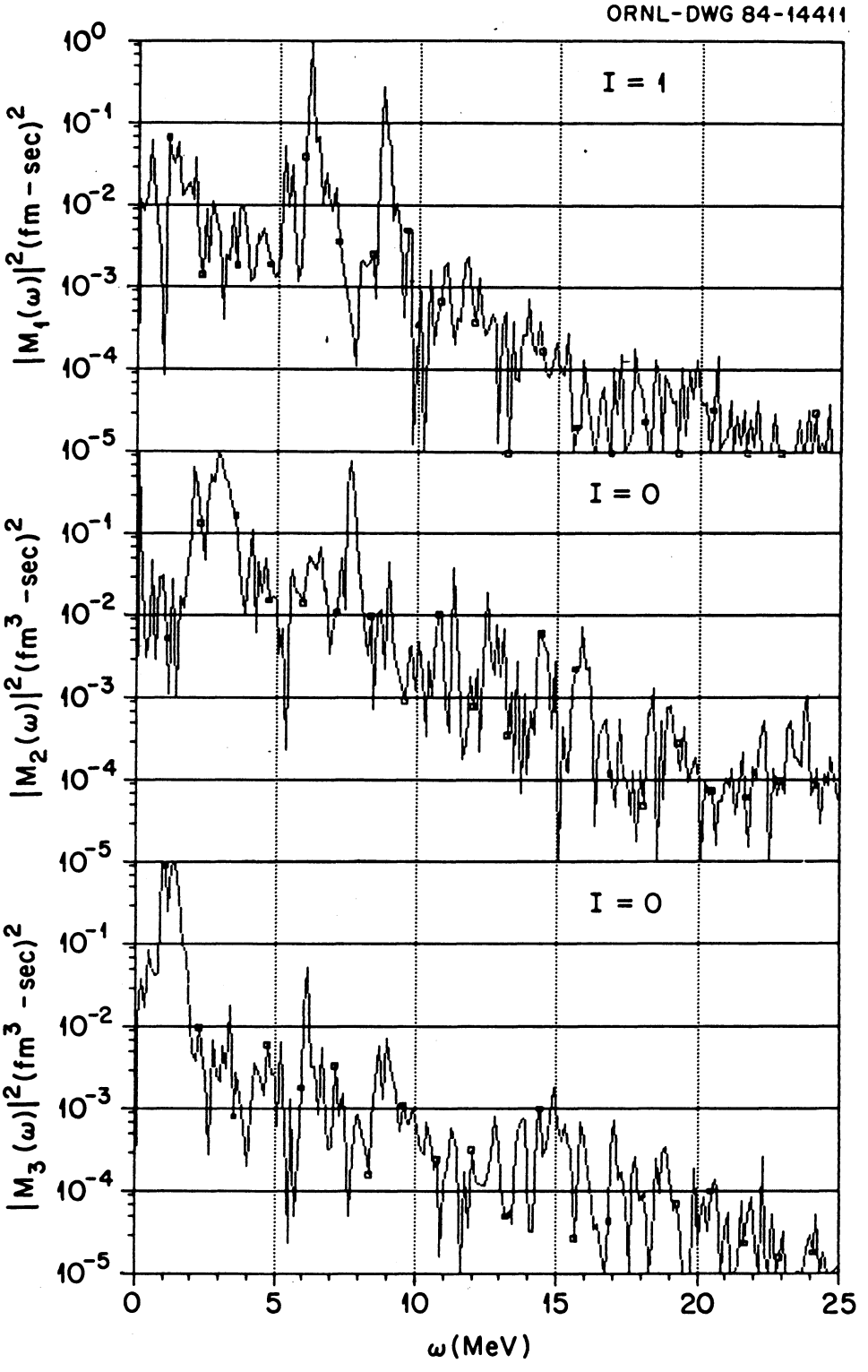
ORNL-DWG 84-14411
I = 1
I = 0
I = 0
$|M_1(\omega)|^2$(fm-sec)^2
$|M_2(\omega)|^2$(fm^3-sec)^2
$|M_3(\omega)|^2$(fm^3-sec)^2
10^0
10^{-1}
10^{-2}
10^{-3}
10^{-4}
10^{-5}
0
5
10
15
20
25
ω(MeV)

Figure 13. Density constrained static Hartree-Fock energies. $E = E(\text{constrained}) - E_o$, $E_o = -143.8$ MeV, as a function of the isoscalar quadrupole and octupole degrees of freedom. Contours are labeled in MeV. The constants q_{20}, q_{30} are $q_{20} = 367.6$ fm^2, and $q_{30} = 2164.3$ fm^3. The point having the energy E_o is a shape isomer of the ^{24}Mg system.

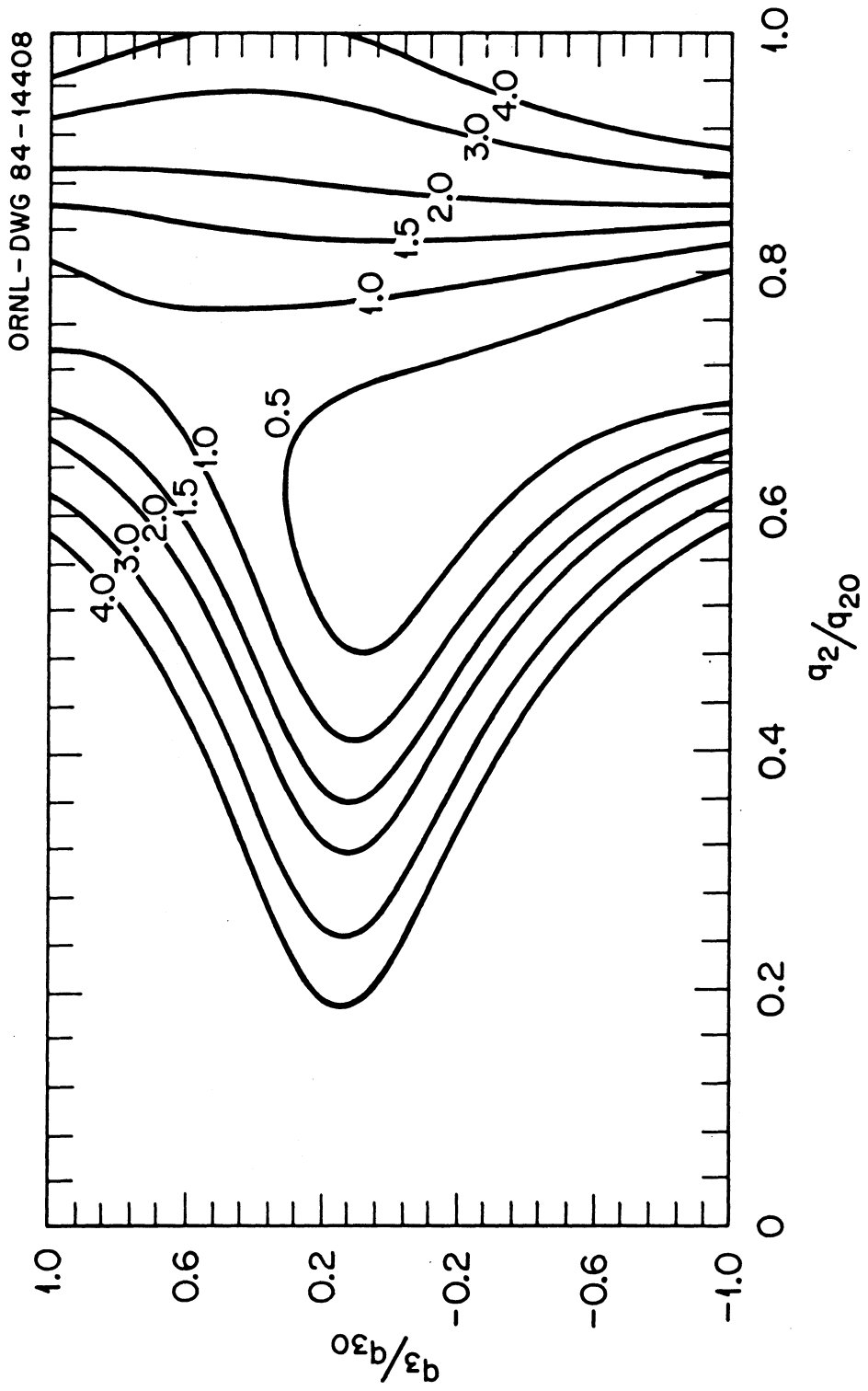
ORNL-DWG 84-14408
0.5
1.0
1.5
2.0
3.0
4.0
1.0
0.6
0.2
-0.2
-0.6
-1.0
q_3/q_{30}
0
0.2
0.4
0.6
0.8
1.0
q_2/q_{20}

Figure 14. The frequency dependence of the isoscalar quadrupole, isoscalar octupole, and the isovector dipole moments for the ^{24}Mg system from an initial configuration $^{4}He+^{20}Ne$.

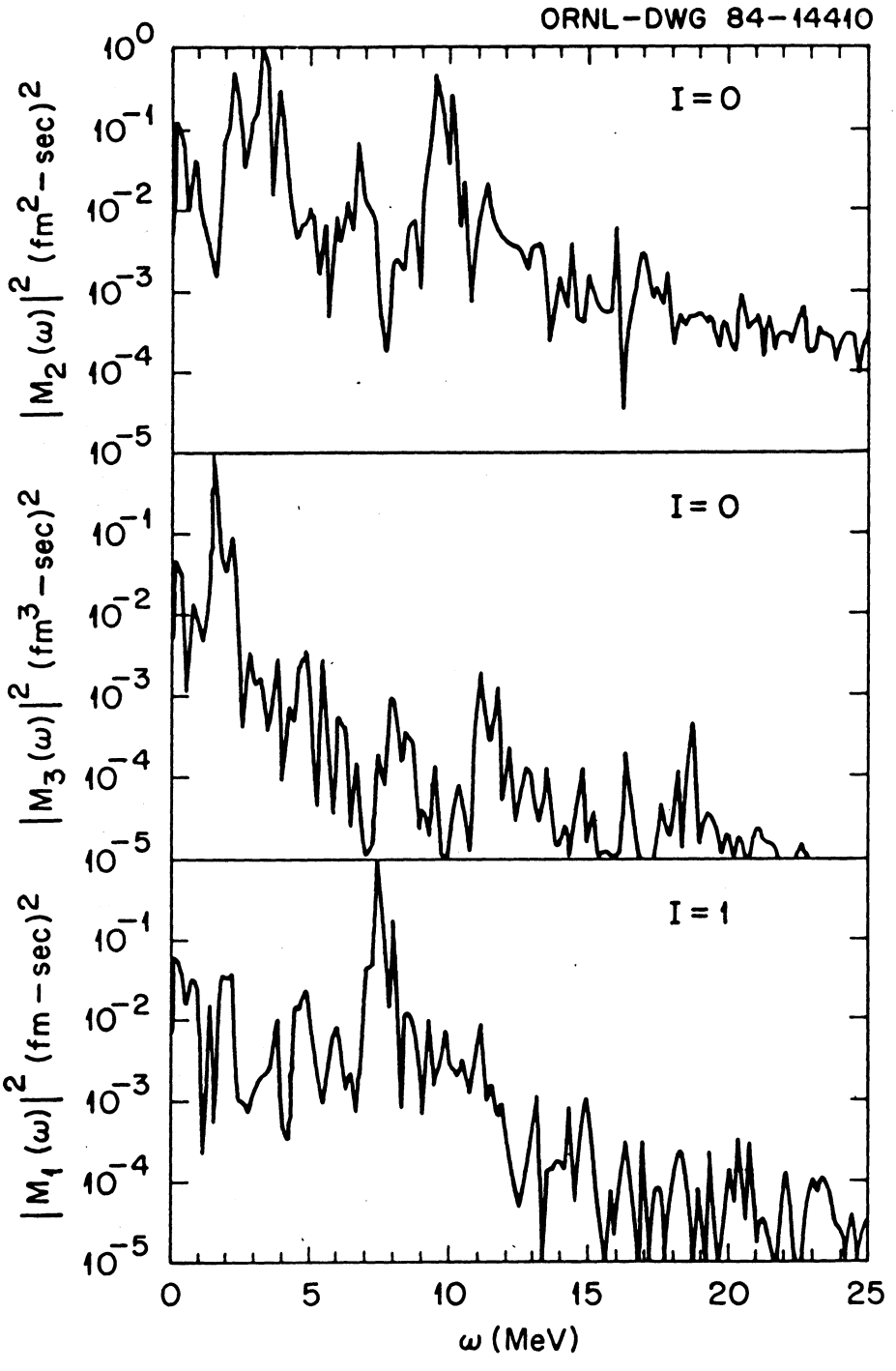
ORNL-DWG 84-14410
I = 0
I = 0
I = 1
$|M_2(\omega)|^2$ (fm^2-sec)^2
$|M_3(\omega)|^2$ (fm^3-sec)^2
$|M_1(\omega)|^2$ (fm-sec)^2
10^0
10^{-1}
10^{-2}
10^{-3}
10^{-4}
10^{-5}
0
5
10
15
20
25
ω (MeV)

of Fig. 12 and this result indicate that both reactions are probing the same part of the ^{24}Mg collective energy surface. Experiments starting from a ^{4}He+^{20}Ne initial configuration have also identified resonances which fit onto the ^{12}C+^{12}C molecular band (Da81).

D. CHAOS

Here we will study the motion of the TDHF path for the ^{12}C+^{12}C(0^+) system using the classifications of (WK82). These authors investigate a variety of requantization schemes for the classical trajectories of the three-level SU(3) model (LK70). For this model, exact quantum-mechanical, as well as closed-form TDHF solutions can be obtained. Upon classifying the motion to be one of the three types: i) periodic, ii) quasiperiodic, and iii) stochastic, they conclude that it is not possible to requantize stochastic motions, whereas different requantization schemes for the quasiperiodic motion all give reasonable results.

In order to interpret the results of section B from this point of view, we plot the Poincaré projects for the motion of the ^{12}C+^{12}C(0^+) system as shown in Fig. 15. We see that both isoscalar quadrupole and octupole modes seem to be filling the available phase space. Another measure for the degree of periodicity is given by the autocorrelation function,

$$C_{LI}(t) = \int_{-\infty}^{+\infty} \frac{d\omega}{2\pi} \exp(i\omega t) \left| M_{LI}(\omega) \right|^2 . \qquad (3.6)$$

The calculated autocorrelation functions (Fig. 16) are small for all of

Figure 15. Poincaré phase space plots of $\dot{M}_{LI}(t)$ vs. $M_{LI}(t)$ for isoscalar quadrupole and isoscalar octupole modes for the ^{24}Mg system.

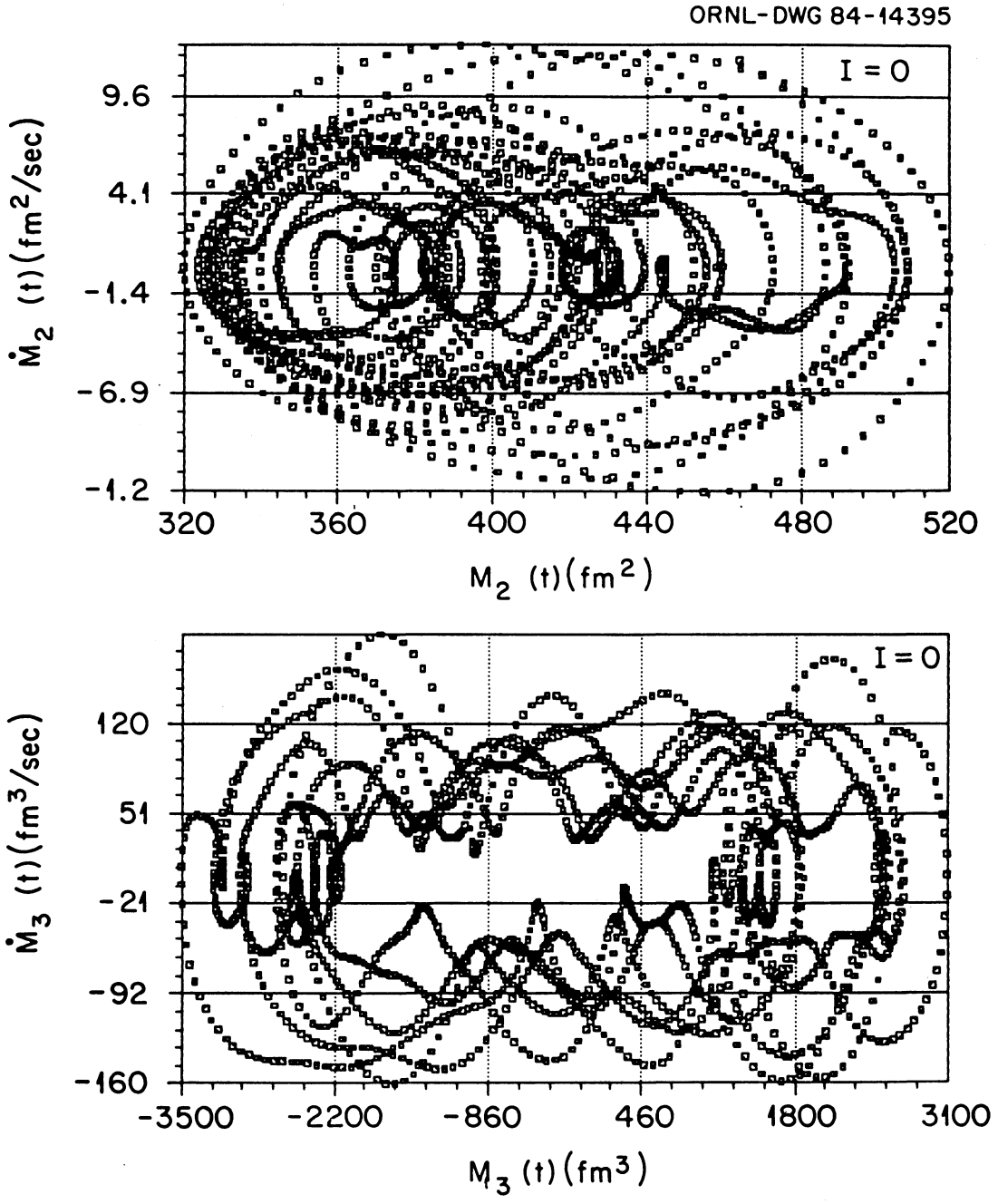
ORNL-DWG 84-14395
I = 0
9.6
4.1
-1.4
-6.9
-1.2
$\dot{M}_2$ (t)(fm^2/sec)
320
360
400
440
480
520
M_2 (t)(fm^2)
I = 0
120
51
-21
-92
-160
$\dot{M}_3$ (t)(fm^3/sec)
-3500
-2200
-860
460
1800
3100
M_3 (t)(fm^3)

Figure 16. The autocorrelation function $C_{LI}(t)$ in units $MeV(fm^{L}\text{-}sec)^{2}$ as a function of time for the isoscalar quadrupole and octupole modes in the ^{24}Mg system.

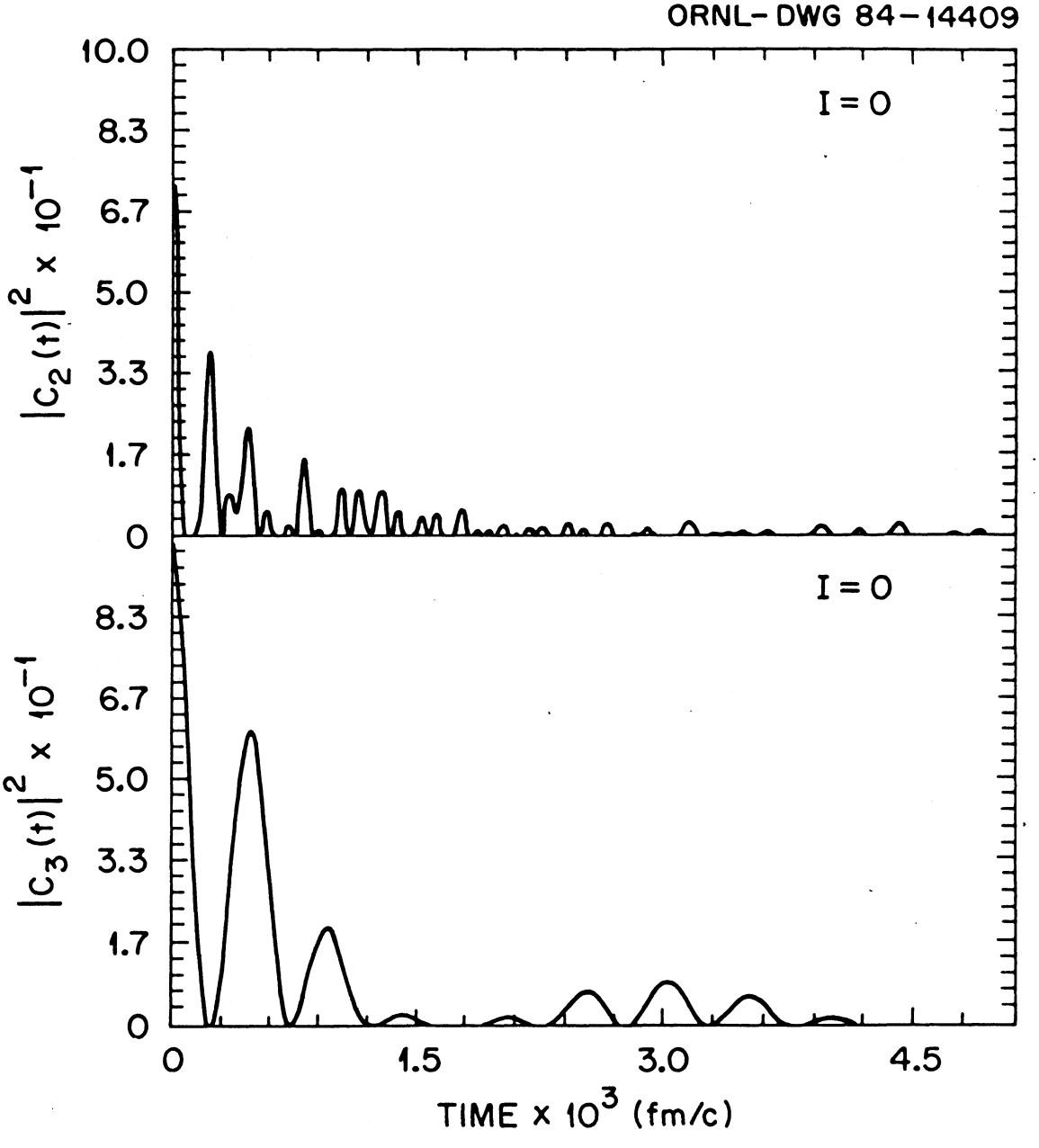
ORNL-DWG 84-14409
10.0
8.3
6.7
5.0
3.3
1.7
0
I = 0
$|C_2(t)|^2 \times 10^{-1}$
I = 0
$|C_3(t)|^2 \times 10^{-1}$
0
1.5
3.0
4.5
TIME x 10^3 (fm/c)

relevant modes indicating that the motion is closer to being stochastic than periodic. These conclusions can be summarized as follows: the initial TDHF trajectory quickly relaxes into a region about the shape isomeric minimum and undergoes a complex, nonlinear motion. Even though the trajectory is focused into the reaction phase space of the isomer, the motion along the path appears to be stochastic and may reflect the formation of a strange attractor near this minimum.

To improve the degree of periodicity, the system must oscillate in the close neighborhood of the isomer. In practice, this can be achieved by localizing the TDHF trajectory via a DCHF minimization to the close proximity of this minimum. To test this idea, we continue the evolution until the system reaches a point in the vicinity of this minimum (after about 700 fm/c). The system is then "cooled" by keeping the density fixed and minimizing the energy. The following evolution starts from this state. Corresponding time-dependence of the isoscalar moments (Fig. 17) are more periodic than the previous calculation, and the dominant low-frequency motion now appears in all of these moments, which must be the case for exact periodicity (see Fig. 18). This trend also continues for the odd isovector moments shown in Figs. 19-20. The even multipoles do not have the expected low-frequency behavior, and they appear to be chaotic. The autocorrelation function associated with the "cooled" motion is shown in Fig. 21. The isoscalar and odd-parity isovector modes show strong correlations in time.

These results are important from the point of view that the quasi-periodic motion represents a known classical limit of quantum

Figure 17. Time dependence of the isoscalar quadrupole, octupole, and hexadecapole moments for the "cooled" modes of the ^{24}Mg system.

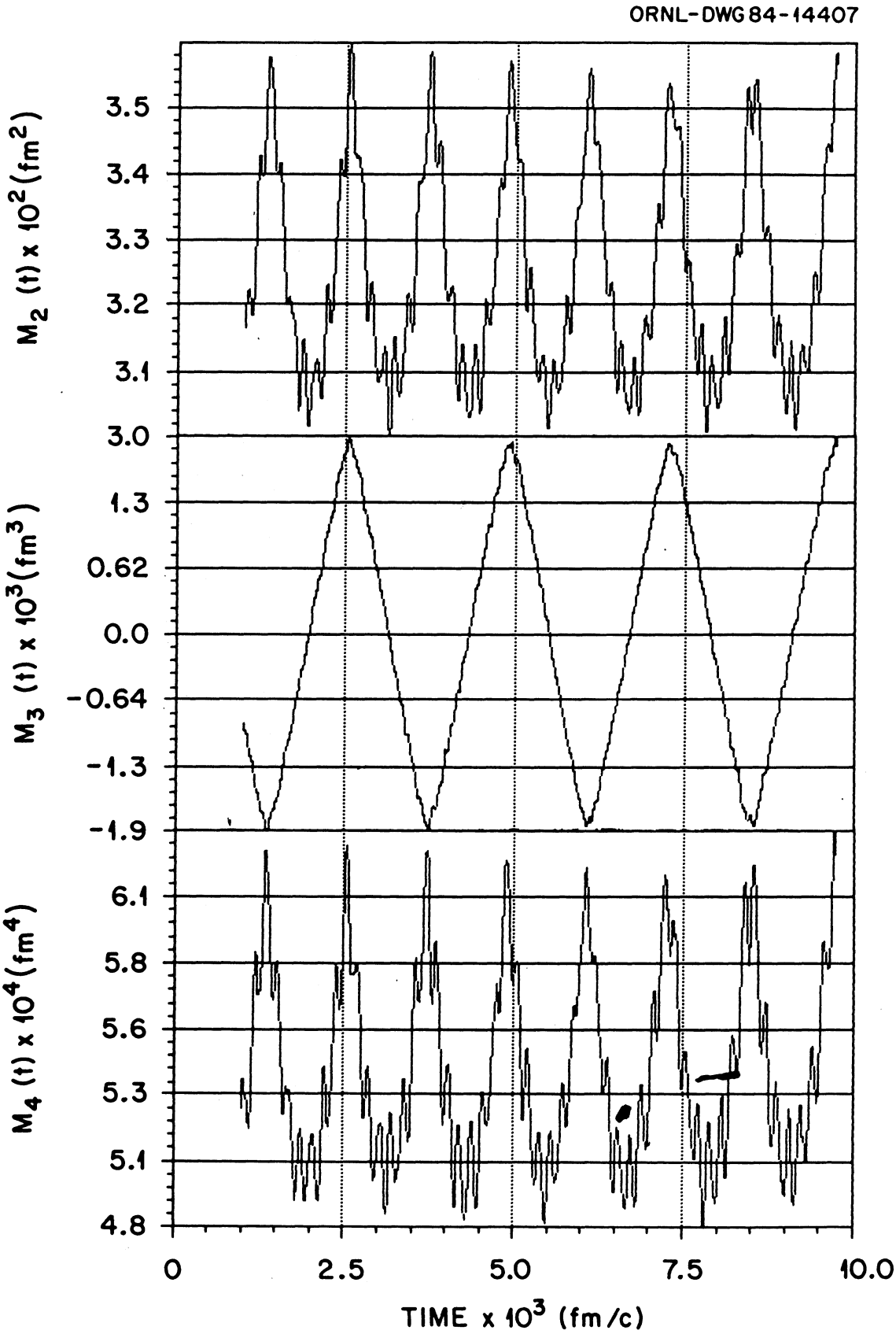
ORNL-DWG 84-14407
M_2 (t) x 10^2(fm^2)
3.5
3.4
3.3
3.2
3.1
3.0
M_3 (t) x 10^3(fm^3)
1.3
0.62
0.0
-0.64
-1.3
-1.9
M_4 (t) x 10^4(fm^4)
6.1
5.8
5.6
5.3
5.1
4.8
0
2.5
5.0
7.5
10.0
TIME x 10^3 (fm/c)

Figure 18. Frequency dependence of the isoscalar quadrupole, octupole, and hexadecapole moments for the "cooled" modes of the ^{24}Mg system.

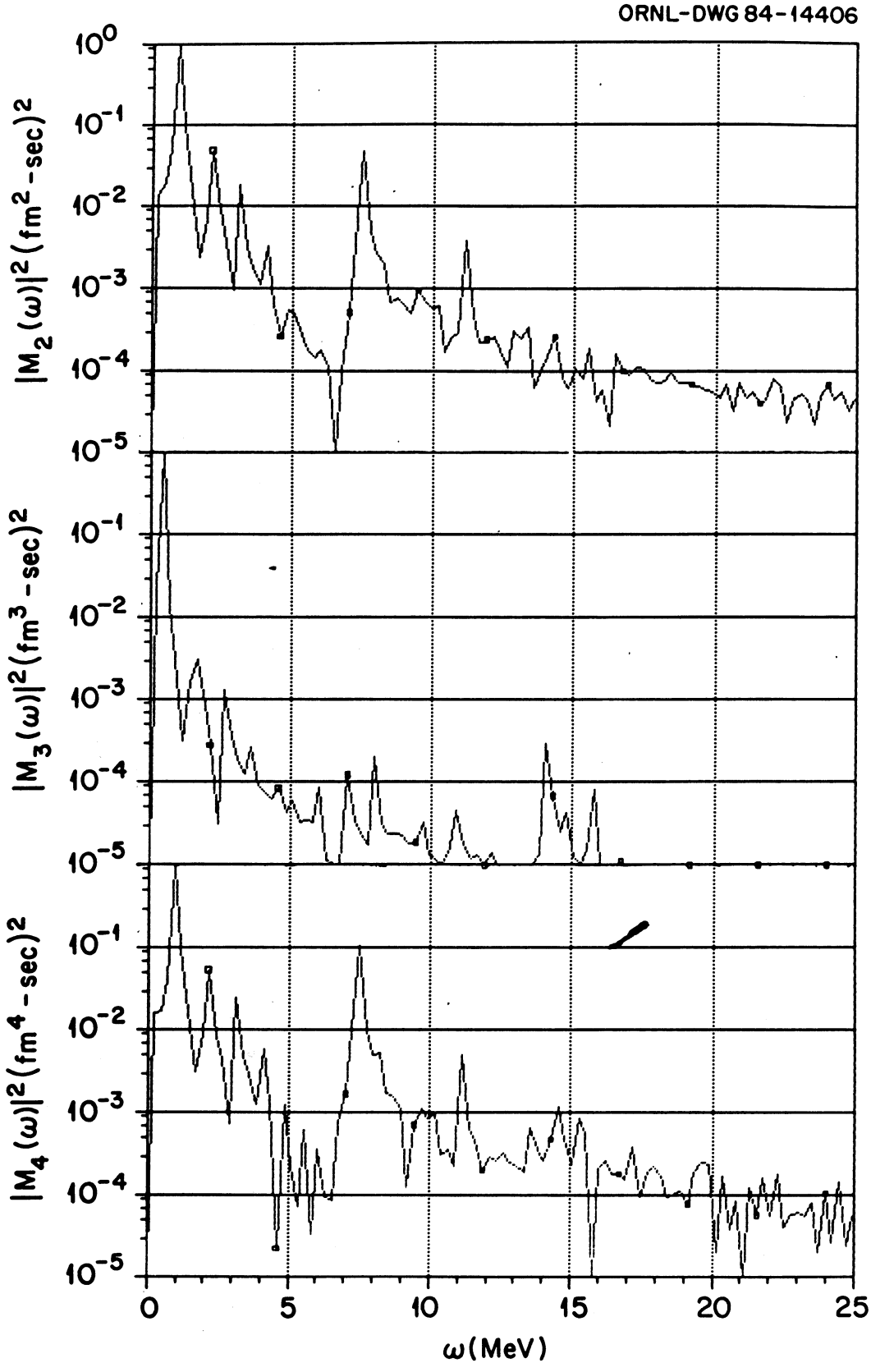
ORNL-DWG 84-14406
$|M_2(\omega)|^2(fm^2-sec)^2$
$|M_3(\omega)|^2(fm^3-sec)^2$
$|M_4(\omega)|^2(fm^4-sec)^2$
10^0
10^{-1}
10^{-2}
10^{-3}
10^{-4}
10^{-5}
0
5
10
15
20
25
ω(MeV)

Figure 19. Time dependence of the isovector dipole, quadrupole, and octupole moments for the "cooled" modes of the ^{24}Mg system.

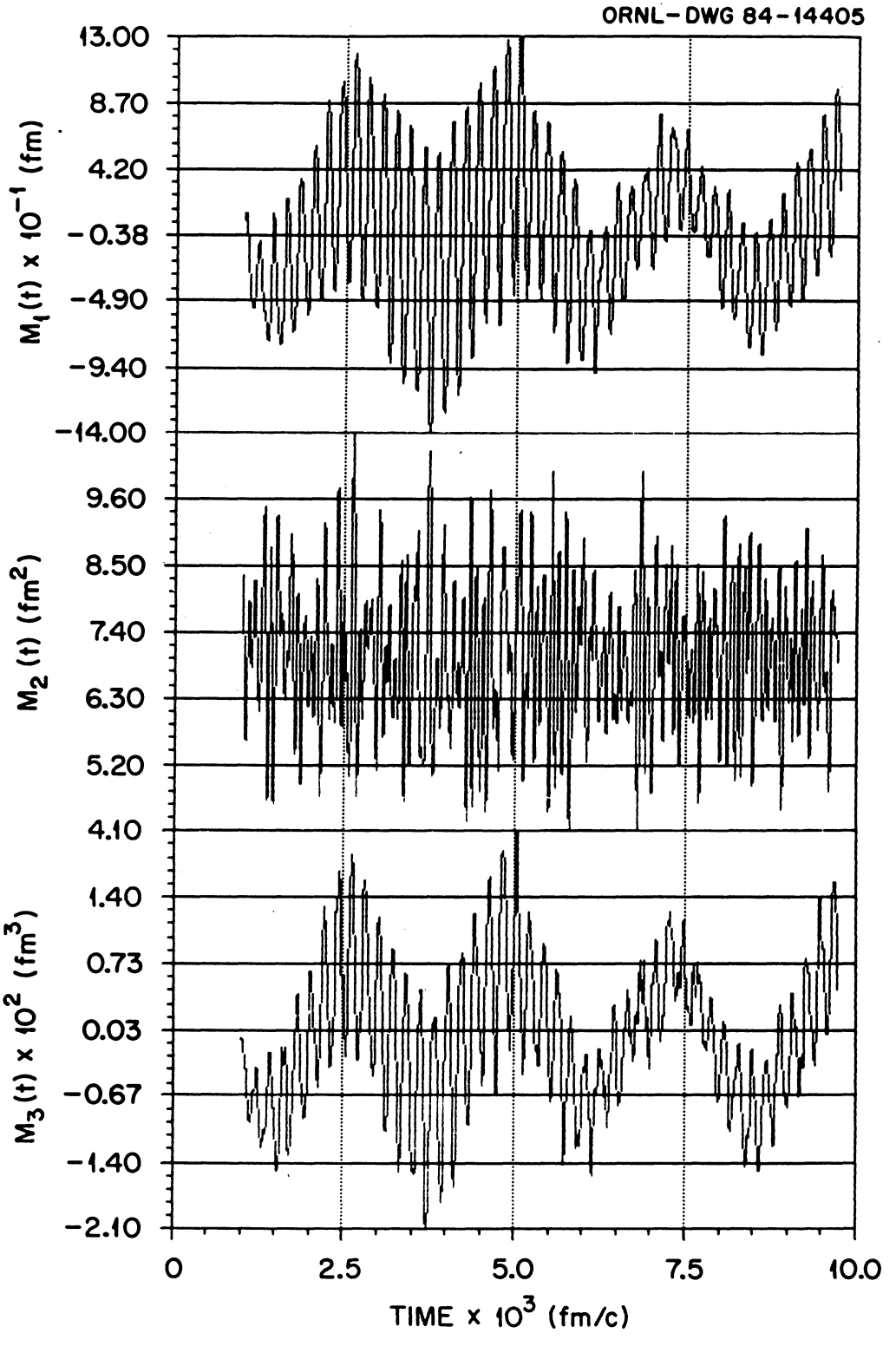
ORNL-DWG 84-14405
13.00
8.70
4.20
-0.38
-4.90
-9.40
-14.00
$M_1(t) \times 10^{-1}$ (fm)
9.60
8.50
7.40
6.30
5.20
4.10
$M_2(t)$ (fm^2)
1.40
0.73
0.03
-0.67
-1.40
-2.10
$M_3(t) \times 10^2$ (fm^3)
0
2.5
5.0
7.5
10.0
TIME x 10^3 (fm/c)

Figure 20. Frequency dependence of the isovector dipole, quadrupole, and octupole moments for the "cooled" modes of the ^{24}Mg system.

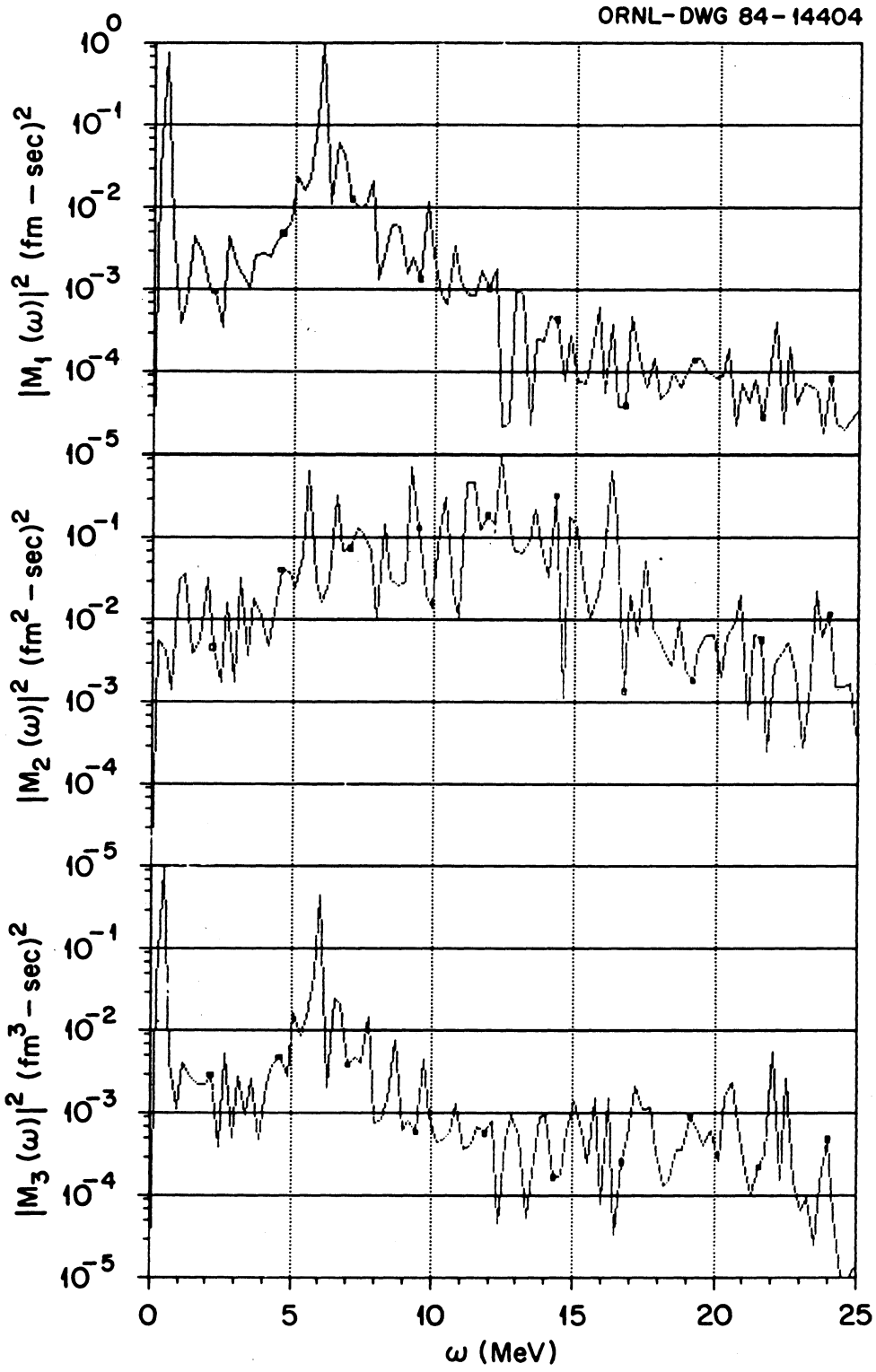
ORNL-DWG 84-14404
$|M_1(\omega)|^2$ (fm − sec)^2
$|M_2(\omega)|^2$ (fm^2 − sec)^2
$|M_3(\omega)|^2$ (fm^3 − sec)^2
10^0
10^{-1}
10^{-2}
10^{-3}
10^{-4}
10^{-5}
0
5
10
15
20
25
ω (MeV)

Figure 21. The autocorrelation function $C_{LI}(t)$ in units $MeV(fm^{L}\text{-}sec)^{2}$ as a function of time for the isoscalar quadrupole and octupole moments for the "cooled" modes of ^{24}Mg.

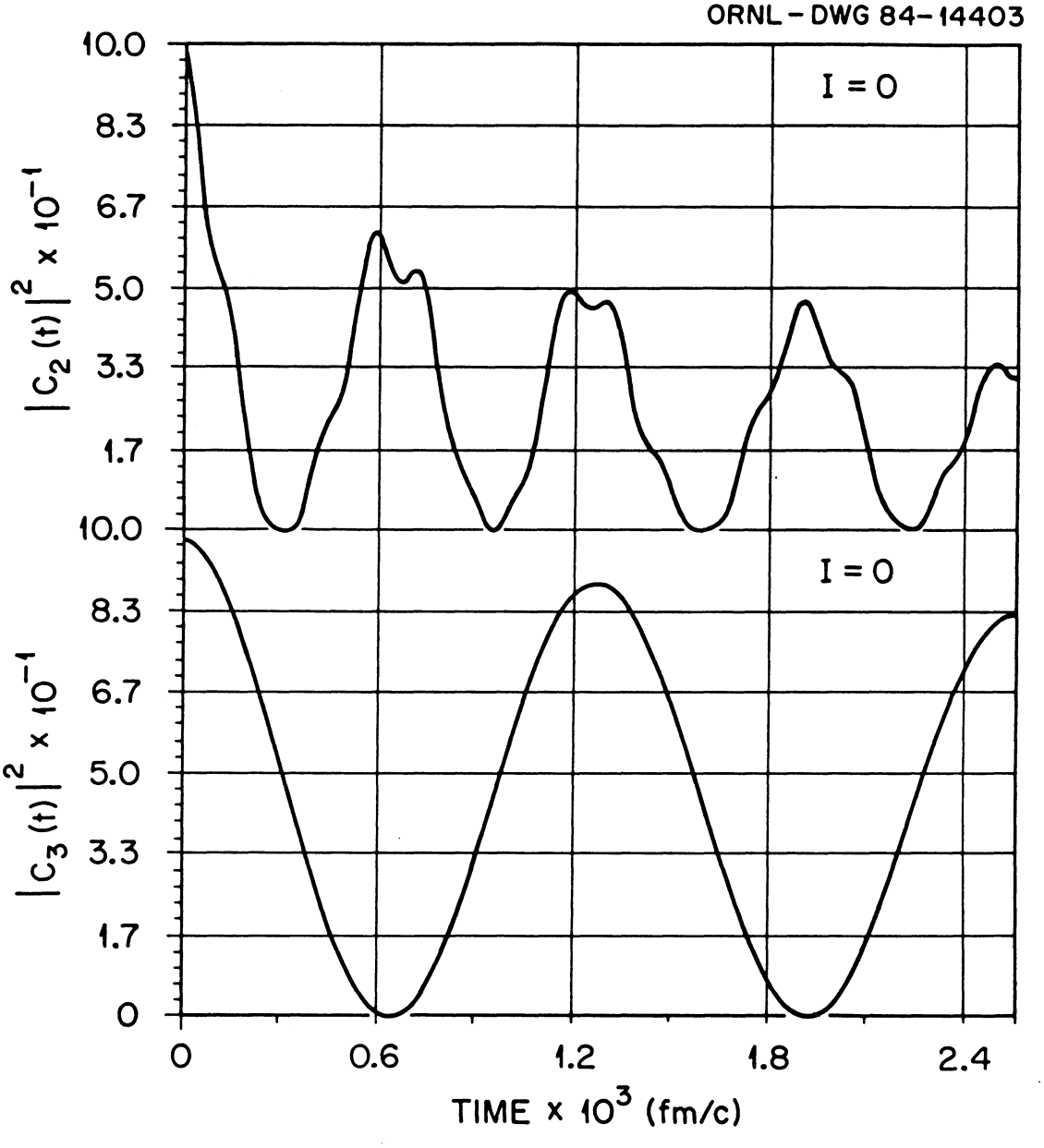
ORNL - DWG 84-14403
I = 0
I = 0
10.0
8.3
6.7
5.0
3.3
1.7
10.0
8.3
6.7
5.0
3.3
1.7
0
0
0.6
1.2
1.8
2.4
$|C_2(t)|^2 \times 10^{-1}$
$|C_3(t)|^2 \times 10^{-1}$
TIME x 10^3 (fm/c)

mechanics, whereas the stochastic motion does not (WK82). It seems that the "trapping" of the TDHF trajectories within the close neighborhood of the shape isomer could be a natural example for studying such a phenomenon.

E. NUCLEAR BREMSSTRAHLUNG

In recent years, the nucleon and pion bremsstrahlung has been widely used to investigate the reaction mechanisms involved in heavy-ion reactions (US84). The inclusive photon spectra obtained during the reaction could also be used for the same purpose.

This section introduces a formalism for photon emission from the charge distributions attained during heavy-ion collisions. The classical treatment of the radiation field results in a continuous spectrum which is related to the time-dependence of the proton density and proton current.

The action S for a system consisting of an electromagnetic field and self-interacting particles is,

$$S = S_N + S_{EM} + S_I \tag{3.7}$$

where S_N is the nuclear action given by Eq. (2.37), S_{EM} is the classical action for the electromagnetic field, and S_I represents the action for the coupling of nuclear and electromagnetic parts. In Gaussian units,

$$\begin{aligned} S_{EM} &= -\frac{1}{16\pi} \int d^4x \; F_{\mu\nu} F^{\mu\nu} \\ S_I &= -\frac{1}{c} \int d^4x \; A_\mu J^\mu \end{aligned} \tag{3.8}$$

with

$$d^4x = dtd^3x.$$

The electromagnetic tensor $F_{\mu\nu}$ is defined as in (Ja75), A_μ is a four-vector having its time component as the scalar potential ϕ and the space component the vector potential $\vec{A}$,

$$A^\mu = (\phi,\vec{A}). \tag{3.9}$$

Similarly, the current four-vector is defined as

$$J^\mu = (c\rho_p,\vec{J}_p), \tag{3.10}$$

where ρ_p and $\vec{J}_p$ are the nuclear proton density and proton current given by Eq. (2.16). The variation of S with respect to the single-particle states yields the TDHF equations (Eq. 2.39) plus a term coming from the variation of S_I, which we neglect. The variation with respect to the fields A_μ, together with the gauge invariance and current conservation, yields the four Maxwell's equations (LL79) in the presence of nuclear densities and currents,

$$\begin{aligned}
\vec{\nabla}\times\vec{B}(\vec{x},t) &= -\frac{1}{c}\frac{\partial E}{\partial t} + \frac{4\pi}{c}\vec{J}_p(\vec{x},t) \\
\vec{\nabla}\cdot\vec{B}(\vec{x},t) &= 0 \\
\vec{\nabla}\times\vec{E}(\vec{x},t) &= -\frac{1}{c}\frac{\partial\vec{B}}{\partial t} \\
\vec{\nabla}\cdot\vec{E}(\vec{x},t) &= 4\pi\rho_p(\vec{x},t).
\end{aligned} \tag{3.11}$$

Using the Fourier transforms,

$$\rho_p(\vec{x},t) = \int_{-\infty}^{+\infty} \frac{d\omega}{2\pi} \exp(-i\omega t)\rho_p(\vec{x},\omega)$$

$$\vec{J}_p(\vec{x},t) = \int_{-\infty}^{+\infty} \frac{d\omega}{2\pi} \exp(-i\omega t)\vec{J}_p(\vec{x},\omega), \tag{3.12}$$

Maxwell's equations for each frequency component become

$$\vec{\nabla}\times\vec{B}(\vec{x},\omega) + \frac{i\omega}{c}\vec{E}(\vec{x},\omega) = \frac{4\pi}{c}\vec{J}_p(\vec{x},\omega)$$

$$\vec{\nabla}\cdot\vec{B}(\vec{x},\omega) = 0$$

$$\vec{\nabla}\times\vec{E}(\vec{x},\omega) = i\omega/c\ \vec{B}(\vec{x},\omega) \tag{3.13}$$

$$\vec{\nabla}\cdot\vec{E}(\vec{x},\omega) = 4\pi\rho_p(\vec{x},\omega).$$

The multipole solution of these equations together with the continuity equation,

$$\vec{\nabla}\cdot\vec{J}(\vec{x},\omega) = i\omega\rho_p(\vec{x},\omega), \tag{3.14}$$

can be obtained by following the method of (Ja75), the only difference being that in our case the Eqs. (3.13-3.14) have to be solved for each frequency component. The asymptotic multipole solution can be written as

$$\vec{B}(\vec{x},\omega) = \frac{e^{ik\rho}}{k\rho}\sum_{LM}(-i)^{L+1}\,a(L,M,\omega)\vec{L}\,Y_{LM}(\hat{\rho})$$

$$\vec{E}(\vec{x},\omega) = \vec{B}(\vec{x},\omega)\times\hat{\rho}, \tag{3.15}$$

where

$$a(L,M,\omega) = \frac{4\pi}{i(2L+1)!!}\left(\frac{L+1}{L}\right)^{1/2}\left(\frac{\omega}{C}\right)^{L+2}$$

$$\times\int_{-\infty}^{+\infty} dt\ \exp(i\omega t)\int d^3\hat{x}\ R^L\ \vec{Y}_{LM}(R)\rho_p(x,t). \tag{3.16}$$

In these expressions ρ denotes an asymptotic distance to the detector,

and the wavenumber k = w/c. Implicit in the solution of these equations is the long-wavelength approximation for the photon. We assume that the wavelength of the photon,

$$\lambda = 2\pi \frac{197.466}{E(MeV)} \quad [fm], \tag{3.17}$$

is much larger than the size of the source $(kr_{max} << 1)$. One interesting outcome of Eqs. (3.15-3.16) is the fact that each term in the multipole expansion of $\vec{E}$ and $\vec{B}$ fields is determined by the time-development of the projection of the same multipole from the proton density.

To calculate the energy spectrum, we define the total radiated energy as an integral,

$$W = \int d\Omega d\omega \frac{d^2W}{d\Omega d\omega}. \tag{3.18}$$

Also, from the knowledge of the Poynting vector $\vec{S}(\vec{x},t)$ one has,

$$W = \int_{-\infty}^{+\infty} dt\ \vec{S}(\vec{x},t)\cdot d\vec{A}, \tag{3.19}$$

where $d\vec{A}$ is the surface area in the radial direction defined by the solid angle $d\Omega$ of the cone

$$d\vec{A} = \hat{\rho}\rho^2 d\Omega.$$

The time integral can be done in the following way,

$$W = \frac{c}{4\pi} \int_{-\infty}^{+\infty} dt\ [E^*(\vec{x},t) \times \vec{B}(\vec{x},t)]\cdot d\vec{A}$$

$$= \lim_{\omega\to 0} \frac{c}{4\pi} \int_{-\infty}^{+\infty} dt\ \exp(i\omega t)[E^*(\vec{x},t) \times \vec{B}(\vec{x},t)]\cdot d\vec{A}.$$

Using the Fourier tranforms for $\vec{E}$ and $\vec{B}$, this becomes

$$W = \int d\omega d\Omega \ \frac{c}{8\pi^2} \left[\vec{E}^*(\vec{x},\omega) \times \vec{B}(\vec{a},\omega)\right]\cdot\hat{\rho}\ \rho^2. \tag{3.20}$$

Using Eq. (3.15) and comparing with Eq. (3.18), one can write

$$\frac{dW}{d\Omega d\omega} = \frac{c}{8\pi^2}\left(\frac{c}{\omega}\right)^2 \sum_{\substack{LM \\ L'M'}} (i)^L(-i)^{L'+1}\ a^*(L,M,\omega)a(L',M',\omega) \times \left(\vec{L}\ Y_{LM}\right)^*\cdot\left(\vec{L}'\ Y_{L'M'}\right). \tag{3.21}$$

Integration over $d\Omega$ yields,

$$\frac{dW}{d\omega} = \frac{c}{8\pi^2}\left(\frac{c}{\omega}\right)^2 \sum_{LM} \left| a(L,M,\omega)\right|^2 . \tag{3.22}$$

The final expression for the classical approximation to the inclusive photon spectrum is given by

$$\frac{dN_\gamma}{d(\hbar\omega)} = \frac{\hbar c}{8\pi^2}\frac{1}{(\hbar\omega)^3}\sum_L (2L+1)\left| a(L,\hbar\omega)\right|^2 , \tag{3.23}$$

where we have performed the M summation using the property of axial symmetry for the proton density,

$$a(L,\hbar\omega) = K_L\left(\frac{E}{\hbar c}\right)^{L+2}\int_{-\infty}^{+\infty} c\ dt\ e^{-iEt/\hbar}\int [2\pi r dr dz] R^L\ Y_{LO}(\hat{R})\rho_p(r,z;t)$$

$$K_L = \frac{4\pi}{(2L+1)!!}\left(\frac{L+1}{L}\right)^{1/2} e \tag{3.24}$$

In this expression e denotes the unit charge, and energy E is $E = \hbar\omega$.

The spectrum for the bremsstrahlung generated by the oscillating proton density of the "cooled" system can be calculated from Eq. (3.23). The magnitude of the spectra falls rapidly with increasing value of L. Figure 22 shows this spectra for the dipole, quadrupole and octupole modes.

Figure 22. The γ spectrum, dN_γ/dE (MeV^{-1}), as a function of the γ energy, E(MeV), for the "cooled" modes of the ^{24}Mg system.

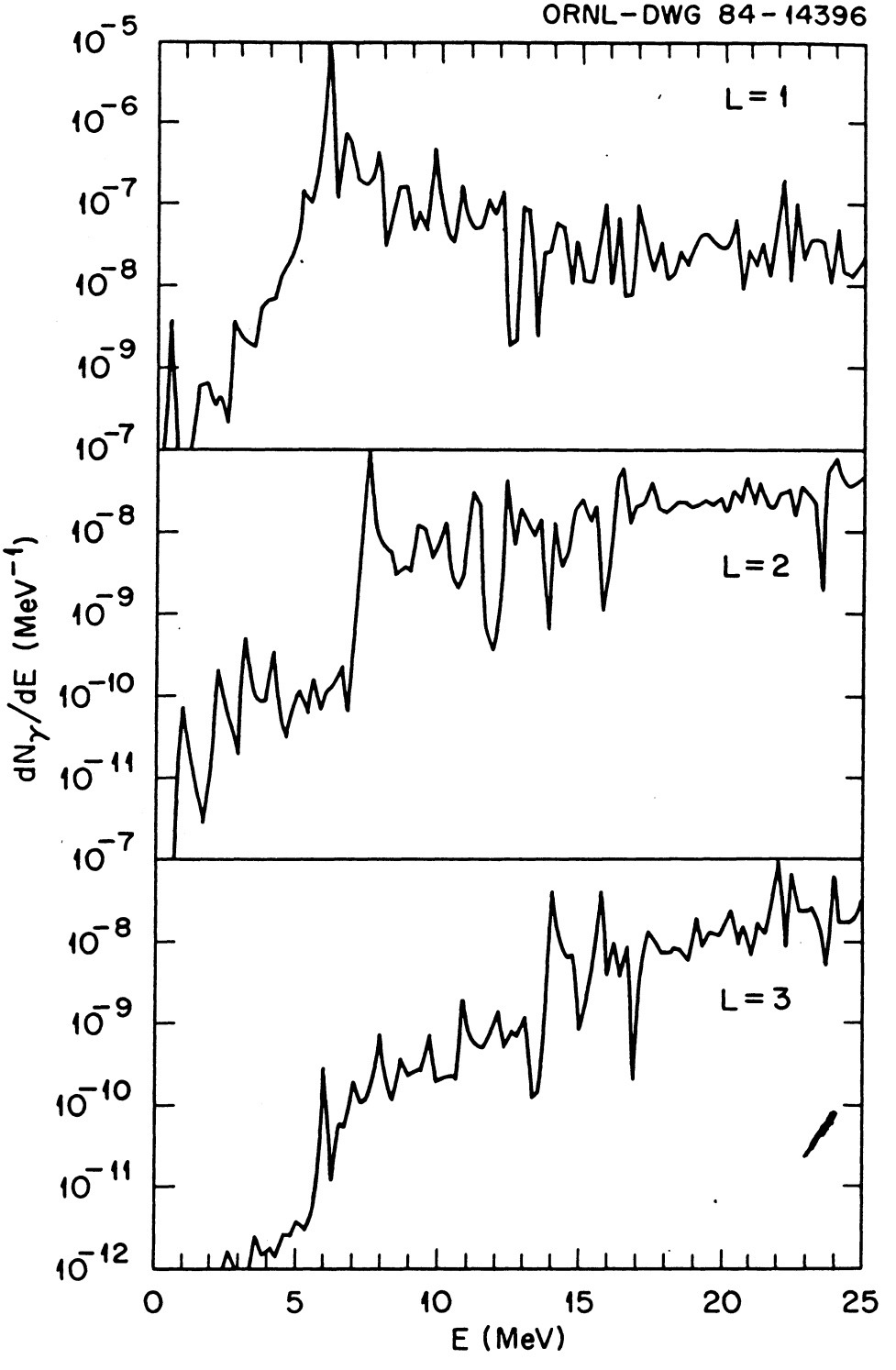
ORNL-DWG 84-14396
L=1
L=2
L=3
dNγ/dE (MeV⁻¹)
E (MeV)
10⁻⁵
10⁻⁶
10⁻⁷
10⁻⁸
10⁻⁹
10⁻⁷
10⁻⁸
10⁻⁹
10⁻¹⁰
10⁻¹¹
10⁻⁷
10⁻⁸
10⁻⁹
10⁻¹⁰
10⁻¹¹
10⁻¹²
0
5
10
15
20
25

IV. A LINEAR RESPONSE CALCULATION

In the TDHF studies of nuclear molecules the focusing of the trajectories onto a region about the shape isomeric minimum was observed. Despite this fact, there are numerous ambiguities and deficiencies associated with this approach. The nonlinearities inherent in TDHF equations lead to non-periodic behavior of the solutions. As a consequence, the observed frequencies are not comparable to the experimental molecular spectra. Another ambiguity has to do with the initialization of the ions. In the case of $^{12}C + ^{12}C$ we have seen that one has to start with two ^{12}C using correlated wavefunctions which also contain admixtures of other configurations and in particular an admixture of configuration B. This might influence the results obtained in the previous chapter, in the sense that the details of how the reaction proceeds may lead to different isomers. Futhermore, TDHF is a theory which is valid in the long mean free path (mean field) approximation. The relaxation of this approximation in principle could lead to a faster equilibration of energy, thus bringing the system closer to the isomer where the motion will be more periodic. In addition, there is the uncertainty about the correct excitation energy of the isomer with respect to the ground state. This problem can be surmounted by calculating the complete spectrum which will then differ from the experimental one by a constant shift in energy.

On the other hand, the classification of the data given by Eq. (1.2) allows to draw simple conclusions about the $^{12}C+^{12}C$ molecular

configuration. If one ignores the doubling or sometimes tripling of the resonances shown in Fig. 2, then a single sequence of I values, belonging to each rotational band, implies that we are dealing with an axially symmetric body constrained to rotate about an axis perpendicular to the symmetry axis. Also, the close agreement with the I(I+1) rule for the members of the rotational bands indicates that the intrinsic motion of the system may be separated from the rotations of the rigid body as a whole (at least for low I states).

The TDHF calculations mentioned above were restricted to axially symmetric geometry. To establish the correct symmetries of the ^{24}Mg isomer under consideration three-dimensional constrained Hartree-Fock calculations (Um82) (a constraint on the quadrupole moment), using oscillator basis expansion up to nine major oscillator shells in Cartesian coordinates, were performed. For the BKN force (the same force used in TDHF calculations) the ground state of ^{24}Mg is found to be a triaxial nucleus with a quadrupole moment of 43 fm^2 whereas the shape isomer corresponds to an axially symmetric configuration with a quadrupole moment of 110 fm^2. These results are also in agreement with Nilsson-Strutinsky calculations (LL75) using phenomenological interactions including the spin-orbit contribution, and other Hartree-Fock calculations (Mu67). In the case of the BKN force the isomer is 12.1 MeV higher than the lowest energy Hartree-Fock configuration. Table 4 shows the deformation and the energy of the isomer for various parametrizations of the Skyrme force. In this table the lowest energy configuration is the axially symmetric approximation to the true triaxial

Table 4. Properties of the ^{24}Mg isomer for various parametrizations of the Skyrme interaction. The ground state configuration is an axially symmetric approximation to the true triaxial ground state and its energy should be taken by caution.

Table 4

Force	E(g.s.) (MeV)	E(*) (MeV)	Q_{20}(g.s.) (fm^2)	Q_{20}(*) (fm^2)
I	-188.78	-182.45	40.91	97.26
II	-188.25	-188.58	42.61	103.4
SkM*	-181.48	-176.16	43.82	104.7
BKN	-179.72	-171.40	42.32	100.0

configuration, and its energy should be interpreted with caution. For the Skyrme I force the density contours of the isomer are shown in Fig. 23. As we see, the structure is considerably different than that of two touching carbons. The structure resembles that of two alpha-like (possibly ^{8}Be) structures attached to a ^{16}O-like structure. It is more probable that in the experiment $^{12}C(^{12}C,^{16}O)^{8}Be$ (WS77) the ^{16}O could be found in its well-known 4p-4h shape isomeric 0^+ state at 6.06 MeV (BG66).

In Fig. 24 a three-dimensional object together with the third component of a body-fixed coordinate system and the z component of a space-fixed coordinate system is shown. The orientation of the body involves three Euler angles (θ,ϕ,γ), and three quantum numbers are needed to specify the state of the motion. The total angular momentum I and its component on the space-fixed z-axis, M, provide two of these quantum numbers. Third is the component of I on the body-fixed axis of symmetry, K. Since we are dealing with an even-even nucleus, where each nucleon is paired with another, the I^{π} of the shape isomer is 0^+. The component of the angular momentum onto the symmetry axis is also zero, $K^{\pi} = 0^+$. As a consequence of axial symmetry, K is a constant of the motion. This is merely a statement that there are no collective rotations about the axis of symmetry. It then follows that the quantum number K represents the angular momentum of the intrinsic motion and has a fixed value for the rotational band based on a given intrinsic state (BM75).

The axially deformed Hartree-Fock wavefunction of the isomer is

Figure 23. Density contours of the shape isomeric configuration of ^{24}Mg using the Skyrme I force. The contour labeled 8 corresponds to 0.15 nucleons/fm^3 and each subsequent contour falls by a factor of two.

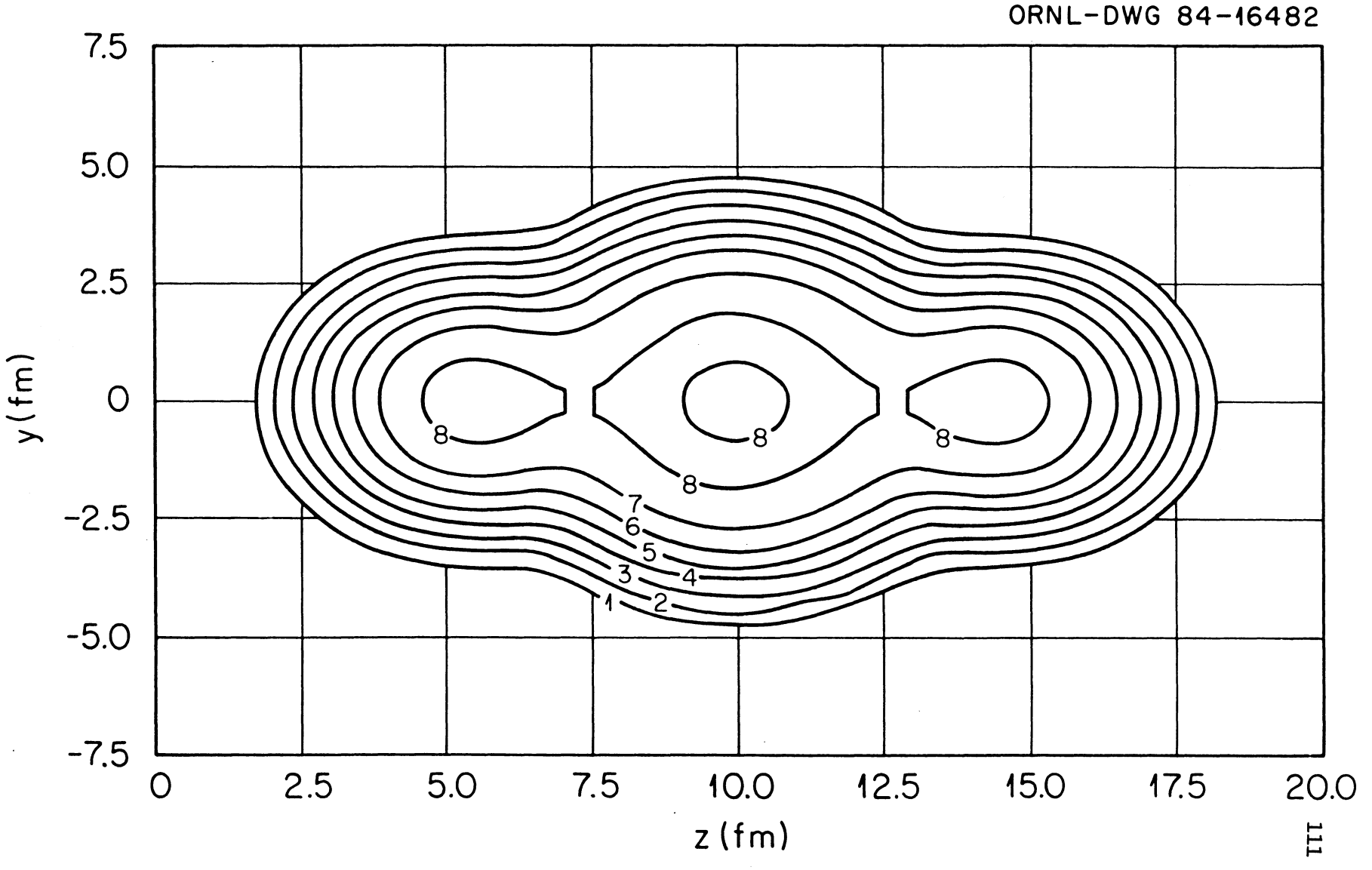
ORNL-DWG 84-16482
7.5
5.0
2.5
0
-2.5
-5.0
-7.5
y (fm)
0
2.5
5.0
7.5
10.0
12.5
15.0
17.5
20.0
z (fm)
8
8
8
8
7
6
5
4
3
2
1

Figure 24. Definitions of various quantities for a deformed body. The axis labeled Z belongs to a space-fixed coordinate system, whereas axis z belongs to a body-fixed frame and in the axis of symmetry. Vector I is the total angular momentum having a component K on the axis of symmetry and a component M on the body-fixed Z-axis.

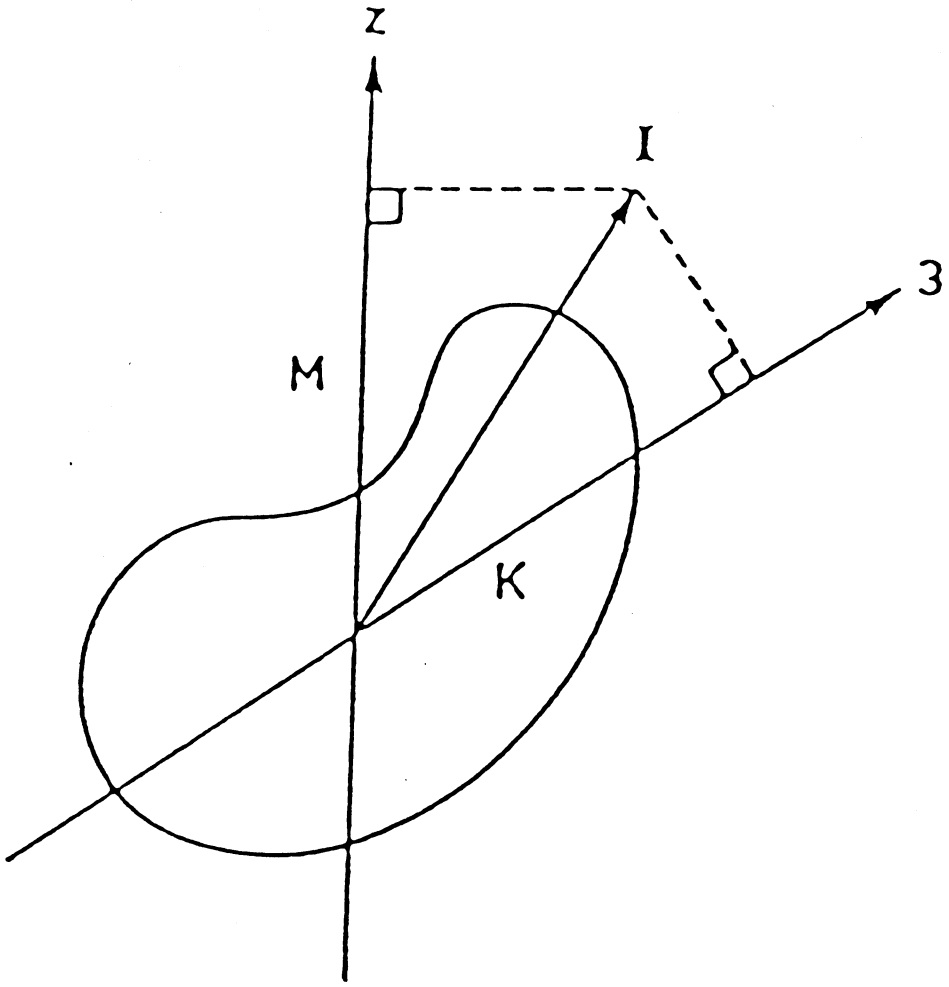
Z
I
3
M
K

not rotationally symmetric and has a preferred direction in space. In principle, it is possible to define a collective rotation of the nucleus which would restore this symmetry (KO77). This rotation, in general, would affect the intrinsic structure of the nucleus. However, the coupling of intrinsic and rotational degrees of freedom becomes important for the high angular momentum states, but could be ignored or treated perturbatively for low angular momenta. As mentioned previously, the experimental justification for neglecting the effects of rotations on the intrinsic motion comes from the fact that the low-lying states of at least six rotational bands in the $^{12}C+^{12}C$ molecular data can be described by a single value for the moment of inertia and with a clear I(I+1) dependence. In this case, the total Hamiltonian for the nucleus can be written as a sum of intrinsic and rotational parts (BM75) (for notational simplicity the intrinsic coordinates will not be explicitly shown),

$$H = H_{int} + h_o \hat{I}^2, \tag{4.1}$$

where h_o depends on the intrinsic coordinates. One should also note that in the collective model, for an axially symmetric nucleus with K = 0, this decoupling is exact (RS80). The vibrational energies associated with H_{int} will be calculated by using the linear response theory developed in section (II.F). Under these conditions, the wavefunction of the nucleus will be of product form

$$| \Psi_{K=0,\nu} \rangle = | X_\nu \rangle \, | Y_{IM}(\theta,\phi) \rangle, \tag{4.2}$$

where X_ν denotes the excited states of H_{int}, and the Legendre functions are the special case of rotation matrices for K = 0 (BM75). The

rotational band for a given vibrational energy E_ν,

$$E_\nu = \langle X_\nu \mid H_{int} \mid X_\nu \rangle, \tag{4.3}$$

becomes

$$E(\nu,I) = E_\nu + \frac{\hbar^2}{2\mathcal{I}_\nu} I(I+1) \tag{4.4}$$

where the moment of inertia $\mathcal{I}_\nu$ is defined through

$$\frac{\hbar^2}{2\mathcal{I}_\nu} \equiv \langle X_\nu \mid h_o \mid X_\nu \rangle. \tag{4.5}$$

Since the moment of inertia is not expected to change appreciably for the small amplitude oscillations about the equilibrium, it can be taken to be constant.

Another restriction on the rotational degrees of freedom comes from the fact that the intrinsic Hamiltonian of the isomer is invariant with respect to 180° rotations about an axis perpendicular to the symmetry axis. This implies that these rotations are part of the intrinsic degrees of freedom and therefore should be excluded from the rotational degrees of freedom. One way of achieving this is to demand that the operator R_e, which performs this rotation by acting on the rotational part of the wavefunction, is the same as the operator R_i, which does the same rotation by acting on the intrinsic wavefunction. Since R_i acting on the intrinsic state has an eigenvalue +1 (invariance), the operator R_e acting on the rotational part ($\theta \to \pi-\theta, \phi \to \pi+\phi$),

$$R_e \mid Y_{IM}(\theta,\phi)\rangle = (-1)^I \mid Y_{IM}(\theta,\phi)\rangle, \tag{4.6}$$

has to have the same eigenvalue. This condition restricts I to even integers only.

To calculate the vibrational spectra, we compute the strength

function $S(\omega)$ of Eq. (2.53) for a transition operator

$$f(\vec{r}) = \begin{cases} \lambda \sum_{i=1}^{A} r_i^L \, Y_{L0}(\hat{r}_i) & , \quad L \neq 0 \\ \lambda \sum_{i=1}^{A} r_i^2 & , \quad L = 0. \end{cases} \tag{4.7}$$

The time dependence of the external field is chosen to be a delta function in time. Because of this delta function, all of the frequencies are excited by the same field. The strength parameter λ was chosen to assure an undamped motion. During the time evolution, the mass number was conserved to better than one part in 10^7 using $\lambda = 0.005$. Making λ smaller does not change any of the results presented here whereas larger values lead to the dampening of the motion due to the emission of the particles which reflect from the walls of the numerical box. The box size used was 20 fm in z and 7.5 fm in r direction with a uniform mesh spacing of 0.5 fm. The time discretization was done with a 0.5 fm/c time-step, and the small amplitude motion was followed up to 16,400 fm/c. This number of time points (2^{15}) is large enough to allow a fast Fourier transform with 75 keV accuracy. The numerical method of solving the TDHF equations presented in Section (II.G) allow the conservation of the total energy to an arbitrary accuracy.

As a check of the linear response formalism and the numerical accuracy, the isoscalar L=2,3,4 giant resonances are calculated for the ^{16}O nucleus. The Hartree-Fock wavefunctions for the spherical ^{16}O nucleus was obtained by the Skyrme II force. Despite the fact that in these calculations the spin-orbit part of the Skyrme interaction was

neglected, the comparison to the full continuum RPA calculations of Ref. (KK77) is excellent. Table 5 tabulates the centroid energies obtained in these calculations together with those of Ref. (KK77).

We next calculate the vibrational states associated with the axially symmetric isomer of ^{24}Mg. Since the THDF equations are solved in axial geometry, this symmetry is always preserved. Thus, the possible vibrational modes are superpositions of vibrations which are parallel and perpendicular to the symmetry axis of the nucleus (AB83), and they can be excited by using an external field $\lambda\ r^2$. The non-axial vibrations are not included, and they are assumed to lie higher in energy. In Fig. 25(a) the time development of the nuclear radius is plotted for the Skyrme I force. The evolution is nearly periodic with slight damping at very large times. The strength function shown in Fig. 25(b) contains six peaks whose centroid energies are tabulated in Table 6. As we see, the spurious zero-frequency peak appears exactly at zero energy which is an indication of the removal of the zero-point energy and the sufficiency of the box size chosen. In the same table we also show the same quantity for the Skyrme M^* force, together with the experimental (I=0) levels and the vibrational energies of the U(4) model. At this point, one should note that the calculated spectrum can be shifted by a constant energy due to the uncertainty in the excitation energy of the isomer. For this table, the lowest vibrational energy was assumed to coincide with that of the U(4) model. The situation for the Skyrme II force is considerably different. For this force, one sees many peaks between 0-7 MeV which do not allow a clear

Table 5. Comparison of the ^{16}O giant resonances calculated in this dissertation and RPA calculations.

Table 5

L	E (this work) (MeV)	E (RPA) (MeV)
2	23.4	24.1
3	9.71	10.2
4	28.3	28.2

Figure 25. a) Time evolution of the nuclear radius for the oscillating ^{24}Mg system (Skyrme I). b) The strength function $S(\omega)$ showing the vibrational frequencies built on the ^{24}Mg isomer.

ORNL-DWG 84-16481

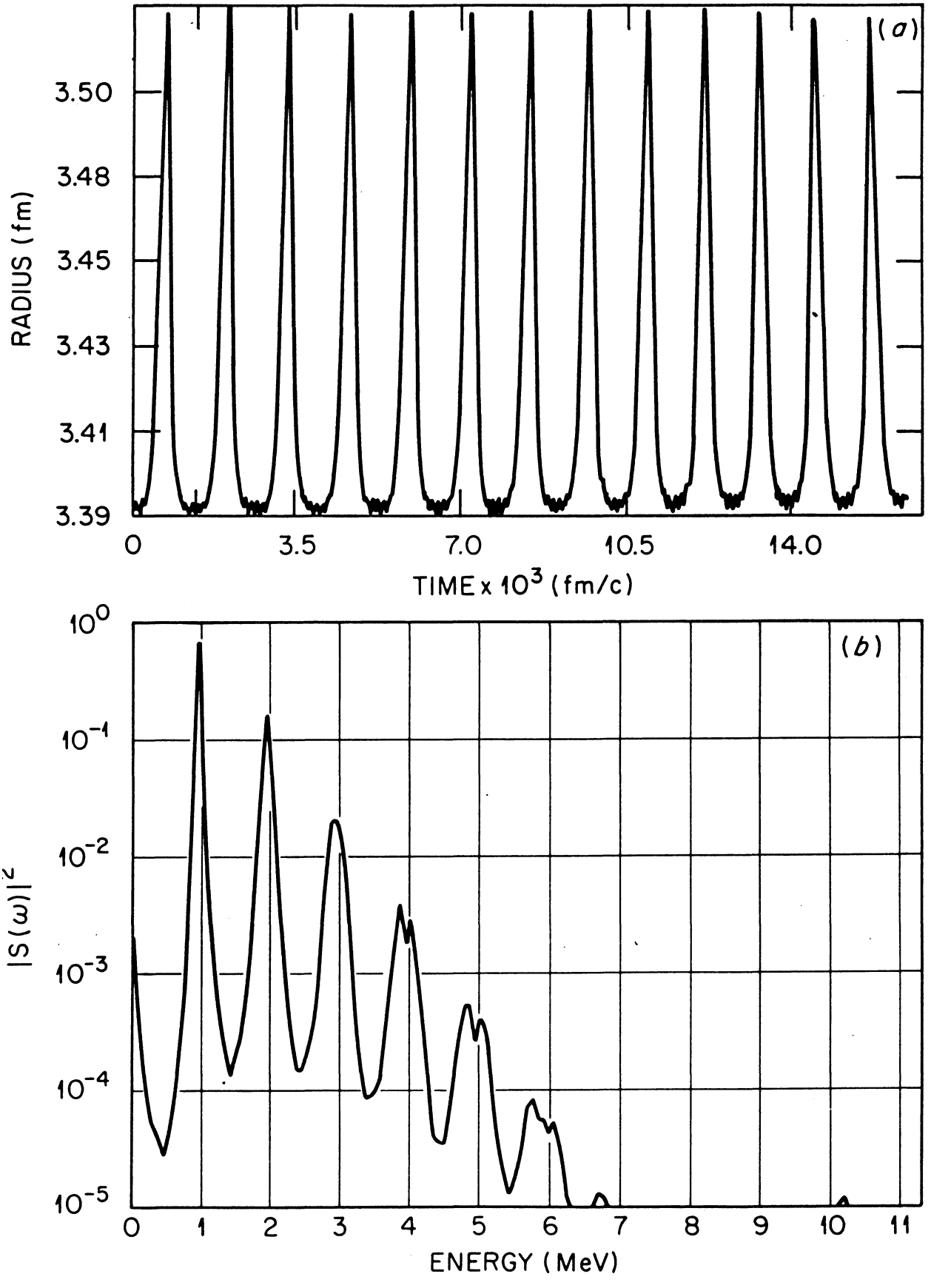

Table 6. Comparison of the experimental (I=0) energies with the results of the present calculation and the vibrational energies of the U(4) model. The data and U(4) energies are from Ref. (EB81).

Table 6

Skyrme I (MeV)	Skyrme M* (MeV)	Experimental (MeV)	U(4) (MeV)
0.98	1.01	-	1.04
1.97	2.12	-	2.58
3.01	3.08	3.17-3.35	3.44
4.00	4.13	4.25	4.44
4.80	5.06	-	5.20
5.75	5.90	5.80	5.84

identification of the vibrational energies. Furthermore, the period of oscillations is about 0.7 times smaller than that of the Skyrme I and M^* forces. These differences between Skyrme I and Skyrme II forces have been observed previously in the calculation of giant resonances (BT75), and they may be attributed to the large differences between the effective masses of these forces as shown in Table 3. Also from Table 4, we note that for Skyrme II force the axially symmetric ground state of ^{24}Mg has about the same energy of the isomer whereas the situation for the other forces is different.

The calculated energies shown in Table 6 are approximately equidistant. Furthermore, the crossover transitions to the ground state of the isomer fall rapidly with the increasing excitation energy. These characteristics suggest that the resonances are multiple excitations from the ground state of the isomer. This is indeed possible, since in the calculation of the response function [Eq. (2.54)], we did not make the harmonic approximation (BT75)

$$\rho(\vec{r},t) = \rho_o(\vec{r}) + \left(\rho^{(1)}(\vec{r})e^{-i\omega t} + c.c.\right).$$

In principle, one could not completely decouple the vibrations that are parallel (longitudinal) and perpendicular (transverse) to the symmetry axis. In order to gain further insight about the nature of the vibrations, one can study the response function for longitudinal and transverse motion by choosing $f(\vec{r})$ as r and $(z-z_{cm})^2$ respectively. The motion in longitudinal direction appears to be large amplitude ($\Delta z \approx$ 4.2 fm) with a very smooth time evolution, whereas the motion in transverse direction is perturbative ($\Delta r < 0.02$ fm) indicating that it is

due to the coupling of the two modes. This result is in agreement with the fact that for strongly deformed nuclei the vibrations in the direction of the smallest incompressibility (for prolate nuclei the longitudinal direction) will produce the low-energy components of the collective excitation. Using the energies from Table 6, together with Eq. (4.4), one gets a relatively good fit to the molecular data provided one uses the empirical moment of inertia of 6.5 MeV^{-1}. The rigid-body moment of inertia of the isomer is 6 MeV^{-1}.

Recently, γ-decay of the 14^+ resonance at E_{cm} = 25.7 MeV to 12^+ state at 19.3 MeV in the $^{12}C+^{12}C$ system has been experimentally observed. The branching ratio (6×10^{-7}) was found to be order of magnitude smaller than expected for E2 radiation emitted by a rigidly rotating di-nuclear complex. Consequently, other mechanisms were suggested as the source of the fine-structure resonances. However, these conclusions are in conflict with the findings of this dissertation. Leaving aside the sensitivity of the results to the details of the experimental procedures, the assumed value of the quadrupole moment, corresponding to the di-nuclear complex (180 fm^2), is considerably larger than the calculated value for the shape isomeric configuration of ^{24}Mg (100 fm^2). Since the electromagnetic transition strength is proportional to the square of the quadrupole deformation, one has to be careful when making predictions based on this value. It is also not clear whether the 14^+ and 12^+ states belong to the same rotational band. In such a case, the transition strength between rotational states belonging to different rotational bands will be drastically reduced due to the

differences in the intrinsic configurations. In conclusion, these experiments do not seem convincing enough to rule out the possibility that these states are built on the composite nuclear system. Furthermore, there exists, as mentioned in the Introduction, a considerable number of particle-decay experiments, which indicate otherwise.

V. CONCLUSION

The origin of the correlated resonances observed in the collisions of light systems has been one of the outstanding questions in low-energy heavy-ion physics. This dissertation addressed this issue from a microscopic standpoint. Unlike previous microscopic calculations, those presented here make no a priori assumptions about the many-body dynamics. In the time-dependent Hartree-Fock calculations of the d dynamics the formation of a nuclear molecule was identified by its long-lived cluster-like character with a definite memory of the entrance channel configuration. Using the newly developed density constrained Hartree-Fock formalism, the position of the time-dependent Hartree-Fock trajectory with respect to the multi-dimensional energy surface of the composite nuclear system was traced. For all of the systems studied ($^{4}He + {}^{14}C$, $^{12}C + {}^{12}C(0^{+})$, $^{4}He + {}^{20}Ne$) the dynamic path was found to be localized about a shape isomeric minimum of the composite system. This result clearly establishes the connection between the observed molecular resonances and the states built on these isomers. In addition, the dynamics are found to be strongly dependent on the inelastic excitations of the target and/or projectile (like in the $^{12}C+{}^{12}C(0^{+})$ case).

The limitations of the time-dependent Hartree-Fock theory, mentioned in Chapters III and IV, do not allow the extraction of detailed quantum-mechanical information concerning the states built on these isomers. To accomplish this, one needs to perform a nuclear structure

calculation. Here, the Hartree-Fock theory, together with the realistic Skyrme interaction, was used to calculate the axially symmetric shape isomer of ^{24}Mg. A linear response calculation, limited only to axially symmetric vibrations, was carried out to determine the states built on this configuration. The results established a multiple excitation of a vibrational mode (I = 0), which has vibrational spacing of approximately 1 MeV, in agreement with the data and the U(4) model.

In summary, this dissertation introduces microscopic evidence relating the observed molecular resonances to the states built on the shape isomeric minimum of the composite nuclear system. Extension of this study is dependent on the development of nuclear structure calculations for strongly deformed configurations. Consideration of non-axial vibrations, effects of rotations on intrinsic configurations, and the dependence of results on effective interactions are some of the possible ways to further pursue the problem.

APPENDIX A

In this appendix the derivation of the Skyrme energy density will be outlined. The derivation is without the spin-orbit interaction.

A. ONE-BODY KINETIC ENERGY

Using the first term of Eq. (2.14), the expectation value of the kinetic energy operator becomes

$$\langle T\rangle = \sum_{i,j=1}^{A} \langle i|t|j\rangle\langle\Phi|a_i^\dagger a_j|\Phi\rangle, \tag{A.1}$$

where Eq. (2.12) was also used. With the help of the anticommutation relations, [Eq. (2.9)] and Eq. (2.12),

$$\langle T\rangle = \sum_i \int d^3r\, \phi_i^*(\vec{r}) \left(-\frac{\hbar^2}{2m}\nabla^2\right) \phi_i(\vec{r}). \tag{A.2}$$

Integrating by parts and using the fact that the wavefunction vanishes at large distances, the final form of the kinetic energy is

$$\langle T\rangle = \int d^3r\, \frac{\hbar^2}{2m}\tau(\vec{r}). \tag{A.3}$$

B. THE TWO-BODY POTENTIAL

Using the second term of Eq. (2.14), the expectation value of the two-body potential is given by

$$\langle V^{(2)}\rangle = \frac{1}{2}\sum_{ijk\ell} \langle ij|v_{12}|k\ell\rangle\langle\Phi|a_i^\dagger a_j^\dagger a_\ell a_k|\Phi\rangle, \tag{A.4}$$

where Eq. (2.12) was also used. Anticommutation relations yield a general form for the expectation of the two-body potential,

$$\langle V^{(2)}\rangle = \frac{1}{2}\sum_{ij} [\langle ij|v_{12}|ij\rangle - \langle ij|v_{12}|ji\rangle]. \tag{A.5}$$

where the first term is known as the "direct" part and the second term as the "exchange". The exchange term can be rewritten in a more compact form through the definition of the particle exchange operator,

$$P_{12} = P_r P_\sigma P_\tau, \tag{A.6}$$

where P_σ and P_τ denote the spin and isospin exchange operators given by Eq. (2.6), and P_r is the radial exchange operator which is unity for zero-range interactions. Using P_{12}, Eq. (A.5) takes the form

$$\langle V^{(2)} \rangle = \frac{1}{2} \sum_{ij} \langle ij \mid v_{12}(1-P_{12}) \mid ij \rangle. \tag{A.7}$$

Here we have also used the invariance of v_{12} under particle exchange.

1. Contribution from the t_0 term.

Using the part of v_{12} proportional to t_o [Eq. (2.5a)] in Eq. (A.7), we obtain

$$V_o = \frac{1}{2} \sum_{ij} \langle ij \mid t_o\, \delta(\vec{r}_1 - \vec{r}_2)(1 + x_o\, P_\sigma)(1 - P_{12}) \mid ij \rangle. \tag{A.8}$$

Since we are dealing with a zero-range force, $P_r = 1$. Also, using the fact that the trace of the spin matrices is zero, and $P_\sigma{}^2 = 1$, V_o takes the form

$$V_o = \frac{t_o}{2} \sum_{ij} \langle ij \mid \left(1 + \frac{x_o}{2}\right) - \left(\frac{1}{2} + x_o\right) \delta q_i q_j \mid ij \rangle, \tag{A.9}$$

and from Eq. (2.16),

$$V_o = \int d^3r\, \frac{t_o}{2} \left[\left(1 + \frac{x_o}{2}\right)\rho^2 - \left(\frac{1}{2} + x_o\right) \sum_q \rho_q{}^2\right]. \tag{A.10}$$

2. Contribution from the t_1 term.

Using the part of v_{12} proportional to t_1 [Eq. (2.5a)] in Eq. (A.7), we obtain

$$V_1 = -\frac{t_1}{16}\sum_{ij} \langle ij \,|\, \delta(\vec{r}_1-\vec{r}_2)(\nabla_1^2 + \nabla_2^2 - 2\vec{\nabla}_1\cdot\vec{\nabla}_2)(1 - P_{12}) \,|\, ij\rangle + c.c. \tag{A.11}$$

Writing the projection operators explicitly, Eq. (A.11) becomes

$$V_1 = -\frac{t_1}{16}\sum_{ij} \langle ij \,|\, (\nabla_1^2 + \nabla_2^2 - 2\vec{\nabla}_1\cdot\vec{\nabla}_2)(1 - \tfrac{1}{2}\delta q_i q_j) \,|\, ij\rangle + c.c. \tag{A.12}$$

For the calculation of these terms we make use of the following relations,

$$\sum_i \phi_i^*(\vec{r})\nabla^2\phi_i(\vec{r}) = \frac{1}{2}\nabla^2\rho(\vec{r}) - \tau(\vec{r})$$

$$\sum_i \phi_i^*(\vec{r})\vec{\nabla}\,\phi_i(\vec{r}) = \frac{1}{2}\vec{\nabla}\rho(\vec{r}) + \vec{ij}(\vec{r}). \tag{A.13}$$

This yields

$$\sum_{ij} \langle ij \,|\, (\nabla_1^2 + \nabla_2^2)\delta(\vec{r}_1-\vec{r}_2) + c.c. = \int d^3r\,[2\rho\,\nabla^2\rho - 4\rho\tau]$$

$$-2\sum_{ij} \langle ij \,|\, \vec{\nabla}_1\cdot\vec{\nabla}_2\,\delta(\vec{r}_1-\vec{r}_2) \,|\, ij\rangle + c.c. = \int d^3r\,[\rho\nabla^2\rho + 4j^2], \tag{A.14}$$

where an integration by parts was performed in the calculation of the first term. The calculation of the exchange term proceeds identically to that of the direct term, and it will not be shown explicitly. Final form for V_1 is

$$V_1 = \int d^3r \left(-\frac{t_1}{16}\right)\Big[3\rho\nabla^2\rho - 4\rho\tau + 4j^2 - \frac{3}{2}\rho_n\nabla^2\rho_n - \frac{3}{2}\rho_p\nabla^2\rho_p + 2\rho_n\tau_n + 2\rho_p\tau_p - 2j_p{}^2 - 2j_n{}^2\Big]. \tag{A.15}$$

3. Contribution from the t_2 term.

Using the part of v_{12} proportional to t_2 in Eq. (A.7), we get

$$V_2 = \frac{t_2}{4}\sum_{ij} \langle ij \,|\, (\vec{\nabla}_1'\cdot\delta(\vec{r}_1-\vec{r}_2)\vec{\nabla}_1 - \vec{\nabla}_2'\cdot\delta(\vec{r}_1-\vec{r}_2)\vec{\nabla}_1)(1-P_{12}) \,|\, ij\rangle, \tag{A.16}$$

where the primes indicate that the gradient operator is acting on the left. The calculation of V_2 is very similar to that of V_1 except this term acts on p-waves; therefore, the Majorana exchange operator P_r has to be replaced by -1 in evaluating the exchange term. To make further use of the operations done for V_1, we integrate the second term by parts to obtain

$$V_2 = \frac{t_2}{4}\sum_{ij} \langle ij \,|\, [2\vec{\nabla}_1'\cdot\delta(\vec{r}_1-\vec{r}_2)\vec{\nabla}_1 + \delta(\vec{r}_1-\vec{r}_2)(\nabla_1{}^2 + \vec{\nabla}_1\cdot\vec{\nabla}_2)]\left(1 + \frac{1}{2}\delta q_i q_j\right) \,|\, ij\rangle. \tag{A.17}$$

Using Eq. (13), and integrating the $(\nabla\rho)^2$ term by parts, the contribution from the t_2 term becomes

$$V_2 = \int d^3r \frac{t_2}{16}\left[4\rho\tau + \rho\nabla^2\rho - 4j^2 + 2\rho_p\tau_p + 2\rho_n\tau_n + \frac{1}{2}\rho_p\nabla^2\rho_p + \frac{1}{2}\rho_n\nabla^2\rho_n - 2j_p{}^2 - 2j_n{}^2\right]. \tag{A.18}$$

4. Contribution from the t_3 term.

To calculate the contribution arising due to the three-body term

of the potential, we use the equivalent two-body form with explicit dependence on the nuclear density [Eq. (2.7)]. In this case, Eq. (A.7) yields

$$V_3 = \frac{t_3}{12} \sum_{ij} \langle ij \mid (1 + P_\sigma)\delta(\vec{r}_1-\vec{r}_2)\rho^\alpha \left(\frac{\vec{r}_1+\vec{r}_2}{2}\right)(1 - P_{12}) \mid ij\rangle. \quad (A.19)$$

After acting with the projection operators, V_3 becomes

$$V_3 = \frac{t_3}{12} \sum_{ij} \langle ij \mid \delta(\vec{r}_1-\vec{r}_2)\rho^\alpha \left(\frac{\vec{r}_1+\vec{r}_2}{2}\right)\left(\frac{3}{2} - \frac{3}{2}\,\delta q_i q_j\right) \mid ij\rangle \quad (A.20)$$

$$= \int d^3r \frac{t_3}{8} [\rho^\alpha \rho^2 - \rho^\alpha \rho_p{}^2 - \rho^\alpha \rho_n{}^2]. \quad (A.21)$$

APPENDIX B

In order to simulate the effects of a finite-range interaction, the surface energy terms, $\rho\nabla^2\rho$, in Skyrme interaction are replaced by the following sum of Yukawa interactions,

$$E_y = \int d\vec{r}\, d\vec{r}' \frac{e^{-|\vec{r}-\vec{r}'|/a}}{|\vec{r}-\vec{r}'|/a}\left[\frac{v_u}{2}\rho(\vec{r})\rho(\vec{r}') + \frac{(v_\ell - v_u)}{2}\sum_q \rho_q(\vec{r})\rho_q(\vec{r}')\right]. \quad (B.1)$$

Instead of doing one of the three-dimensional integrals, we can solve the associated Helmholtz equation,

$$\Phi(\vec{r}) = 4\pi a^3\rho(\vec{r}) + a^2\nabla^2\Phi(\vec{r}), \quad (B.2)$$

which has the solution,

$$\Phi(\vec{r}) = \int d^3\vec{r}'\ \rho(\vec{r}')\frac{e^{-|\vec{r}-\vec{r}'|/a}}{|\vec{r}-\vec{r}'|/a}. \quad (B.3)$$

Iterating Eq. (B.2), we obtain

$$\Phi(\vec{r}) = 4\pi a^3[\rho(\vec{r}) + a^2\nabla^2\rho(\vec{r}) + \text{higher order terms}]. \qquad (B.4)$$

This expansion is then used to replace one of the integrals in Eq. (B.1),

$$E_Y = \int d\vec{r}\; 4\pi a^3 \left\{ \frac{V_u}{2}\rho^2 + a^2\frac{V_u}{2}\rho\nabla^2\rho - \frac{V_\ell - V_u}{2}\sum_q \rho_q{}^2 - a^2\frac{V_\ell - V_u}{2}\sum_q \rho_q\nabla^2\rho_q \right\}. \qquad (B.5)$$

Note that in this expansion we also have terms proportional to ρ^2. Comparison of the coefficients of $\rho\nabla^2\rho$ terms in Eq. (B.5) with those of Eq. (2.15) yield the relations given by Eq. (2.18). Similarly, the ρ^2 terms result in modifications given by Eq. (2.19).

APPENDIX C

The action of the tri-diagonal matrices H and V on wavefunctions g_ℓ are given by Eqs. (2.72-2.79). On the other hand, the time-evolution operator G_{PR} given by Eq. (2.86) requires the inversion of tri-diagonal matrices of the form

$$\left[1 + \frac{i\Delta t}{2\hbar} H\right]^{-1}. \qquad (C.1)$$

Instead, the inversion can be done by solving the tri-diagonal system of equations using a special form of the Gaussian elimination method,

$$\left(1 + \frac{i\Delta t}{2\hbar} H\right) g''(t) = g'(t), \qquad (C.2)$$

where g' is defined as

$$g'(t) = \left[1 - \frac{i\Delta t}{2\hbar} V\right] g(t). \qquad (C.3)$$

Since H acting on g'' only changes the discrete coordinate index j, Eq. (C.2) can be cast into the form

$$C_{j-1}g''(i,j-1) + C_j\, g''(i,j) + C_{j+1}g''(i,j+1) = g'(i,j), \qquad (C.4)$$

where the coefficients are obtained from Eq. (2.72) as

$$\begin{aligned} C_{j-1} &= B^{(+)*}(i,j-1) \\ C_j &= 1 + \frac{i\Delta t}{2\hbar}\left(B^{(o)}(i,j) + \frac{1}{2}\, h_o(i,j)\right) \\ C_{j+1} &= B^{(+)}(i,j). \end{aligned} \qquad (C.5)$$

Note that for notational simplicity we have suppressed the time indices. A recursive solution of Eq. (C.4) can be obtained by defining

$$g''(i,j) = E_j\, g''(i,j+1) + F_j \quad , \quad j = N_z-1,\ldots,1 \qquad (C.6)$$

together with the boundary condition,

$$g''(i,N_z) = 0. \qquad (C.7)$$

To obtain the arrays E and F, we substitute $g''(i,j-1)$ from Eq. (C.6) into Eq. (C.4),

$$g''(i,j) = -\frac{C_{j+1}}{C_{j-1}\,E_{j-1} + C_j}\, g''(i,j+1) + \frac{g'(i,j)-C_{j-1}\,F_{j-1}}{C_{j-1}\,E_{j-1} + C_j}. \qquad (C.8)$$

Comparing Eq. (C.8) and Eq. (C.6), we can write the following recursion relations for E and F,

$$E_j = -\frac{C_{j+1}}{C_{j-1}\,E_{j-1} + C_j}\ ;\ F_j = \frac{g'(i,j)-C_{j-1}\,F_{j-1}}{C_{j-1}\,E_{j-1} + C_j},\ j = 1,2,\ldots,N_z, \qquad (C.9)$$

together with boundary conditions,

$$E_0 = F_0 = 0. \qquad (C.10)$$

APPENDIX D

In Section II.G we have discussed the gradient iteration step for solving the static Hartree-Fock equations. Here, we will incorporate the constrained Hartree-Fock calculations into the gradient iteration step. We will first illustrate the derivation for a general constraining field, and afterwards, we will write the equations for the density constraint. We start with an imaginary time iteration step of Eq. (2.89),

$$|\chi_\lambda^{k+1}\rangle = \mathcal{O}\{|\chi_\lambda^k\rangle - \varepsilon(\hat{h}^k - \varepsilon_\lambda^k)|\chi_\lambda^k\rangle\}. \tag{D.1}$$

It is possible to rewrite Eq. (B.1) via the use of the projection operator,

$$\hat{P}_\lambda^k = 1 - |\chi_\lambda^k\rangle\langle\chi_\lambda^k|, \tag{D.2}$$

as

$$|\chi_\lambda^{k+1}\rangle = \mathcal{O}\{|\chi_\lambda^k\rangle - \varepsilon\, \hat{P}_\lambda^k\, \hat{h}^k|\chi_\lambda^k\rangle\}. \tag{D.3}$$

The aim of this appendix is to devise an iteration scheme such that the expectation value of an arbitrary operator $\hat{Q}$ does not change from one iteration to the next

$$\sum_\lambda \langle\chi_\lambda^{k+1}|\hat{Q}|\chi_\lambda^{k+1}\rangle = \sum_\lambda \langle\chi_\lambda^k|\hat{Q}|\chi_\lambda^k\rangle. \tag{D.4}$$

Furthermore, we wish this expectation value to be equal to a fixed number Q_o. To achieve this, we use the method of Lagrange multipliers,

$$|\chi_\lambda^{k+1}\rangle = \mathcal{O}\{|\chi_\lambda^k\rangle - \varepsilon\, \hat{P}_\lambda^k(\hat{h}^k + \lambda\hat{Q})|\chi_\lambda^k\rangle\}. \tag{D.5}$$

where λ is to be determined from Eq. (D.4). The application of the Gram-Schmidt orthogonalization procedure yields, to order ε^2,

$$|\chi_\lambda^{k+1}\rangle = (1-\hat{A}_\lambda)\,|\chi_\lambda^k\rangle + \sum_{\mu=1}^{\lambda-1}\left[\langle\chi_\lambda^k|\hat{A}_\lambda^\dagger|\chi_\mu^k\rangle + \langle\chi_\lambda^k|\hat{A}_\mu|\chi_\mu^k\rangle\right]|\chi_\mu^k\rangle, \tag{D.6}$$

where we have defined

$$\hat{A}_\lambda = \hat{P}_\lambda^k\,\varepsilon(\hat{h}^k + \lambda\hat{Q}). \tag{D.7}$$

From Eq. (D.6) we calculate the lefthand side of Eq. (D.4) to obtain

$$\lambda = \frac{\langle x|\,\hat{Q}(\hat{h}^k + \lambda\hat{Q})\,|x\rangle}{\langle x|\,\hat{Q}^2\,|x\rangle}, \tag{D.8}$$

where

$$\langle x|\,\hat{A}\hat{B}\,|x\rangle = \sum_\lambda \langle\chi_\lambda^k|\,\hat{A}\hat{B}\,|\chi_\lambda^k\rangle - 2\sum_\lambda\sum_{\mu=1}^{\lambda-1}\langle\chi_\lambda^k|\,\hat{A}\,|\chi_\mu^k\rangle\langle\chi_\mu^k|\,\hat{B}\,|\chi_\lambda^k\rangle. \tag{D.9}$$

The difference between the expectation value of $\hat{Q}$ in each iteration step will be of order ε^2. To further correct for this error, we add a term which is solely driven by this difference,

$$\delta\lambda = \frac{\left[\sum_\lambda \langle\chi_\lambda^k|\,\hat{Q}\,|\chi_\lambda^k\rangle - Q_o\right]/2\varepsilon}{\langle x|\,\hat{Q}^2\,|x\rangle}. \tag{D.10}$$

This is then the most optimal value of λ to be used at each iteration step. As we see, the calculation of the exchange terms is rather costly. Instead, it is possible to formulate an iterative scheme for determining λ at each iteration step. To do this, we perform an intermediate step,

$$|\chi_\lambda^{k+1/2}\rangle = \mathcal{O}\{|\chi_\lambda^k\rangle - \varepsilon(\hat{h}^k + \lambda^k\,\hat{Q} - \varepsilon_\lambda^k)\,|\chi_\lambda^k\rangle\}, \tag{D.11}$$

and calculate the difference

$$\delta Q^{k+1/2} = \sum_{\lambda} \langle \chi_{\lambda}^{k+1/2} | \hat{Q} | \chi_{\lambda}^{k+1/2} \rangle - \sum_{\lambda} \langle \chi_{\lambda}^{k} | \hat{Q} | \chi_{\lambda}^{k} \rangle . \tag{D.12}$$

We then correct λ to reduce this difference,

$$\lambda^{k+1} = \lambda^{k} + C_{o} \frac{\delta Q^{k+1/2}}{2\varepsilon \sum_{\lambda} \langle \chi_{\lambda}^{k} | \hat{Q}^{2} | \chi_{\lambda}^{k} \rangle + d_{o}}, \tag{D.13}$$

where we have replaced the exchange term by the constant d_o. In terms of these intermediate states, the (k+1)st step is given by

$$| \chi_{\lambda}^{k+1} \rangle = \mathcal{O} \{ | \chi_{\lambda}^{k+1/2} \rangle - \varepsilon (\lambda^{k+1} - \lambda^{k} + \delta\lambda^{k}) \hat{Q} | \chi_{\lambda}^{k+1/2} \rangle \}, \tag{D.14}$$

where

$$\delta\lambda^{k} = \frac{\sum \langle \chi^{k} | \hat{Q} | \chi^{k} \rangle - Q_{o}}{2\varepsilon \sum_{\lambda} \langle \chi_{\lambda}^{k} | \hat{Q}^{2} | \chi_{\lambda}^{k} \rangle + d_{o}} . \tag{D.15}$$

The extension of this method to the density constraints is a trivial one. In this case, we would like to constrain a continuous density,

$$\rho^{k}(r) = \sum_{\lambda} | \chi_{\lambda}^{k}(r) |^{2}, \tag{D.16}$$

to be equal to $\rho_o(r)$. The operator $\hat{Q}$ becomes the density operator $\hat{\rho}(r)$ defined as

$$\langle \chi_{\lambda}^{k} | \hat{\rho}(r) | \chi_{\lambda}^{k} \rangle = | \chi_{\lambda}^{k}(r) |^{2}, \tag{D.17}$$

and the product $\lambda\hat{Q}$ becomes an integral,

$$\lambda\hat{Q} \rightarrow \int d^{3}r \, \lambda(r) \, \hat{\rho}(r). \tag{D.18}$$

Note that in coordinate space $\hat{\rho}(r)$ is a delta function, and

$$\int d^3r\ \lambda(r)\hat{\rho}(r) = \lambda(r). \tag{D.19}$$

From these equations the iterative scheme for $\lambda^k(r)$ can be written as

$$\lambda^{k+1}(r) = \lambda^k(r) + C_o \frac{\delta\rho^{k+1/2}}{2\varepsilon\rho^k(r)+d_o}, \tag{D.20}$$

where

$$\delta\rho^{k+1/2}(r) = \rho^{k+1/2}(r) - \rho_o(r) \tag{D.21}$$

is obtained from the half-time iteration step

$$|\chi_\lambda^{k+1/2}\rangle = \mathcal{O}\{|\chi_\lambda^k\rangle - \varepsilon(\hat{h}^k + \lambda^k(r) - \varepsilon_\lambda^k)|\chi_\lambda^k\rangle\}. \tag{D.22}$$

Using these wavefunctions, the (k+1)st iteration becomes

$$|\chi_\lambda^{k+1}\rangle = \mathcal{O}\{|\chi_\lambda^{k+1/2}\rangle - \varepsilon(\lambda^{k+1}(r)-\lambda^k(r) + \delta\lambda^k(r))|\chi_\lambda^{k+1/2}\rangle\}, \tag{D.23}$$

where

$$\delta\lambda^k(r) = c_o \frac{\rho^k(r)-\rho_o(r)}{2\varepsilon\rho_o(r)+d_o}.$$

In practical calculations the parameter ε of Eq. (D.1) has been replaced by the damping operator of Eq. (2.91), and the constants c_o and d_o were chosen to be 0.9 and 7×10^{-5} respectively.

REFERENCES

AB63 E. Almqvist, D.A. Bromley, J.A. Kuehner, and B. Whalen
Phys. Rev. 130 (1963), 1140.

AB83 F. Arickx, J. Broeckhove, E. Caurier, E. Deumens, and P.V. Leuven
Nucl. Phys. A398 (1983), 467.

BA76 Z. Basrak, F. Auger, B. Fernandez, J. Castebois, and N. Cindro
Phys. Lett. 65B (1976), 119.

Be71 H.A. Bethe
Ann. Rev. Nucl. Sci. 21 (1971), 93.

Be73 G.F. Bertsch
Phys. Rev. Lett. 31 (1973), 121.

Be75 G.F. Bertsch
Nucl. Phys. A249 (1975), 253.

BF75 M. Beiner, H. Flocard, N.V. Giai, and P. Quentin
Nucl. Phys. A238 (1975), 29.

BF79 J. Blocki and H. Flocard
Phys. Lett. 85B (1979), 163.

BG66 G.E. Brown and A.M. Green
Nucl. Phys. 75 (1966), 401.

BG76 J.P. Blaizot, D. Gogny, and B. Grammaticos
Nucl. Phys. A265 (1976), 315.

BG80 J.F. Berger and D.Gogny
Nucl. Phys. A333 (1980), 302.

BK60 D.A. Bromley, J.A. Kuehner, and E. Almqvist
Phys. Rev. Lett. 4 (1960), 365

BK76 P. Bonche, S.E. Koonin, and J.W. Negele
Phys. Rev. C13 (1976), 1226.

B180 J.P. Blaizot
Phys. Rep. 64 (1980), 171.

B181 J.P.Blaizot
Phys. Lett. 107B (1981), 331.

BM75 A.Bohr and B.R. Mottelson
"Nuclear Structure", (W.A. Benjamin, Massachussetts, 1975),
Vol. II, pp. 7, 4, 23, 35, 8.

BQ82 J. Bartel, P. Quentin, M. Brack, C. Guet, and H.B. Hakansson
Nucl. Phys. A386 (1982), 79.

BT75 G.F. Bertsch and S.F. Tsai
Phys. Rep. 18 (1975), 125.

BT77 A. Bonaccorso, M. Di Toro, and G. Russo
Phys. Lett. 72B (1977), 27.

CC75 E.R. Cosman, T.M. Cormier, K.V. Bibber, A. Sperduto,
G. Young, J. Erskine, L.R. Greenwood, and O. Hansen
Phys. Rev. Lett. 35 (1975), 265.

CD79 J. Cugnon, H. Doubre, and H. Flocard
Nucl. Phys. A331 (1979), 213.

CG83 N. Cindro and W. Greiner
J. Phys. G9 (1983), L175.

CH76 R.Y. Cusson, R. Hilko, and D. Kolb
Nucl. Phys. A270 (1976), 437.

CR85 R.Y. Cusson, P.-G. Reinhard, M.R. Strayer, J.A. Maruhn, and W. Greiner
Z. Phys. A320 (1985), 475.

CM78 H. Chandra and U. Mosel
Nucl. Phys. A298 (1978), 151.

CS82 R.Y. Cusson, H. Stocker, M.R. Strayer, A.S. Umar, D.A. Bromley, J.A. Maruhn, and W. Greiner
in proceedings of "Time-Dependent Hartree-Fock and Beyond", (Springer-Verlag, NY, 1982), ed. K. Goeke, P.-G. Reinhard, p. 22.

Da81 C. Davis
Phys. Rev. C24 (1981), 1891.

Di30 P.A.M. Dirac
Proc. Cambridge Phil. Soc. 26 (1930), 376.

DD85 K.T.R. Davies, K.R.S. Devi, S.E. Koonin, and M.R. Strayer
in "Treatise on Heavy-Ion Science", ed. D.A. Bromley, (Plenum, NY, 1985), Vol. 3, p. 3.

DF80 K.T.R. Davies, H. Flocard, S. Krieger, and M.S. Weiss
Nucl. Phys. A342 (1980), 111.

DR80 M. Di Toro, G. Russo, and F. Duggan
Phys. Rev. C21 (1980), 2054.

DK81 K.T.R. Davies and S.E. Koonin
Phys. Rev. C23 (1981), 2042.

EB75 Y.M. Engel, D.M. Brink, K. Goeke, S.J. Krieger, and D. Vautherin
Nucl. Phys. A249 (1975), 215.

EB76 K.A. Erb, R.R. Betts, D.L. Hanson, M.W. Sachs, R.L. White, P.P. Tung, and D.A. Bromley
Phys. Rev. Lett. 37 (1976), 670.

EB81 K.A. Erb and D.A. Bromley
Phys. Rev. C23 (1981), 2781.

EB85 K.A. Erb and D.A. Bromley
in "Treatise on Heavy-Ion Science", (Plenum, NY, 1985), ed. D.A. Bromley, Vol. 3, p. 201.

EM75 K.A. Eberhard, E. Mathiak, J. Stettmeier, W. Trombik, A. Weidinger, L.N. Wustefeld, and K.G. Bernhardt
Phys. Lett. 56B (1975), 445.

EN73 H. Emling, R. Nowotny, D. Pelte, and G. Schrieder
Nucl. Phys. A211 (1973), 600.

FH80 H. Flocard, P.H. Heenen, and D. Vautherin
Nucl. Phys. A339 (1980), 336.

FP57 E. Fermi, J. Pasta, and S. Ulam
"Studies of Nonlinear Problems", Sci. Rep. LA-1940, (LASL, 1957).

FW71 A.L. Fetter and J.D. Walecka
"Quantum Theory of Many-Particle Systems", (McGraw-Hill, NY, 1971) pp. 171.

GR83 M. Gai, M. Ruscev, A.C. Hayes, J.F. Ennis, R. Keddy, E.C. Schloemer, S.M. Sterbenz, and D.A. Bromley
Phys. Rev. Lett. 50 (1983), 239.

GT77 W. Galster, W. Treu, P. Duck, H. Frohlich, and H. Voit
Phys. Rev. C15 (1977), 950.

He81 R.G.H. Helleman
"Chaos and Universality", Nordisk Institut für Theoretisk Atomfysik, 1981, p. 165.

HN77 P. Hoodbhoy and J.W. Negele
Nucl. Phys. A288 (1977), 23.

Ia81 F. Iachello
Phys. Rev. C23 (1981), 2778.

Ja75 J.D. Jackson
"Classical Electrodynamics", (Wiley, NY, 1975), p. 739.

JF78 D.R. James and N.R. Fletcher
Phys. Rev. C17 (1978), 2248.

KD77 S.E. Koonin, K.T.R. Davies,V. Maruhn-Rezwani, H. Feldmeier, S.J. Krieger, and J.W. Negele
Phys. Rev. C15 (1977), 1359.

KE79 S.K. Korotky, K.A. Erb, S.J. Willet, and D.A. Bromley
Phys. Rev. C20 (1979), 1014.

KK76 A.K. Kerman and S.E. Koonin
Ann. Phys. 100 (1976), 332.

KK77 S. Krewald, V. Klemt, J. Speth, and A. Faessler
Nucl. Phys. A281 (1977), 166.

Ko69 H.S. Kohler
Nucl. Phys. A139 (1969), 353.

Ko75 S.E. Koonin
Ph.D. Thesis, Massachusetts Institute of Technology, unpublished (1975).

Ko80 S.E. Koonin
Progr. in Part. & Nucl. Phys. 4 (1980), 283.

KO77 A.K. Kerman and N. Onishi
Nucl. Phys. A281 (1977), 373.

KT80 H. Krivine, J. Treiner, and O. Bohigas
Nucl. Phys. A336 (1980), 155.

LB76 K.F. Liu and G.E. Brown
Nucl. Phys. A265 (1976), 385.

LK70 S.Y. Li, A. Klein, and R.M. Dreizler
J. Math. Phys. 11 (1970), 975.

LL75 G. Leander and S.E. Larsson
Nucl. Phys. A239 (1975), 43.

LL79 L.D. Landau and E.M. Lifshitz
"The Classical Theory of Fields", (Pergamon Press, NY, 1979), p. 66.

LN80 S. Levit, J.W. Negele, and Z. Paltiel
Phys. Rev. C21 (1980), 1603.

MH77 N. Marquardt, W. Hoppe, and D. Siegel
Phys. Rev. C16 (1977), 2291.

MK83 V. Metag, W. Kuhn, R. Novotny, H.J. Hennrich, A. Lazzarini, D. Habs, D. Schwalm, and H. Gemmeke
in proceedings of "Nuclear Physics with Heavy Ions", (Harwood Academic, NY, 1983), ed. P. Braun-Munzinger, p. 391.

MV74 N. Marquardt, R. Volders, C. Cardinal, and J. L'Ecuyer
Phys. Rev. Lett. 33 (1974), 1389.

Mo70 S.A. Moszkowski
Phys. Rev. C2 (1970), 402.

Mu67 R. Muthukrishnan
Nucl. Phys. A93 (1967), 417.

Ne70 J.W. Negele
Phys. Rev. C1 (1970), 1260.

Ne82 J.W. Negele
Revs. Mod. Phys. 54 (1982), 913.

NV72 J.W. Negele and D. Vautherin
Phys. Rev. C5 (1972), 1472.

NV75 J.W. Negele and D. Vautherin
Phys. Rev. C11 (1975), 1031.

Pa76 K.-H. Passler
Nucl. Phys. A257 (1976), 253.

PG77 J.Y. Park, W. Greiner, and W. Scheid
Phys. Rev. C16 (1977), 2276.

PS74 J.Y. Park, W. Scheid, and W. Greiner
Phys. Rev. C10 (1974), 967.

RC82 P.-G. Reinhard and R.Y.Cusson
Nucl. Phys. A378 (1982), 418.

Ro66 D.J. Rowe
Nucl. Phys. 80 (1966), 209.

RS80 P. Ring and P. Schuck
"The Nuclear Many-Body Problem", (Springer-Verlag, NY, 1980), p. 22.

SB75 S. Shlomo and G.F. Bertsch
Nucl. Phys. A243 (1975), 507.

SB76 P. Sperr, T.H. Braid, Y. Eisen, D.G. Kovar, F.W. Prosser, J.P. Schieffer, S.L. Tabor, and S. Vigdor,
Phys. Rev. Lett. 37 (1976), 321.

SC84 M.R. Strayer, R.Y. Cusson, A.S. Umar, P.-G. Reinhard, D.A. Bromley and W. Greiner
Phys. Lett. 135B (1984), 261.

SF74 A. de Shalit and H. Feshbach
"Theoretical Nuclear Physics", Vol. I (Wiley, NY, 1974).

Sk56 T.K.R. Skyrme
Phil. Mag. 1 (1956), 1043.

Sk59 T.K.R. Skyrme
Nucl. Phys. 9 (1959), 615; 9 (1959), 635.

SK78 A.M. Sandorfi, L.R. Kilius, H.W. Lee, and A.E. Litherland
Phys. Rev. Lett. 40 (1978), 1248.

St81 M.R. Strayer
private communication.

SZ73 R.W. Sharp and L. Zamick
Nucl. Phys. A208 (1973), 130.

TA71 N. Takigawa and A. Arima
Nucl. Phys. A168 (1917), 593; and references therein.

Um82 A.S. Umar
unpublished.

US84 A.S. Umar, M.R. Strayer, D.J. Ernst, K.R.S. Devi
Phys. Rev. C30 (1984), 1934; and references therein.

US85 A.S. Umar, M.R. Strayer, R.Y. Cusson, P.-G. Reinhard, D.A. Bromley
Phys. Rev. C32 (1985) in press.

Va73 D. Vautherin
Phys. Rev. C7 (1973), 296.

VB70 D. Vautherin and D.M. Brink
Phys. Lett. 32B (1970), 149.

VB72 D. Vautherin and D.M. Brink
Phys. Rev. C5 (1972), 626.

VG77 H. Voit, W. Galster, W. Treu, H. Frohlich, and P. Duck
Phys. Lett. 67B (1977), 399.

WK82 R.D. Williams and S.E. Koonin
Nucl. Phys. A391 (1982), 72.

WS77 R. Wada, J. Schimizu, and K. Takimoto
Phys. Rev. Lett. 38 (1977), 1341.

ZM75 P.G. Zint and U. Mosel
Phys. Lett. 56B (1975), 424.

SZ73 R.W. Sharp and L. Zamick
Nucl. Phys. A208 (1973), 130.

TA71 N. Takigawa and A. Arima
Nucl. Phys. A168 (1917), 593; and references therein.

Um82 A.S. Umar
unpublished.

US84 A.S. Umar, M.R. Strayer, D.J. Ernst, K.R.S. Devi
Phys. Rev. C30 (1984), 1934; and references therein.

US85 A.S. Umar, M.R. Strayer, R.Y. Cusson, P.-G. Reinhard, D.A. Bromley
Phys. Rev. C32 (1985) in press.

Va73 D. Vautherin
Phys. Rev. C7 (1973), 296.

VB70 D. Vautherin and D.M. Brink
Phys. Lett. 32B (1970), 149.

VB72 D. Vautherin and D.M. Brink
Phys. Rev. C5 (1972), 626.

VG77 H. Voit, W. Galster, W. Treu, H. Frohlich, and P. Duck
Phys. Lett. 67B (1977), 399.

WK82 R.D. Williams and S.E. Koonin
Nucl. Phys. A391 (1982), 72.

WS77 R. Wada, J. Schimizu, and K. Takimoto
Phys. Rev. Lett. 38 (1977), 1341.

ZM75 P.G. Zint and U. Mosel
Phys. Lett. 56B (1975), 424.